Formation and Removal of SO_x and NO_x in Pressurized Oxy-fuel Coal Combustion

by

Muhammad Jahangir Malik

A thesis
presented to the University of Waterloo
in fulfilment of the
thesis requirement for the degree of
Master in Applied Science
in
Chemical Engineering

Waterloo, Ontario, Canada, 2019

Author's Declaration

I hereby declare that I am the sole author of this thesis. This is a true copy of the thesis, including any required final revisions, as accepted by my examiners.

I understand that my thesis may be made electronically available to the public.

Abstract

Growing concerns over greenhouse gas emissions have driven extensive research in carbon capture, storage and sequestration. Oxy-fuel combustion is a promising technology in CO_2 capture, as the combustion products consists primarily of CO_2 and H_2O with contaminants like NO_x and SO_x. More recently, oxy-fuel combustion under pressurized conditions has gained attention due to its overall higher net efficiency, while decreasing the auxiliary power consumption in the process.

The need for a better understanding of the coal combustion in oxy-fuel conditions under elevated pressures and the formation of SO_x and NO_x in such conditions inspired this research project. In this thesis, the effect of pressurized oxy-fuel combustion on SO_x and NO_x formation from coal combustion and their removal from the flue gas was investigated. The combustion modelling for lignite coal was conducted in ANSYS Fluent, under oxy-fuel environment at atmospheric pressure and elevated pressures (5 atm, 10 atm, 15 atm). The results showed an increase in SO_3 formation and rapid decrease in NO in the flue gas as the pressure was increased in the combustor. At 15 atm, the NO_x emissions were found to be below 100 ppm, which is an acceptable concentration of NO_x for CO_2 transport and storage.

In order to investigate the influence of pressure on SO_x and NO_x in the flue gas in the post-combustion zone, the system was subjected to a temperature profile representative of an actual plant boiler, where the residence time is around 2 seconds. The results showed that the rate of SO_2 and NO oxidation to SO_3 and NO_2, respectively, were influenced by the rate of temperature decrease, and the effect of pressure was not as significant. It was observed that flue gas composition remained constant below 550 K, as all SO_3 present in the flue gas converted to gaseous H_2SO_4.

Lastly, simulations for SO_x and NO_x removal from flue gas via absorption were performed at 15 atm to purify the flue gas to meet the requirements for CO_2 transportation. The results showed complete removal of SO_x in the form of H_2SO_4 and SO_4^{2-} and around 30% NO_x removal, mostly in the form of HNO_3. A sensitivity analysis was performed on the reflux ratio of liquid in the absorber and the results showed increased NO_x removal at lower reflux ratio. The investigation helped conclude that pressurized oxy-fuel combustion results in lower SO_x and NO_x emissions, and require less sophisticated separation techniques to meet the pipeline threshold for CO_2 transportation in storage and sequestration.

Acknowledgments

First and foremost, I would like to thank God Almighty for His uncountable blessings and giving me courage and strength in completing this thesis.

I sincerely thank my supervisors, Dr. P.L. Douglas and Dr. Eric Croiset, for their invaluable comments, guidance, patience and encouragement, without which this project would not have been possible.

I would also like to thank my committee members, Dr. X. Feng and Dr. D. Simakov for serving as my committee members and for their time.

I would like to acknowledge King Abdulla University of Science and Technology (KAUST) and Natural Sciences and Engineering Research Council (NSERC) for their funding of my research.

To my colleagues and friends at the university, I thank you for sharing your knowledge with me, your support, care, and all the memorable time we spent together.

Finally, to my parents, sister and fiancée for their personal support, encouragement, and great patience through this study. I would have never even thought of this if I did not have their prayers.

Table of Contents

Author's Declaration ii

Abstract iii

Acknowledgments v

List of Figures ix

List of Tables xi

Nomenclature xii

1 Introduction 1

1.1 Carbon capture technologies for coal fired power plants 3

1.2 Oxy-fuel combustion technology 5

1.3 Research objectives and contribution 8

1.4 Thesis Outline 9

2 Literature review 11

2.1 Oxy-fuel combustion technology development 11

2.2 CFD studies in oxy-fuel combustion 12

2.2.1 CFD studies in atmospheric oxy-fuel combustion 13

2.2.2 CFD studies in pressurized oxy-fuel combustion 14

2.3 Pollutant emissions 14

2.3.1 NO_x formation 14

2.3.2 SO_x formation 17

2.3.3 Interactions between SO_x and NO_x 19

2.4 Removal of SO_x and NO_x from flue gas 20

3 Mathematical modelling and methodology 24

3.1 Introduction 24

3.2 CFD modelling for coal combustion 25

3.2.1 Governing equations 26

3.2.2 Turbulence Flow 27

3.2.3 Gas phase model 28

3.2.4 Particle phase model 29

3.2.5 Radiation model 33

3.2.6 Nitric Oxide (NO) Modelling 34

3.2.7 Sulphur Oxide (SO_x) Modelling 38

3.3 Kinetic model for the flue gas 40

3.4 Removal of SO_x and NO_x from flue gas 43

4 CFD simulation of pressurized oxy-fuel combustion 47

4.1 Validation of the CFD simulation at atmospheric pressure 47

4.1.1 Coal 47

4.1.2 Furnace and burner geometry 48

4.1.3 Boundary conditions 50

4.1.4 Results and discussion 52

4.2 Effect of pressure in oxy-fuel combustion of coal 55

4.2.1 Results and discussion 56

5 Effect of pressure on NO_x and SO_x concentrations in the flue gas 64

5.1 Gas phase kinetic model 66

5.2 Results and discussion 68

5.2.1 Fixed geometry 68

5.2.2 Constant residence time 74

6 Removal of SO_x and NO_x in the absorber column 78

6.1 Design specifications 79

6.2 Results and Discussion 80

6.3 Effect of recycle ratio on NO_x and SO_x removal 82

7 Conclusions and recommendations 85

7.1 Conclusions 85

7.2 Recommendations 88

References 90

Appendix A Gas phase reactions for sulphur in ANSYS Fluent 102

Appendix B Kinetic mechanism for flue gas reactions 103

Appendix C Henry's law constants used in ASPEN Plus 136

List of Figures

Figure 1.1 Overview of carbon capture technologies [5] 3

Figure 1.2 Oxy-fuel combustion power plant with CO_2 capture 6

Figure 2.1 Timeline of pilot scale oxy-fuel combustion projects[37] 12

Figure 2.2 The overall NO formation and reduction mechanism [12] 16

Figure 2.3 Schematic for 2 column absorbers for NO_x and SO_x removal [65]..... 22

Figure 2.4 Single column absorber proposed by Iloeje et al. [65]..... 22

Figure 3.1 Schematic representing the methodology and the simulation software used.. 24

Figure 3.2 Heat, mass, and momentum transfer between particle and gas phase..... 30

Figure 3.3 Formation and destruction of fuel nitrogen 37

Figure 3.4 Temperature profile of flue gas in typical coal fired power plant. 41

Figure 3.5 Flowsheet for the reactive absorber column in ASPEN Plus 44

Figure 4.1 (a) Chalmers 100 kW combustor unit [105] (b) Cross section of the burner configuration of the combustor. 49

Figure 4.2 Axisymmetric 2D mesh for 100 kW Chalmers vertical combustor 50

Figure 4.3 Temperature profile of oxy-fuel combustion at 1 atm..... 53

Figure 4.4 Temperature profiles of the model and the experimental data 54

Figure 4.5 Flame temperature distribution in the furnace..... 57

Figure 4.6 Concentration of CO_2 in the furnace at different pressures..... 58

Figure 4.7 Contour for the concentration of O_2 at different pressures..... 59

Figure 4.8 Contour for the concentration of H_2O at different pressures..... 59

Figure 4.9 NO concentration at the furnace exit at different pressures. 61

Figure 4.10 Contour of SO_2 concentration at different pressures. 62

Figure 4.11 SO_3 concentration at the outlet of combustor at different pressures. 62

Figure 5.1 (a) represents the temperature profile of flue gas in a typical coal power plant (b) represents the enlarged view of the dashed portion of Figure 1.1 (a) 67

Figure 5.2 NO_2 concentration across the PFR at (a) 1 atm (b) 5 atm (c) 10 atm (d) 15 atm. The dashed line represents the temperature in K. 69

Figure 5.3 Rate of reactions ($mol.m^{-3}.s^{-1}$) for the production of NO_2 at (a) 1 atm (b) 5 atm (c) 10 atm (d) 15 atm. The dashed line represents temperature profile in K. 70

Figure 5.4 SO_3 concentration across the PFR at (a) 1 atm (b) 5 atm (c) 10 atm (d) 15 atm. The dashed line represents the temperature in K. 71

Figure 5.5 Rate of reactions ($mol.m^{-3}.s^{-1}$) for the production of SO_3 at (a) 1 atm (b) 5 atm (c) 10 atm (d) 15 atm. The dashed line represents temperature profile in K. 72

Figure 5.6 H_2SO_4 concentration across the PFR at (a) 1 atm (b) 5 atm (c) 10 atm (d) 15 atm. The dashed line represents the temperature in K 73

Figure 5.7 NO_2 concentration in the PFR at different pressures..... 75

Figure 5.8 (a) SO_3 concentration and (b) H_2SO_4 concentration in the PFR at different pressures..... 76

Figure 6.1 NO_x removal and NO_x concentration in the flue gas at different recycle ratio 82

Figure 6.2 Temperature profiles of gas and liquid in the absorber at different recycle ratio 83

List of Tables

Table 2-1 Reactions involved in the removal of SO_x and NO_x 21

Table 3-1 Design specifications of the reactive absorber column 44

Table 3-2 Gas and liquid reaction implemented in the reactive absorber column 45

Table 4-1 Proximate and ultimate analysis of the Lusatian lignite coal 48

Table 4-2 Operating conditions of the oxy-fuel combustion at 1 atm 51

Table 4-3 Boundary conditions at the walls 52

Table 4-4 Inlet conditions at atmospheric and elevated pressures 55

Table 4-5 Composition of the flue gas exiting the furnace 60

Table 5-1 Flue gas composition (molar basis) at the PFR inlet at different pressures 67

Table 5-2 Inlet and Outlet concentrations of SO_x, NO_x and H_2SO_4. 74

Table 5-3 Dimensions used for the PFR model at different pressures 75

Table 5-4 Inlet/Outlet concentrations of SO_x, NO_x and H_2SO_4. 77

Table 6-1 Composition (molar basis) of the inlet and outlet products in the absorber column 80

Table A-1 Reduced mechanism for sulphur reaction in ANSYS Fluent 102

Table C-1 Temperature dependent Henry's Law constants used in ASPEN Plus 136

Nomenclature

Abbreviations

1D	One Dimensional
2D	Two Dimensional
ADP	Acid Dew Point
AR	As Received
ASU	Air Separation Unit
CCS	Carbon Capture And Sequestration
CFD	Computational Fluid Dynamics
CO2CPU	CO_2 Compression And Purification Unit
DAF	Dry, Ash Free
DCC	Direct Condenser Column
DO	Discrete Ordinates
DRW	Discrete Random Walk
EDC	Eddy Dissipation Concept
EDM	Eddy Dissipation Model
EFR	Entrained Flow Reactor
EOR	Enhanced Oil Recovery
FGD	Flue Gas Desulphurizer
GHG	Greenhouse Gases
HHV	High Heating Value
HRSG	Heat Recovery Steam Generator

IEA	International Energy Agency
IGCC	Integrated Gasification Combined Cycle
IPCC	Intergovernmental Panel On Climate Change
LES	Large Eddy Simulation
NOx	Oxides Of Nitrogen
PFR	Plug Flow Reactor
ppb	Parts Per Billion
ppm	Parts Per Million
RANS	Reynolds-Averaged Navier-Stokes
RNG	Dynamic Renormalization Group
RTE	Radiative Transfer Equation
SCR	Selective Catalytic Reduction
SCU	Sour Compression Unit
SOx	Oxides Of Sulphur
SPOC	Staged Pressurized Oxy-Fuel Combustion
SST	Shear-Stress Transport
WSGGM	Weighted Sum Of Grey Gases Model

Symbols

A	Pre-exponential factor
A_c	Pre-exponential factor of char combustion
A_v	Pre-exponential factor of volatilization
a	Absorption coefficient
b	Temperature exponent
C_i	Mass diffusion limited constant
D_0	Diffusion rate of oxygen to the particle's external surface
d_p	Particle diameter
E	Activation energy
E_c	Activation energy of char combustion
E_v	Activation energy for volatilization
F	Drag force
f_v	Mass fraction of the volatiles
f_w	Mass fraction of the moisture
g	Gravity
H	Henry's solubility
H^o	Henry's solubility at T^o
I	Spectral radiation intensity
J	Diffusion flux
K_v	Rate constant for volatilization
K_c	Char kinetic rate

k	Turbulent kinetic energy
k_{cond}	Thermal conductivity
k_f	Rate constants of the forward reactions
k_r	Rate constants of the reverse reactions
m_p	Mass of the particle
n	Refractive index
P	Pressure
$\dot{Q}_{rad}$	Radiation
R	Gas Constant
R_r	Rate of reaction
s	Path length
T	Local temperature
T_∞	Gas temperature in the cell
T^υ	Standard temperature
t	Time
u_i	Direction vector in i-direction
v_i	Stoichiometric coefficients
$v'_{i,r}$	Stoichiometric coefficient of reactants
$v''_{j,r}$	Stoichiometric coefficient of products
Y	Mass fraction
$\Delta_{sol}h$	Molar enthalpy of dissolution
δij	Kronecker delta

ρ	Density
σ_s	Scattering coefficient
τ_{ij}	Stress tensor
λ	Stoichiometric ratio
ε	Turbulent dissipation rate
Φ	Phase function
Ω'	Solid angle
$\dot{\omega}$	Molar rate of production

1 Introduction

The annual world-wide demand for energy is constantly rising. This increased demand is caused by the increase in population, and by economic development in many emerging economies [1]. In 2017, global power generation increased by 2.8%, where 94% of the increase was contributed by the emerging economies [1]. The global demand for electricity will increase by 28% by 2030, especially in China and India, due to their expanding economies and growing populations [2].

At the same time as global demand for electricity is increasing, calls to reduce greenhouse gases (GHG) and pollutant emissions, to counteract global warming, are intensifying. According to the Intergovernmental Panel on Climate Change (IPCC), the world temperature is expected to rise between 2 and 4°C by 2050, due to global warming caused by anthropogenic emissions of GHG [3].

Coal has been and will continue to be one of the largest contributor to energy resources because of its availability and competitively low prices, especially in developing countries. Despite the huge policy efforts to encourage cleaner fuels and renewables to reduce GHG, it still continues to be the dominant fuel in the power sector, contributing nearly 39% of total electricity generation and 44% of total CO_2 emissions globally [2]. Apart from CO_2, coal-fired power plants also emit other pollutants such as nitrogen oxides (NO_x), sulphur oxides (SO_x) and other trace metals.

In the long term, the conversion from coal to cleaner fuels, is unavoidable. Nevertheless, it is also unrealistic to meet the growing electricity demand without the use of coal, at least up to

year 2050. Therefore, CO_2 emissions reduction in the interim is required for the existing and newly installed power plants.

The continued use of fossil fuels, without CO_2 reduction, will result in an increase in CO_2 emissions from the current level of about 33 Gt- CO_2/year to over 60 Gt- CO_2/year by 2030 [4]. Therefore, in order to achieve significant reductions, CO_2 abatement strategies have to be implemented. Carbon capture and sequestration (CCS) from coal-fired power plants provide an opportunity to continue using coal resources. Once CO_2 is captured from the power plants it is often injected into geological formations, such as depleted oil and gas field, saline aquifers and for enhanced oil recovery (EOR) [5]. According to a report by the International Energy Agency (IEA), power plants with CCS will account for 6% of the energy generation by 2035 and 10% by 2040 [6].

1.1 Carbon capture technologies for coal fired power plants

Several carbon capture technologies have been proposed for reducing CO_2 emissions from coal-fired power plants, such as pre-combustion capture, post combustion capture combustion and oxy-fuel combustion and capture as shown in Figure 1.1 [7].

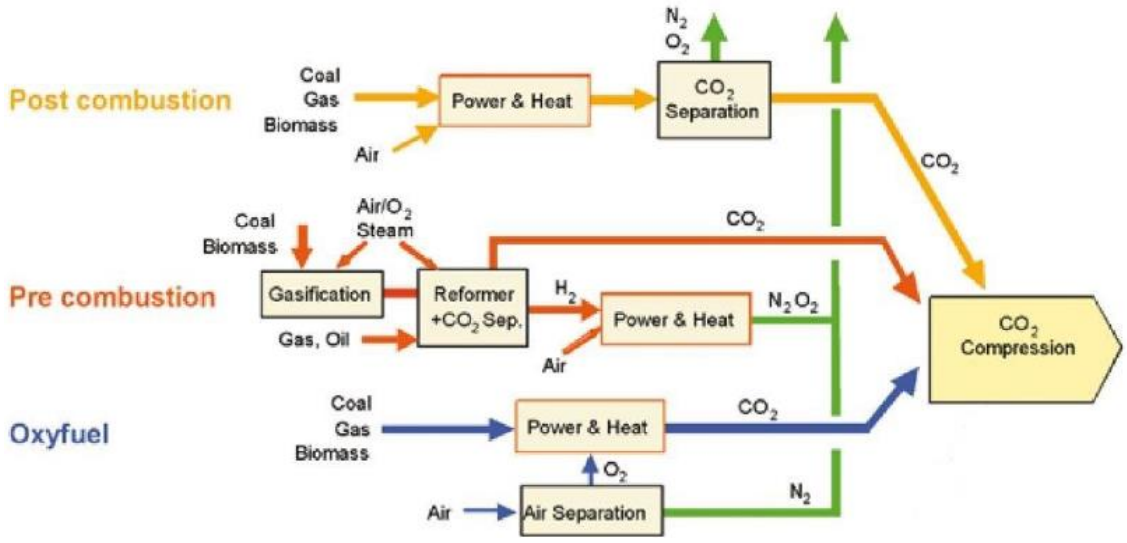

Figure 1.1 Overview of carbon capture technologies [5]

Pre-combustion capture technology uses a high pressure gasifier to convert coal into syngas, which is composed of CO and H_2. CO_2 can be separated and removed in a water-gas shift reactor, leaving pure H_2 to be used as fuel. An integrated gasification combined cycle (IGCC) for coal is an example of pre-combustion capture system. However, high electricity cost and plant complexity have limited this technology's demand in the power industry [8].

In post combustion capture technology, CO_2 is separated from flue gas without changing the combustion process. Several technologies have been investigated to remove CO_2, including absorption, adsorption, and membrane separation. The most economical and mature capture

process is currently absorption which utilizes mainly amine solvents to capture CO_2 from the flue gas. A major drawback is the high operating costs incurred by the high energy demand to regenerate the solvent.

Oxy-fuel combustion is a promising technology for CCS, as mixture of pure oxygen (O_2) and CO_2 is used as an oxidant for combustion instead of air. Due to the absence of nitrogen (N_2) in the oxidizer stream, the combustion products are predominantly CO_2 and H_2O, and the CO_2 can be separated easily by removing H_2O via condensation. The flue gas produced from combustion is further processed to remove pollutants such as NO_x, SO_x and excess O_2 to meet the purity requirements for CO_2 transport in pipelines for utilization or sequestration. However, the major challenge for oxy-fuel combustion is the high energy costs associated with oxygen production in the air separation unit (ASU).

1.2 Oxy-fuel combustion technology

Oxy-fuel combustion was first proposed almost three decades ago for CO_2 reduction and enhanced oil recovery (EOR) [9], [10]. With the increasing concerns about the effect of CO_2 emissions on global warming, oxy-fuel combustion has gained attention as a useful process to capture the anthropological CO_2 from power plants to reduce GHG from the environment [11].

The concept of oxy-fuel combustion is to burn fuel in O_2, instead of air thereby producing a flue gas that is primarily CO_2 and H_2O and with small amount ofN_2. In the presence of pure O_2, the temperature in the boiler may rise up to 3000°C, therefore a fraction of the flue gas is recycled back to act as a diluent. The recycled flue gas is used not only to control combustion temperature but also to make up the volume of the missing N_2 to ensure there is enough gas for heat transfer through the boiler [7], [12].Typically, around 30% O_2 is required in the oxidant to maintain the flame temperature similar to that in a conventional boiler [13]. The resulting flue gas mainly consists of CO_2 and H_2O along with some impurities, such as oxides (SO_x), nitrogen oxides (NO_x) and unreacted O_2. This process eliminates the need for a complex and expensive post combustion process to capture CO_2 from a N_2-rich flue gas as in a conventional boiler. This stream is condensed to remove the moisture and impurities before it can be compressed and transported for storage and sequestration. Most of the oxy-fuel combustion plants have been designed at atmospheric pressure (1 atm) for the proof of concept. Figure 1.2 shows a typical oxy-fuel combustion power plant at atmospheric pressure.

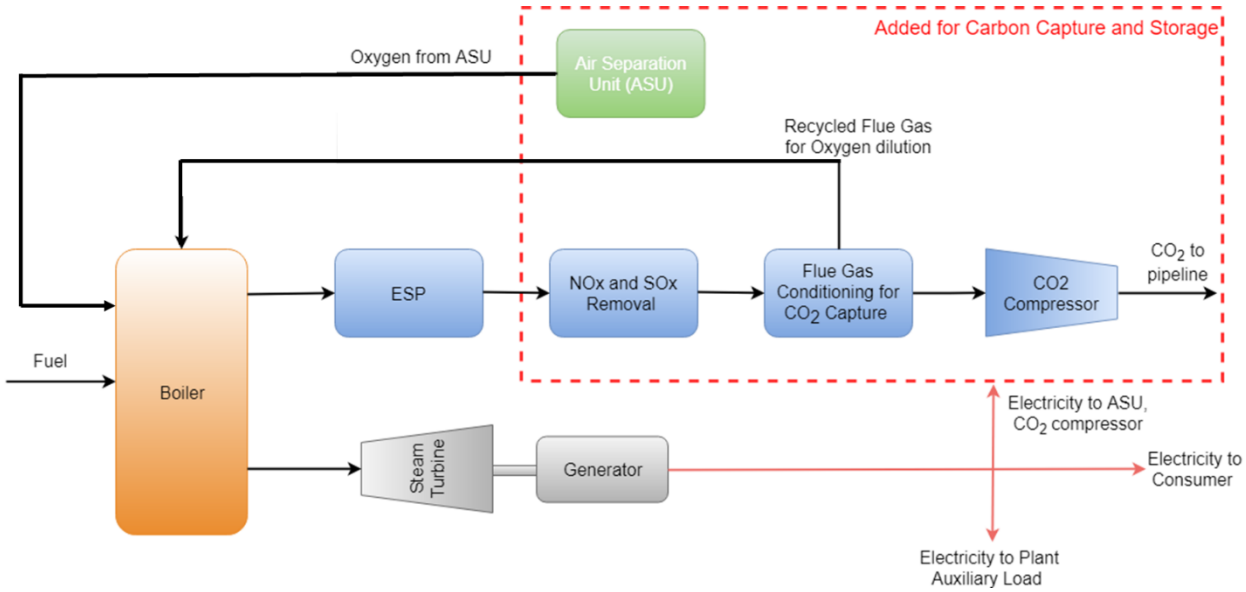

Figure 1.2 Oxy-fuel combustion power plant with CO_2 capture

The design of an oxy-fuel combustion power plant is very similar to a conventional power plant; therefore, it can be retrofitted to an existing power plants. There are two additional processes, air separation unit (ASU), and CO_2 compression and purification unit (CO_2CPU). An ASU is usually a cryogenic distillation unit used to separate O_2 from nitrogen (N_2). The flue gas exiting the boiler is processed in the CO_2CPU, where flue gas is compressed and CO_2 is removed.

Pressurized oxy-fuel combustion systems have been proposed recently, and several studies have been conducted on the technical and economic feasibility of the process [8], [14]–[18]. In pressurized oxy-fuel combustion, the combustion of fuel takes place at elevated pressure in oxy-fuel environment. They are in agreement that the overall process efficiency and thermal recovery improves with increasing operating pressure, mainly due to the latent heat recovery from the flue gases at higher temperatures. A potential advantage of using this technology is the utilization of cheap low grade coal, with high moisture content [19]. Thus, pressurized oxy-fuel combustion is expected to increase the efficiency of carbon capture.

The primary benefits of pressurized oxy-fuel combustion include:

i. The utilization of the latent heat of condensation, as the moisture in the flue gas condenses at higher temperature.
ii. Reduction in the size and cost of equipment, since the gas volume is greatly reduced at higher pressures.
iii. Increase in the convective heat transfer in the boiler, as the increase in the flue gas density produces an increased Reynolds number [20].

However, a major concern in adopting oxy-fuel combustion (atmospheric or pressurized) is the increased SO_x concentration in the flue gas [21]. Sulphur present in the coal is released as sulphur dioxide (SO_2) during devolatilization and char oxidation process. SO_2 concentration from oxy-fuel combustion is higher than that from air combustion due to flue gas recirculation [22]. Moreover, high pressures enhance the production of acid gases, including sulphur trioxide (SO_3) and nitrogen dioxide (NO_2) [23],which could significantly increase the risk of corrosion at lower temperatures in the CO_2CPU. It has been suggested in the literature that SO_x and NO_x interaction becomes important at higher pressures and the presence of NO favours the production of SO_3 [24].

1.3 Research objectives and contribution

Most of the research published on pressurized oxy-fuel combustion has focused on the feasibility, design and thermal performance of pressurized oxy-fuel combustion [19], [25], [26].To the best of author's knowledge, none of the published research explores the formation of SO_x and NO_x in the pressurized oxy-fuel combustion environment.

The main objective of this thesis is to model coal combustion in oxy-fuel environment and investigate the effect of pressure on the formation and removal of SO_x and NO_x in the flue gas. Lignite coal has been used as a feedstock, due to its high sulphur content.

To fulfil the objective, the thesis is divided into three sections:

1. Model oxy-fuel combustion of coal at high pressures using ANSYS Fluent CPD software. The numerical simulation of combustion has been conducted at different pressures and the sub-model for the production of SO_x and NO_x has been integrated to investigate the effect of pressure on the evolution of SO_x and NO_x during combustion.
2. Model a plug flow reactor in CHEMKIN-PRO and investigate the effect of pressure and temperature on the flue gas reactions in oxy-fuel environment, based on the reaction mechanism of Geminez-Lopez et al. [27]. The mechanism is modified by Chaoudhury et al. [28] and reaction for SO_x – NO_x interaction are incorporated to understand the effect of pressure and temperature on the formation of SO_3.
3. Model a reactive absorber column in ASPEN Plus to purify the flue gas and remove the SO_x and NO_x at high pressures. Reactions involved in the gas phase and liquid phase are added to the model, based on the work of Meunier et al. [29]

1.4 Thesis Outline

The thesis is divided into the following seven chapters:

Chapter 1 discusses the impact of CO_2 emissions from power plants on global warming, and the carbon capture technologies to reduce CO_2 emission, particularly oxy-fuel combustion. The chapter also introduces the objective of this thesis.

Chapter 2 provides a literature review on CFD modelling of oxy-fuel combustion at atmospheric and elevated pressures. This chapter also includes the formation of SO_x and NO_x in oxy-fuel combustion. Lastly, the methods for SO_x and NO_x removal from flue gas are discussed.

Chapter 3 discusses the modelling techniques and the methodology required for coal combustion, flue gas reactions and flue gas purification. The models used in the CFD for coal combustion and the kinetic mechanism for flue gas reactions utilized in the CHEMKIN-PRO model are explained. The design and specifications of the absorber to remove SO_x and NO_x are also included.

Chapter 4 presents CFD simulation of coal combustion in oxy-fuel environment. Validation results of the 100 kW oxy-fuel combustor model at atmospheric pressure are presented in this chapter. Most importantly, the results of oxy-fuel coal combustion at different pressures are discussed, including the temperature and species concentrations during combustion.

Chapter 5 discusses the effect of pressure and temperature on the flue gas reactions, and the important reactions are identified.

Chapter 6 provides details of the operating conditions in a reactive absorber column. It also details the technical evaluation of SO_x and NO_x removal in the liquid phase at 15 atm.

Chapter 7 presents the conclusions learned from this research along with the recommendations for future research.

2 Literature review

2.1 Oxy-fuel combustion technology development

Oxy-fuel combustion has been used in industrial furnaces in the glass, steel and cement industries for decades to obtain extremely high temperatures and radiating flames. Research in carbon dioxide capture involving oxy-fuel combustion started almost three decades ago, originally intended to utilize CO_2 from power plants for enhanced oil recovery [9]. However, with the increasing concerns of global warming and CO_2 emissions, the possibility of using oxy-fuel combustion for power plants with CO_2 capture has gained attention among researchers and is being widely explored.

Lab scale research was initially conducted to investigate the characteristics of oxy-fuel combustion under different operating conditions. These characteristics included coal ignition behaviour [30], heat transfer [31],[32], flame stability [33], and species concentration [34] in oxy-fuel environment. Comprehensive description of these characteristics in oxy-fuel combustion have been reviewed by Toftegaard et al. [12], Chen et al. [35], and Wall et al. [36]. To overcome the difficulties in applying oxy-fuel combustion at large scale, several pilot scale as well as demonstration oxy-fuel combustion facilities have been constructed around the world, such as the Vattenfall Schwarze Pumpe project in Germany and the Callide oxy-fuel project in Australia [37]. Figure 2.1 shows the timeline of the pilot scale projects for oxy-fuel combustion around the world.

Pressurized oxy-fuel combustion is still in its infancy. The Enel Group had built a small pilot scale plant for 4 MW pressurized oxy-fuel combustion, based on Isotherm Pwr® process, a patented technology developed by ITEA, a company based in Italy. The experimental results showed an increased heat transfer rate in the heat recovery steam generator (HRSG) compared to

atmospheric oxy-fuel combustion [8]. However, there have been numerous modelling-based studies on the feasibility and performance of pressurized oxy-fuel combustion of coal, with results proving that pressurized oxy-fuel combustion can effectively increase the performance of the coal power plant.

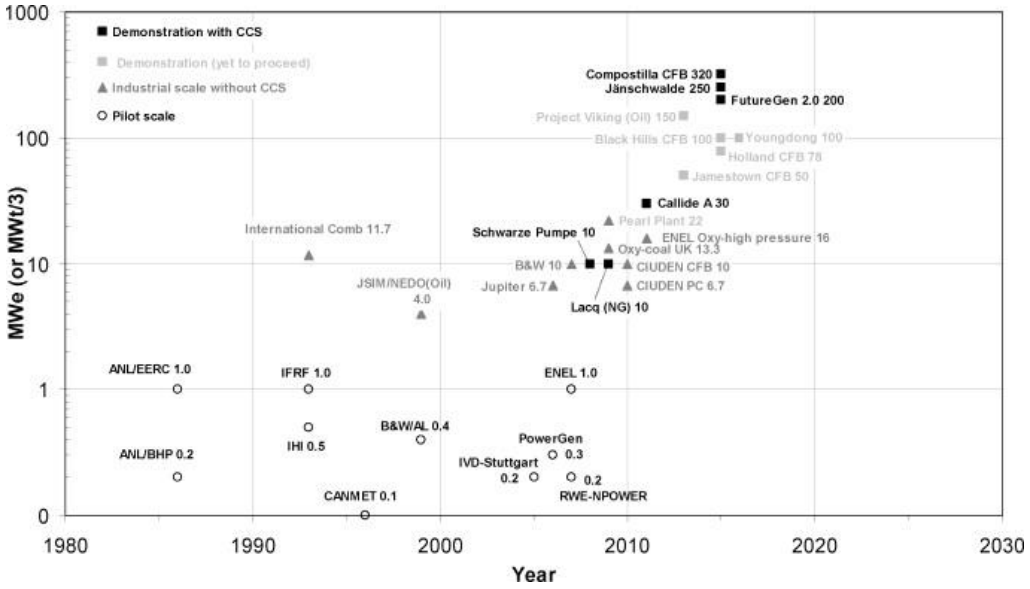

Figure 2.1 Timeline of pilot scale oxy-fuel combustion projects[37]

2.2 CFD studies in oxy-fuel combustion

An alternative to experimental measurements, is to perform computational simulations of oxy-fuel combustion, to gain greater insight of the physical and chemical processes. Computational fluid dynamics (CFD) modelling can comprehensively provide a wide range of information for the burner, that can reduce the cost and time spent on experimental investigation.

CFD codes are based on the numerical approximation of Navier-Stokes equations that describe fluid motion. The CFD model can predict the flame structure, gas temperature distribution, heat transfer and chemical species concentrations at a given operating condition.

2.2.1 CFD studies in atmospheric oxy-fuel combustion

Comprehensive details of oxy-combustion of mathematical modelling in CFD has been reviewed by Chen et al. [35], Yan et al. [38] and Edge et al. [39], providing in-depth details on the models for turbulence, radiative properties of gas mixtures, coal devolatilization, char combustion and pollutant formation at atmospheric pressure

Chen et al. [40] performed simulation of oxy-fuel combustion of lignite coal using different turbulence models, such as standard k-ε model, the RNG k-ε model, the SST k-ω model, and the LES model. The turbulence models showed different performance, especially the prediction of coal combustion and temperature distribution. When compared to the experimental results, SST k-ω model captured the flow structure and improved the O_2 diffusion prediction. However, LES showed more accurate results for flame length and temperature, but at a higher computational cost.

Toporov et al. [41] modelled a CFD application based on experiments done in a 100 kW pilot-scale furnace at the Institute of Heat and Mass transfer (RWTH) in Germany. Adapted models for homogeneous and heterogeneous reactions sub-models were used to design a burner that enhanced the flame stabilization using O_2/CO_2 content similar to that of air. The simulation results showed a good match with experimental results for the gas velocities, temperature distribution and gas composition.

Abbas et al. [42] investigated the effect of O_2 concentration in oxy-fuel combustion environment for lignite coal. The predicted results showed a reasonably good agreement against the measured data for 21% to 29% O_2 concentration in the oxidizer. Different chemical reaction mechanisms for both homogeneous and heterogeneous combustion were also investigated; a 3-step-reaction proved

to be more accurate as it captured the CO/CO_2 production rate and the equilibrium between H_2 and H_2O, especially in the flame zone, in terms of temperature profile and species concentrations.

2.2.2 CFD studies in pressurized oxy-fuel combustion

Since, it is still a novel idea, there is limited literature on the numerical modelling of pressurized oxy-fuel combustion using CFD. Chen et al. [43] simulated the combustor design of Isotherm Pwr® process and studied the effect of pressure on oxy-coal combustion, such as flow patterns, coal conversion, heat transfer and slag behaviour at 4 bar, 20 bar and 40 bar with progressively increasing burner velocities. Similar flow fields were maintained, resulting in similar gas temperature and coal conversion. The author concluded that it is possible to operate the reactor at a higher thermal load at elevated pressures, by taking advantage of char conversion kinetics [44].

Gopan et al. [45] introduced Staged Pressurized Oxy-fuel Combustion (SPOC) as an alternative to increase plant efficiency by staging fuel in multiple boilers to control heat flux and gas temperature. Xia et al. [46] used CFD simulation to access the boiler performance for SPOC, and the simulation results showed a relatively uniform heat flux distribution on the walls on all the boilers. However, these results are not expected in a traditional pressurized boiler, which typically employs high mixing rates that result in complex flow fields.

2.3 Pollutant emissions

2.3.1 NO_x formation

Due to the concerns regarding NO_x formation in air-fired power plants, significant research including experimental investigation and numerical modelling have been done. Experimental

studies have shown that the mechanism for NO_x formation and destruction during oxy-fuel combustion are similar to air combustion [47]. Therefore, available models, such as extended Zeldovich mechanism [48] and de Soete's fuel NO mechanism [49] are adopted for oxy-fuel combustion conditions.

Generally, NO_x emissions from coal combustion are generated from three sources:

- Thermal NO_x,
- Prompt NO_x,
- Fuel NO_x.

Thermal NO is dominating the high temperature combustion (above 1500°C), where N_2 and O_2 react, due to the presence of radicals. The thermal NO mechanism consists of three reactions, known as the extended Zeldovich mechanism.

$$O + N_2 \rightleftharpoons NO + N \quad (2\text{-}1)$$

$$N + O_2 \rightleftharpoons NO + O \quad (2\text{-}2)$$

$$N + OH \rightleftharpoons NO + H \quad (2\text{-}3)$$

Prompt NO is produced due to the nitrogen reaction with hydrocarbon radicals such as CH, C_2H, and CH_2 in the fuel rich zones, which subsequently form NO when oxidized.

Fuel NO is produced when O_2 is reacted with the nitrogen bounded (mainly HCN, NH_3) in the volatile and as well as char phase of the coal. The volatile nitrogen reacts to form either NO or N_2, while nitrogen in the char reacts heterogeneously along with char oxidation. The division between the nitrogen in volatile and char are dependent upon the type of the coal, its nitrogen

content and its volatility. Figure 2.2 shows the pathways for the NO_x formation and destruction in oxy-fuel combustion.

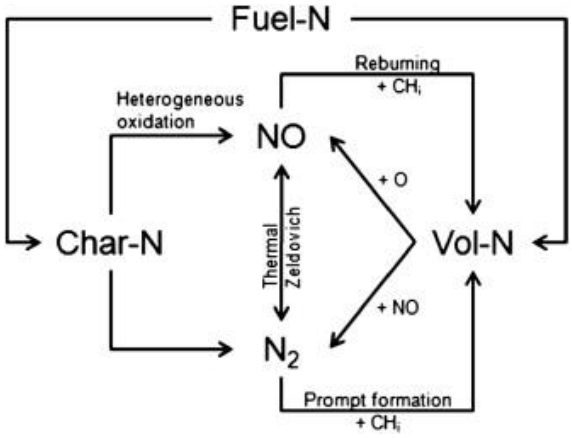

Figure 2.2 The overall NO formation and reduction mechanism [12]

It has been shown that for oxy-fuel combustion NO_x in the flue gas decreases by 30% as compared to air-fired combustion [22], [50]. The reduction is primarily due to the absence of N_2 in the oxidizer gas, thus minimizing the formation of thermal NO and also due to the recirculation process of the combustion flue gas.

Numerical modelling of NO formation and destruction was performed by Cao et al. [51] for oxy-fuel combustion conditions. Hydrogen cyanide (HCN) was assumed to be released in the volatile which yields NO and NH_3 by reacting with O_2 and H_2O in the environment. The predicted results showed a good agreement with measured data

Abbas et al. [42] compared NO_x emissions in air-fired combustion and oxy-fuel combustion. Significant decrease in NO_x emission was predicted in oxy-fuel combustion, principally due to the absence of thermal NO formation, and only nitrogen bound compounds of the coal were contributing to the fuel-NO.

Alvarez et al. [52] performed simulation of a entrained flow reactor (EFR) to model the devolatilization and release of NO_x precursors in the coal (NH_3/HCN). The predicted NO emissions showed the importance of accurate determination of fuel-N_2 distribution between char and volatile when modelling NO formation.

An important aspect concerning pressurized combustion is the production of NO_2. Tsukahara et al. [53] suggested that the NO oxidation to NO_2 is favourable at higher pressures and lower temperatures. This is a well-known reaction, describing NO_2 formation in the industrial production of nitric acid (HNO_3) at pressures around 10 bar [54]. NO_2 formation is possible in the flue gas where the temperatures are decreasing and require long residence time before NO_x can be removed.

2.3.2 SO_x formation

Sulphur emissions is of great importance due to the use of low-grade coal in pressurized oxy-fuel combustion. Sulphur content in coal may vary from 0.2 to 11% depending on the rank of the coal. Desulfurization is required for high sulphur coal, but generally the coal used for combustion is less than 4 wt.% sulphur content.

Sulphur in coal is bounded mostly as sulphides and organic sulphur compounds and traces amounts of sulphates and elemental sulphur [55]. During volatilization, most of the organic sulphur and sulphides are released in the gas phase, and sulphates are released during the char combustion. The sulphur compounds react with O_2 at high temperatures (>1273 K) to form SO_2. However, a portion of sulphur remains unburnt in the ash.

Due to the absence of N_2 in the environment as a diluent, the concentrations of SO_x is significantly higher [56]. According to Croiset et al. [34], the relatively difference in SO_2 emissions in different combustion medium and oxygen concentrations is negligible, therefore the specific SO_2 emissions are almost exclusively dependent on the sulphur content of the coal.

It has been observed that the only prominent sulphur species formed is SO_2, under typical flame and O_2 rich conditions [57]. However, at lower temperatures below 800 K, the equilibrium shifts towards SO_3, and the SO_3/ SO_x conversion ratio for coal combustion is usually <4% under atmospheric pressure [58] through reactions (2-4) to (2-6).

$$SO_2 + O + M \rightleftharpoons SO_3 + M \quad (2\text{-}4)$$

$$SO_2 + OH + M \rightleftharpoons HOSO_2 + M \quad (2\text{-}5)$$

$$SO_2 + OH + M \rightleftharpoons SO_3 + HO_2 \quad (2\text{-}6)$$

SO_3 is formed at temperatures above 1500 K through reaction (2-4). At temperatures below 1150 K, reaction (2-5) and (2-6) are active and these are termed as secondary formation pathways [59]. Since the SO_3 formation increases with temperature decrease, the cooling rate of the flue gas governs SO_3 formation. Furthermore, the formation of SO_3 is heavily dependent upon the concentration of SO_2 and O_2. The generated SO_3 can convert to sulphuric acid (H_2SO_4) below 700K through reaction (2-7) and, around 450K, almost all the SO_3 is likely to be in the form of H_2SO_4.

$$SO_3 + H_2O \rightleftharpoons H_2SO_4 \quad (2\text{-}7)$$

There are only few studies of the numerical modelling of SO_x using in oxy-fuel combustion, as compared to air-fired combustion. Muller et al. [60] predicted the fate of sulphur

in coal under oxy-fuel combustion. Organic sulphur compounds were assumed to be released as H_2S during pyrolysis, and a simplified global reaction was used to describe the oxidation of H_2S in the homogeneous gas phase. SO_x release from inorganic sulphur, bounded to the char was calculated via char oxidation model. The results showed a deviation between the simulation and the experimental results, as the model failed to predict the SO_x concentration close to the burner as well as SO_2 reduction in the O_2-depleted zones in the combustor. The author recommended to use a multi-step scheme for SO_x model to improve the model's accuracy.

2.3.3 Interactions between SO_x and NO_x

In the flue gas resulting from combustion, NO and SO_2 are the dominant NO_x and SO_x species. The rate of oxidation of NO to NO_2 is thermodynamically favoured by lower temperatures and elevated pressures, similar to that of pressurized oxy-fuel combustion flue gas. It has been suggested that a homogeneous reaction of SO_2 and NO_2 occurs under conditions relevant for pressurized flue gases from oxy-fuel combustion [61]–[63].

During the compression of flue gas, formation of H_2SO_4 and HNO_3 has been observed in the condenser water in a number of experiments [64]. White et al. [23] observed that an increase in NO_x enhances the removal of SO_2 from the gas phase. The reaction path for the homogenous gas phase oxidation of SO_2 and NO_2, also known as lead-chamber reaction is described by reaction (2-8). The SO_3 will be absorbed in water and react to produce H_2SO_4.

$$SO_2 + NO_2 \rightarrow SO_3 + NO \qquad (2\text{-}8)$$

Armitage and Cullis [61] studies the reaction in a batch reactor at high temperatures and sub-atmospheric pressures and proposed a rate expression. Wendt et al. [62] suggested that SO_3

formation, as a result from such reaction, is significant when NO concentrations are above 1000 ppmv.

Mueller et al. [63] studied the SO_x and NO_x interaction in a plug flow reactor at 950 K and elevated pressures up to 10 atm. It was suggested that at lower pressures, SO_3 formation occurs primarily through reaction (2-4), but at higher pressures where the fractional conversion of NO to NO_2 increases, SO_3 formation via reaction (2-8) becomes more important.

Integrated SO_x / NO_x removal through condensation is another motivation to study the SO_2 and NO_2 interaction as this will eliminate the need for a selective catalytic reduction (SCR) and flue gas desulphurizer (FGD) from the pressurized oxy-fuel combustion power plant.

2.4 Removal of SO_x and NO_x from flue gas

NO_x and SO_x can be removed from the flue gas using conventional processes like SCR and FGD. However, they may not be viable solution for pressurized flue gas, as they would add a significant capital cost and energy penalty in order to keep the system under pressure [65].

An alternative method to remove SO_x and NO_x for CO_2 purification is the flue gas condenser. Flue gas condensers are a common feature in oxy-fuel power plants to remove moisture from the flue gas. The column has a dual role. It is primarily used to remove moisture from the flue gas, which can be removed from the bottom stage. The second purpose is to remove SO_x and NO_x, via conversion to H_2SO_4 and HNO_3. It was reported by Zanganeh et al. [64] that at high pressure and low temperatures, NO_x and SO_x can be recovered from the condenser via lead chamber reaction. The proposed mechanism for SO_x and NO_x removal are shown in Table 2-1.

Table 2-1 Reactions involved in the removal of SO_x and NO_x

Reaction	Phase
$2\,NO + O_2 \rightleftharpoons NO_2$	Gas
$NO_2 + SO_2 \rightleftharpoons SO_3 + NO$	Gas
$2\,NO_2 \rightleftharpoons N_2O_4$	Gas
$N_2O_4 + H_2O \rightleftharpoons HNO_2 + HNO_3$	Liquid
$3\,HNO_2 \rightleftharpoons HNO_3 + 2\,NO + H_2O$	Liquid
$SO_3 + H_2O \rightleftharpoons H_2SO_4$	Liquid

White et al. [66] proposed a process to remove SO_x and NO_x as HNO_3 and H_2SO_4 using an intermediate and a high pressure reactive absorber columns at low temperature, as shown in Figure 2.3. The first column is maintained at 15 bar and removed the majority of the SO_x, while the second column removes NO_x at 30 bar. The simulated results showed all of the SO_x and 90% of the NO_x can be removed from the flue gas.

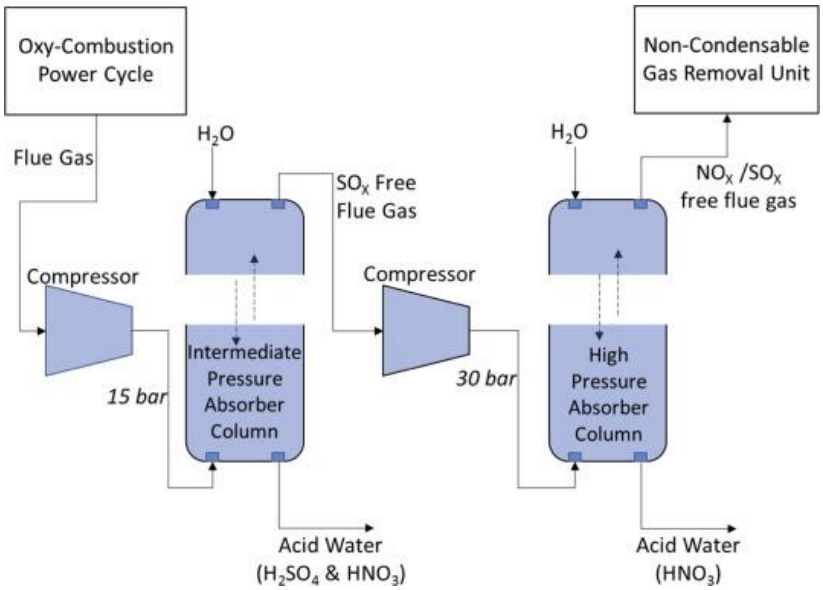

Figure 2.3 Schematic for 2 column absorbers for NO_x and SO_x removal [65]

A single absorber column was suggested by Iloeje et al. [65] to remove SO_x and NO_x (Figure 2.4). The predicted results showed that the process is strongly dependent on pressure. Vapour holdup volume in the absorber and feed water flowrate have a significant impact on NO_x / SO_x removal.

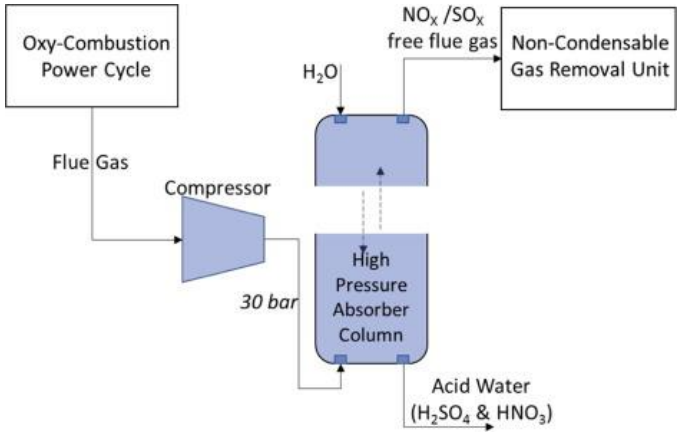

Figure 2.4 Single column absorber proposed by Iloeje et al. [65]

More recently, Ajdari et al. [67] observed that SO_x and NO_x abatement through the sulphur – nitrogen interaction to produce H_2SO_4 takes place once SO_2 and NO_2 have been dissolved in the liquid. It was observed that the oxidation of NO to NO_2 is the rate limiting reaction in the gas phase while different liquid phase reactions are dependent on the pH.

Gopan et al. [45] simulated the single direct condenser column (DCC), with the lead chamber reactions for pressurized oxy-fuel combustion system It was observed that the flue gas entering the condenser is at a higher temperature, in order to avoid the acid dew point temperature and risk of corrosion.

3 Mathematical modelling and methodology

3.1 Introduction

This chapter discusses the modelling techniques and methodologies utilized in this study, to determine the physical and chemical characteristics of coal combustion at elevated pressures, the subsequent reactions in the flue gas, and the reactions involved in the removal of pollutants (SO_x, NO_x) for further purification prior to entering the CO_2CPU. A schematic of the methodology used in this study is presented in Figure 3.1, highlighting the three components being simulated here, that is (i) combustion chamber, (ii) flue gas reactions after the flame and during transport through pipes, and (iii) flue gas reactive absorber to remove NO_x and SO_x. This figure also indicates the software used for each component.

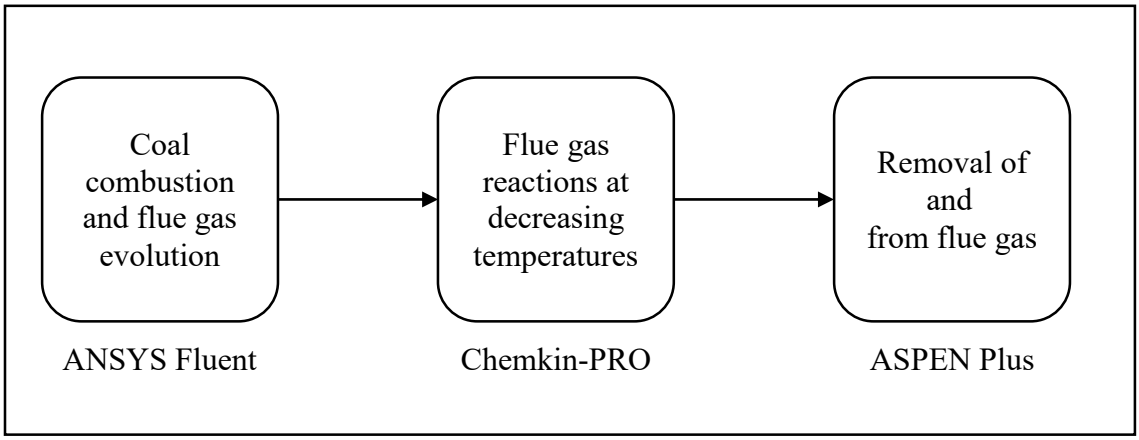

Figure 3.1 Schematic representing the methodology and the simulation software used

In order to determine accurately physical and chemical characteristics of coal combustion and pollutant formation in oxy-fuel conditions, a two-dimensional (2D) model axisymmetric was developed using combustion computational fluid dynamic (CFD) software, ANSYS Fluent 18.0 [68] . This method is preferred for coal combustion to include turbulence in the flow which can

alter the flame structure, as reactions are highly sensitive to the flame temperature during combustion.

Next, the effect of pressure on flue gas at lower temperatures is determined via a plug flow reactor modelled in Chemkin-PRO [69] as it allows to simulate reaction kinetics in the gas phase. A reaction mechanism for oxy-fuel combustion is modelled to determine the effect of pressure and temperature change, that occur in a typical coal combustion boiler in the post-combustion zone.

To remove SO_x and NO_x from the flue gas, a reactive absorber is modelled using ASPEN Plus V8.8 [70] process simulator. The reactions simulated in the absorber include both equilibria as well as kinetic reactions in the gas and liquid phases.

3.2 CFD modelling for coal combustion

The numerical simulation of coal combustion is a complex process as compared to the combustion of other fossil fuels because it includes several complicated physical and chemical processes, which have not been completely understood. Coal combustion is modelled as a two-phase (solid and gas) reacting flow using a Eulerian-Lagrangian approach for continuous and discrete phases, respectively, using ANSYS Fluent. The mass, momentum and energy interaction between the gas phase and the solid particles are calculated using the "particle-source-in-cell" method [71], which updates the particle state and its trajectories.

Appropriate sub-models were coupled with the CFD to account for the chemical reactions (devolatilization, char burnout, SO_x, and NO_x formation, etc.) and heat transfer, which will be discussed in this chapter.

3.2.1 Governing equations

Conservation of Mass

The mass conservation or continuity equation can be written in differential form is given by Equation

$$\frac{\partial \rho}{\partial t} + \frac{\partial \rho u_i}{\partial x_i} = \dot{S}_{mass} \tag{3-1}$$

where the first term represent the change of density ρ in time t, and the second term represent the convective transport of mass with velocity u_i in the x_i direction. A mass source term $\dot{S}_{mass}$ accounts for the interchange of mass between the solid and the gas phase during coal combustion, due to the release of volatiles from coal particles to the gaseous phase.

Conservation of Species

The change in chemical composition of the gaseous mixture can be described by:

$$\frac{\partial \rho Y_\alpha}{\partial t} + \frac{\partial \rho u_i Y_\alpha}{\partial x_i} = -\frac{\partial J_{\alpha,i}}{\partial x_i} + \dot{R}_\alpha + \dot{S}_{Y,\alpha} \tag{3-2}$$

where Y_α is the mass fraction of species α. The diffusion flux $J_{\alpha,i}$ combines the effect of mass diffusion due to concentration gradients, temperature gradients and pressure gradients. The chemical source term $\dot{R}_\alpha$ represents the net rate of production or destruction of species α due to chemical reaction. Finally, the source term $\dot{S}_{Y,\alpha}$ has been added to account for the addition of mass to the gas phase from the solid phase.

Conservation of Momentum

Similar to mass, momentum is a conserved quantity. Newton's second law of motion relates the change of momentum of an object to the external forces acting upon it. Therefore, the

change in the momentum ρu_i of a fluid can be related to the forces on the fluid due to stresses τ_{ij} and pressure P , and the gravitational effect ρg_i:

$$\frac{\partial \rho u_i}{\partial t} + \frac{\partial \rho u_i u_j}{\partial x_j} = -\frac{\partial P}{\partial x_i} + \frac{\partial \tau_{ij}}{\partial x_j} + \rho g_i + \dot{S}_{mom,i} \tag{3-3}$$

A source term $\dot{S}_{mom,i}$ is added to the momentum equation to account for the effect of the particle acceleration on the gas phase. All gases are considered to be Newtonian fluids. A stress applied to a Newtonian fluid can be expressed using Stoke's hypothesis mentioned in Equation

$$\tau_{ij} = \mu \left(\frac{\partial u_j}{\partial x_i} + \frac{\partial u_i}{\partial x_j} \right) - \frac{2}{3} \mu \frac{\partial u_i}{\partial x_i} \delta_{ij} \tag{3-4}$$

Where μ is the molecular viscosity and δ_{ij} is the Kronecker delta (δ_{ij} = 1 for $i = j, \delta_{ij} =$ 0, otherwise).

Conservation of energy

The conserved energy equation used in this work is described by:

$$\frac{\partial \rho E}{\partial t} + \frac{\partial}{\partial x_i} (u_i(\rho E + P) = \frac{\partial}{\partial x_j} \left(k_{cond} \frac{\partial T}{\partial x_j} + u_i(\tau_{ij}) \right) + \dot{Q}_{rad} + \dot{S}_h \tag{3-5}$$

where E is the energy, k_{cond} is the thermal conductivity of the fluid, T is the local temperature. The heat source term $\dot{Q}_{rad}$ represents the enthalpy change due to radiation and the term $\dot{S}_h$ has been included to account for the heat exchange between the gas phase and the particle phase.

3.2.2 Turbulence Flow

One of the most important phenomena in the combustion process is dominated by turbulence, which complicates the prediction of combustion characteristics.

The simulation for the gas phase is done by solving the Navier – Stokes equations using the Reynolds Averaged Navier – Stokes equation (RANS), which focuses on the mean flow and effect of turbulence on mean flow properties. In the RANS based approach, dependent variables are decomposed into space-time averaged components and fluctuations. The resulting Reynolds fluxes are modelled by solving transport equations for the turbulent quantities, such as turbulent viscosity, kinetic energy, turbulent dissipation rate, etc., at all scales. The Reynolds stresses in this simulation are modelled by using the shear stress transport *SST k-ω model.* This model is used over the widely used *standard k-ε model,* as it gives better predictions for complex flows with swirl and pressure gradients [40]. The *SST k-ω model* blends the robust and accurate formulation by applying the *standard k-ω model* in the near-wall region but switch to *standard k-ε model* in the domain far away from the wall. This is achieved by applying a blending factor, the value of which is one in the near-wall region and zero in a region away from the wall.

3.2.3 Gas phase model

Turbulence-chemistry interaction is an important aspect of coal combustion modelling. Eddy Dissipation Model (EDM) [72], [73] was used to simulate the turbulence-chemistry interaction, which is a popular and efficient model in combustion calculations and has proven to predict accurate results in oxy-fuel combustion [40]. In EDM, the chemical reaction rate is fast relative to the transport processes in the flow, and the overall rate of reaction is controlled by the turbulence mixing of the reactants. In non-premixed flames, turbulence slowly mixes the fuel and the oxidizer into the reaction zones where they burn quickly. The chemical reaction is governed by large eddy mixing timescale $\left({}^{k}/_{\varepsilon}\right)$. The net rate of production $(R_{\alpha,r})$ of species α due to reaction r, is given by the smaller of the following two equations [73]:

$$\dot{R}_{\alpha,r} = A\,\nu'_{\alpha,r} M_{w,\alpha} \rho \frac{\varepsilon}{k} \min\left(\frac{Y_R}{\nu'_{R,r} M_{w,R}}\right) \tag{3-6}$$

$$\dot{R}_{\alpha,r} = A\,B\,\nu'_{\alpha,r} M_{w,\alpha} \rho \frac{\varepsilon}{k} \frac{\sum_P Y_p}{\sum_j^N \nu''_{\beta,r} M_{w,\beta}} \tag{3-7}$$

Where $\nu'_{\alpha,r}$ and $\nu''_{\beta,r}$ are the stoichiometric coefficients for reactant α and β in reaction r, $M_{w,\alpha}$ is the molecular weight of the species α , $Y_R$and Y_p are the mass fractions of reactants and products, respectively, A and B are empirical constants equal to 4.0 and 0.5, respectively.

Two gas phase reactions, including a global reaction, are considered for coal combustion as described by Westbrook et al. [74]:

$$volatile + \ v_1 O_2 \ \rightarrow v_2 CO + \ v_3 H_2 O + \ v_4 N_2 + \ v_5 SO_2 \tag{3-8}$$

$$CO + \ 0.5\, O_2 \ \rightarrow \ CO_2 \tag{3-9}$$

Reaction (3-8) and (3-9) represent volatiles combustion and oxidation reaction of CO in the gas phase, respectively. In this mechanism, the volatile species are lumped into one hydrocarbon species $\left(C_x H_y O_z N_a S_b\right)$ based on the coal's proximate and ultimate analysis. EDM does not incorporate finite rate kinetics, so it can only be used to predict the major products species for the stable diffusion flame in which the reaction rates are controlled by turbulent mixing.

3.2.4 Particle phase model

The particle phase model is utilized to compute the particle trajectories and the mass and energy balances of the particles. The particle phase is described in the Lagrangian frame, while the continuous fluid field is computed in a Eulerian frame. Two-way coupling between particle phase and the continuous phase allows the continuous phase transfers turbulence and momentum transfer to the particle, while the particle influences the continuous phase through the source term. This is illustrated in Figure 3.2.

Turbulent dispersion of the particles is essential as it defines the trajectories of the particles. The effect of turbulence on particle trajectories is modelled using the Discrete Random Walk (DRW) model, based on the instantaneous fluid flow [75].

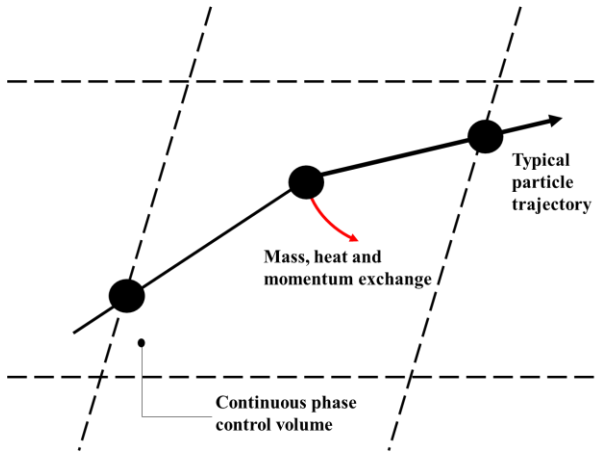

Figure 3.2 Heat, mass, and momentum transfer between particle and gas phase

During the evolution of coal particle in combustion, a particle experiences mass and heat exchange between the particle and the continuous phase, which are governed by the following laws:

(1) Inert particle heating/cooling

(2) Vaporization

(3) Boiling

(4) Devolatilization

(5) Char combustion

In the initial phase, the particle is heated until all the existing moisture starts to evaporate. In this phase, the energy exchange for the particle is modelled by convection and radiation interchange. As the temperature of the particle reaches the evaporation temperature of the

moisture, the latent energy is included in the particle energy balance. After all the moisture in the particle is boiled off, the particle temperature continues to increase until the devolatilization temperature is reached.

During coal devolatilization, hydrocarbons from coal (volatiles) are released into the continuous phase, which reacts with oxygen to produce carbon monoxide and water mostly, as described in reaction (3-8)and (3-9). In the present simulation, the single kinetic rate model [76] is applied to simulate the coal devolatilization, which assumes that the rate of devolatilization is first-order dependent on the amount of volatiles remaining in the particle:

$$-\frac{dm_p}{dt} = K_v \left[m_p - \left(1 - f_{v,0}\right)\left(1 - f_{w,0}\right)m_{p,0}\right] \tag{3-10}$$

where m_p and $m_{p,0}$ are the current and the initial mass of the particle, $f_{v,0}$ is the mass fraction of the volatiles on dry basis, and $f_{w,0}$ is the mass fraction of the moisture initially present in the coal. The rate constant, K_v, is given by

$$K_v = A_v e^{-\left(\frac{E_v}{RT_p}\right)} \tag{3-11}$$

where $R = 8314\, J/(kmol.K)$ is the ideal gas constant and T_p is the particle temperature. The pre-exponential factor, A_v, activation energy, E_v, were taken as $20{,}000\, s^{-1}$ and $4.94 \times 10^7\, J.kmol^{-1}$, respectively, as suggested by Al-Abbas et al. [77].

After devolatilization, the particle is assumed to be composed of carbon as graphite and ash, i.e., char. The remaining char in the coal particle reacts slowly with the surrounding gases. Due to the complexity of char oxidation mechanism, the oxidant and product species are defined with the following simplified approach:

$$C_{char} + O_2 \rightarrow CO_2 \tag{3-12}$$

The kinetic/diffusion-limited rate model is used for char oxidation reaction in this simulation. The model assumes that the char reaction rate is governed by an effective char kinetic rate, K_c and diffusion rate of oxygen to the particle's external surface, D_0:

$$\frac{dm_p}{dt} = -A_p p_i \frac{D_0 K_c}{D_0 + K_c} \tag{3-13}$$

where A_p is the external surface area of the char particle, $p_i$is the partial pressure of species *i* in the bulk gas. The kinetic rate of the char external surface reactions, R_i, is represented by Arrhenius form:

$$K_c = A_c e^{-\left(\frac{E_c}{RT_p}\right)} \tag{3-14}$$

Due to the lack of measured char reactivity data, the recommended values for the pre-exponential factor, A_c, and activation energy, E_c, used in the simulation are $497\ kg.(m^2.s.Pa)^{-1}$ and $7.1 \times 10^7\ J.kmol^{-1}$ as suggested by Al-Abbas et al. [77] The diffusion rate of oxygen, D_0,often controls the char oxidation at high temperatures and is expressed by

$$D_0 = C_i \frac{\left[(T_p + T_\infty)/2\right]^{0.75}}{d_p} \tag{3-15}$$

where T_∞ is the gas temperature in the cell, d_p is the particle diameter, and C_i is the mass diffusion limited constant.

After char oxidation, the particle is composed of ash, which continues to exchange heat with its surrounding but no more chemical reactions occur.

3.2.5 Radiation model

Due to the high temperatures during oxy-fuel coal combustion, radiation dominates the heat transfer, especially within the flame zone, with hot solid particles participating in the radiation heat transfer. Therefore, it is important to calculate the radiant heat flux during combustion. Heat transfer is modelled by solving the radiative transfer equation (RTE), which is given as

$$\frac{dI(\vec{r},\vec{s})}{ds} + (a+\sigma_s)I(\vec{r},\vec{s}) = an^2\frac{\sigma T^4}{\pi} - + \frac{\sigma_s}{4\pi}\int_0^{4\pi} dI_\lambda(\vec{r},\vec{s}')\Phi(\vec{s}\cdot\vec{s}')d\Omega' \qquad (3\text{-}16)$$

where s is the path length, a is the absorption coefficient, σ_s is the scattering coefficient, n is the refractive index, $I(\vec{r},\vec{s})$ is the spectral radiation intensity which is dependent on position $\vec{r}$ and direction $\vec{s}$, T is the local temperature and Φ is the phase function and $\Omega'$is solid angle.

The total absorption coefficient is the sum of the absorption coefficient of the gas mixture and particles. According to Al-Abbas et. al. [77], the recommended emissivity of the particles is 0.7, which is used in this simulation.

In this study, Discrete Ordinates (DO) model [78] is used to calculate the radiation, as it can account for the effect of radiation exchange between gas and particle phases as well as scattering Each octet of the angular space is discretized into 3×3 solid angles. Gaseous absorption is considered by a domain-based Weighted Sum of Grey Gases Model (WSGGM). In WSGGM, the absorption coefficient of the gas mixture is assumed to be the weighted average of several gravy gases and a transparent gas, therefore it is a function of H_2O and CO_2 concentrations and gas temperature [79].

3.2.6 Nitric Oxide (NO) Modelling

In ANSYS Fluent, the nitric oxide (NO) formation is simulated from three different sources:

i. Thermal NO
ii. Prompt NO
iii. Fuel NO

In the present study, the main sources of NO formation used are thermal NO and fuel NO, since the prompt NO formation was ignored because it is only important in fuel-rich mixtures [80]. Since the detailed chemistry for NO formation is computationally expensive due to the complexity in turbulence, heterogeneous reactions, heat transfer, etc., a simplified approach of the chemical kinetics is more suitable. Since the overall NO formation rate is slow compared to fuel oxidation reactions, a simplified approach consists in performing NO formation simulation as a post-processing step, based on the results of the main combustion process. This simplified approach used in ANSYS Fluent for NO formation is appropriate for complex combustion applications, thereby maintaining the accuracy of the results and no loss of essential information due to simplified mechanism [81].

Thermal NO_x

The formation of thermal NO is determined is determined from the extended Zeldovich mechanism [48]. The principal reactions governing the NO formation from molecular N_2 are as follows:

$$O + N_2 \rightleftharpoons N + NO \quad (3\text{-}17)$$

$$N + O_2 \rightleftharpoons O + NO \quad (3\text{-}18)$$

$$N + OH \rightleftharpoons NO + H \tag{3-19}$$

Reactions (3-17) and (3-18) show the formation of NO from the dissociation of molecular N_2. Reaction (3-19) takes into account the hydrogen radical's effect on NO formation and has shown to contribute in NO formation at near-stoichiometric conditions and in the fuel-rich conditions [48]. The net rate of NO formation via reactions (3-17) to (3-19) can be given as follows:

$$\begin{aligned}\frac{d[NO]}{dt} = {} & k_{f,1}[O][N_2] + k_{f,2}[N][O_2] + k_{f,3}[N][OH] \\ & - k_{r,1}[NO][N] - k_{r,2}[NO][O] - k_{r,3}[NO][H]\end{aligned} \tag{3-20}$$

where the concentrations are in $mol.m^{-3}$, and $k_{f,i}$ and $k_{r,i}$ are the rate constants of the forward and reverse reactions, respectively. All rate constants have the unit $m^3.(mol.s)^{-1}$.

The expressions for the rate constants used in thermal NO formation have been critically evaluated by Hanson and Salimian [82] and are given as follow:

$$k_{f,1} = 1.8 \times 10^8 e^{-\frac{38370}{T}} \qquad k_{r,1} = 3.8 \times 10^7 e^{-\frac{425}{T}}$$

$$k_{f,2} = 1.8 \times 10^4 T e^{-\frac{4680}{T}} \qquad k_{r,2} = 3.81 \times 10^3 T e^{-\frac{20820}{T}}$$

$$k_{f,3} = 7.1 \times 10^7 e^{-\frac{450}{T}} \qquad k_{r,3} = 1.7 \times 10^8 e^{-\frac{24560}{T}}$$

where the *T* is the temperature in K.

In fuel-lean combustion, when there is adequate amount of O_2 in the combustion zone, a quasi-steady state can be established for the consumption and formation of free nitrogen atoms [83]. Therefore, the NO formation rate becomes

$$\frac{d[NO]}{dt} = k_{f,1}[O][N_2]\frac{\left(1-\frac{k_{r,1}k_{r,2}[NO]^2}{k_{f,1}[N_2]k_{f,2}[O_2]}\right)}{\left(1+\frac{k_{r,1}[NO]}{k_{f,2}[O_2]+k_{f,3}[OH]}\right)} \quad (3\text{-}21)$$

The kinetics of thermal NO formation is much slower than the hydrocarbon oxidation rate, and most of the thermal NO are formed after the completion of combustion. The thermal NO formation mechanism can be decoupled from the fuel oxidation process and simulated in the post-processing step, where the concentration of [O] and [OH] can be calculated by the partial equilibrium approach [84]. The partial equilibrium concentrations of the [O] and [OH] can be given by the following expressions:

$$[O] = 36.64\, T^{0.5}[O_2]^{0.5} e^{-\frac{27123}{T}} \quad (3\text{-}22)$$

$$[OH] = 2.129 \times 10^2\, T^{-0.57}[O_2]^{0.5}[H_2O]^{0.5} e^{-\frac{-4595}{T}} \quad (3\text{-}23)$$

where concentrations are in $mol.m^{-3}$, and T is in K.

Generally, in air-fired combustion, thermal NO is the main contributor of NO in the flue gas. However, in oxy-fuel combustion, due to the near absence of N_2, the effect of thermal NO will be minimized.

Fuel NO_x

Nitrogen in coal, which is generally present in both the volatile and char, contributes to the formation of NO during combustion. During coal devolatilization, intermediate nitrogen species, such as hydrogen cyanide (HCN), ammonia (NH_3), nitrogen atom (N), etc., are released in the gas phase. HCN and NH_3 are the dominant intermediate species, particularly in lignite coal, where it has been investigated that the level of NH_3 are higher in lignite coal and subbituminous coal, whereas, HCN is more dominant species in the bituminous coal [8]. The routes for the formation

and destruction of nitrogen in coal are still not completely understood due to the complexity of the reactions. Therefore, the in-built ANSYS Fluent's global simplified fuel NO pathway is taken into consideration, which is used in various studies for NO_x [42], [80], [85]. Figure 3.3 shows the pathway for the formation of NO from fuel nitrogen.

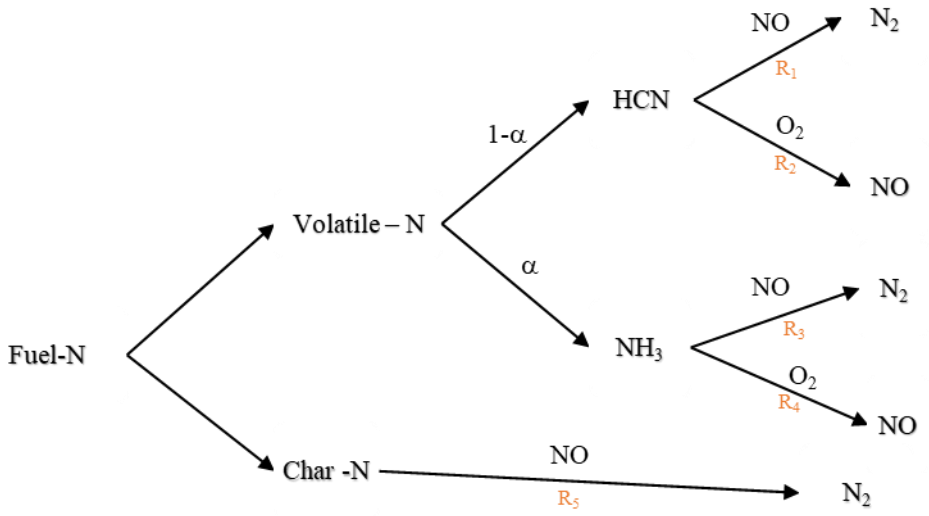

Figure 3.3 Formation and destruction of fuel nitrogen

According to the literature [42], [80], [85], fuel nitrogen is equally distributed between the volatile matter and char, and the amount of nitrogen is calculated from the ultimate analysis and proximate analysis of the coal. Nitrogen in lignite coal volatiles is released as NH_3 and HCN with a ratio (α) of 9:1 [8]. NH_3 and HCN conversion through oxidation from O_2 and reduction from NO are calculated based on the work of De Soete [86]. The char nitrogen is released directly to the gas phase as NO, and the corresponding kinetic parameters are adopted from the char oxidation reaction parameters as shown in Equation (3-9).

3.2.7 Sulphur Oxide (SO_x) Modelling

All coal contains sulphur, which can exist as one of the following fractions [87]:

i. Organic sulphur, which is an integral part of the coal structure,
ii. Inorganic sulphur, mostly present as pyrite, and
iii. Sulphates as salts of metals such as calcium and iron.

During combustion, sulphur species from coal are released and oxidized to produce SO_2 and SO_3. The reaction mechanisms are influenced by various factors such as the coal type, and its sulphur compounds, and the combustion conditions. The organic sulphur in coal is less stable and is distributed in the volatile as H_2S as the dominant species along with COS, SO_2 and CS_2 [88], [89]. The inorganic sulphur remains trapped in the char, which is subsequently released during char burnout. For CFD study, the sulphur transformation is assumed to occur as following:

i. The release of coal-bound sulphur during devolatilization,
ii. Gas phase reaction of the sulphur species in the gas phase,
iii. Oxidation of inorganic sulphur during char burnout.

It is assumed that the organic sulphur released during devolatilization comprises of only H_2S, and the release rate parameters are adopted from the parameters of volatile devolatilization mentioned in Equations (3-10) and (3-11). The inorganic sulphur retained in char during devolatilization is assumed to be converted to SO_2 during char burnout as a single step process [90]. The release rate of SO_2 from char is calculated from the kinetic parameters of the char oxidation reaction parameters as stated in Equations (3-13), (3-14) and (3-15). For this study, the sulphur content in coal is equally distributed between the volatile and char and the amount of sulphur is calculated from the proximate and ultimate analysis of the coal.

In this study, due to the relatively small impact of sulphur chemistry on temperature and the flow fields as compared to hydrocarbon combustion, the sulphur chemistry model is applied in the post-processing step based on the results of the main coal combustion simulation.

Gas phase reactions of sulphur species

For modelling of the volatile sulphur species (H_2S) within ANSYS Fluent, the default sulphur species reaction mechanism is used, which is an eight-step reduced mechanism based on the detailed model developed by Kramlich et al. [91].

$$H_2S + H \rightleftharpoons SH + H_2 \quad (3\text{-}24)$$

$$H_2S + OH \rightleftharpoons SH + H_2O \quad (3\text{-}25)$$

$$H_2S + O \rightleftharpoons SH + OH \quad (3\text{-}26)$$

$$H_2S + M \rightleftharpoons SH + H + M \quad (3\text{-}27)$$

$$SH + O \rightleftharpoons SO + H \quad (3\text{-}28)$$

$$SO + OH \rightleftharpoons SO_2 + H \quad (3\text{-}29)$$

$$SO + O_2 \rightleftharpoons SO_2 + O \quad (3\text{-}30)$$

$$SO + O + M \rightleftharpoons SO_2 + M \quad (3\text{-}31)$$

The equilibrium is modelled by treating both the forward and backward pathways of reactions individually and the rate constants for the forward and reverse reactions are listed in Appendix A. The concentrations for O and OH radicals have been calculated through the partial equilibrium assumption based on the O_2 and H_2O concentration, as stated in Equations (3-22) and (3-23).

In addition, SO_2 may be further oxidized to form SO_3. The following two reactions are included in the model to simulate SO_3 formation:

$$SO_2 + O + M \rightleftharpoons SO_3 + M \quad (3\text{-}32)$$

$$SO_2 + O_2 \rightleftharpoons SO_3 + O \quad (3\text{-}33)$$

The reactant constants are taken from Hunter et al. [92].

3.3 Kinetic model for the flue gas

The CFD simulation of coal allows us to determine the temperature and flow field during combustion. In addition, it also determines the composition of flue gas in the combustor. However, in a thermal power plant, the flue gas is utilized to produce steam, that reduce the flue gas temperature to temperatures below 473 K as it flows out of the boiler. Kinetic modelling of the flue gas is an essential method to understand the changes in the chemistry of the flue gas in the boiler system of an oxy-fuel power plant at high pressures. This will help to predict the final composition of the flue gas as it cools down in super-heater and economizer section of the boiler.

The method employed in the current study is to determine the sulphur and nitrogen chemistry occurring in the oxy-fuel combustion environment at different pressures. It has been suggested in the literature that SO_x and NO_x interaction becomes important at higher pressures and the presence of NO favours the production of SO_3 [24]. Kinetic simulation is conducted to investigate the effect of NO_x on the evolution of SO_3 under a temperature profile similar to actual conventional boiler conditions.

In the present work, the calculation for the flue gas kinetics is performed with the Chemkin-PRO software. The model assumes plug flow reactor (PFR) and a temperature profile for the pulverized coal-fired power plant, adopted from Senior et al. [93] and shown in Figure 3.4.

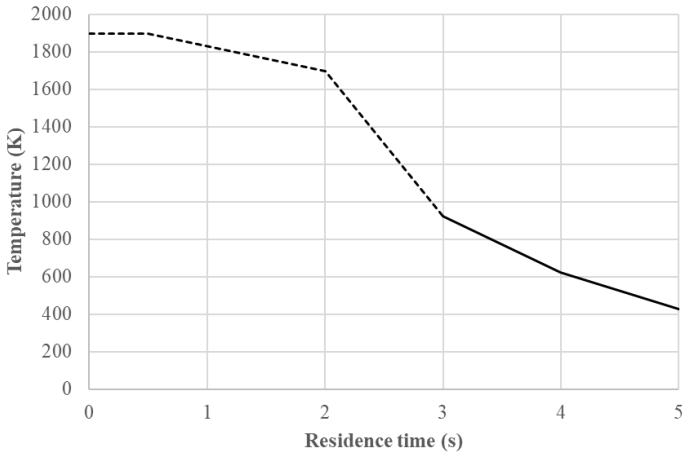

Figure 3.4 Temperature profile of flue gas in typical coal fired power plant. The dashed line represents the temperature in the combustor, the solid line represents the temperature of flue gas considered in CHEMKIN-PRO [93]

The equations governing the behaviour of a PFR are simplified versions of the general relations for conservation of mass and momentum. In this work, it is assumed that (a) the flow of the gas in the axial direction, (b) axial diffusion is negligible relative to the corresponding convective term. In this way, the overall mass balance for the gas is as follows:

$$\frac{d(\rho u A)}{dx} = 0 \tag{3-34}$$

Where ρ is the density and u is the axial velocity of the gas. The quantity A is the cross sectional area of the reactor.

A similar equation for the conservation of gas species can be written for each species, individually:

$$\rho u \frac{dY_\alpha}{dx} = \dot{\omega}_\alpha M_{w,\alpha} \tag{3-35}$$

where Y_α is the mass fraction of species α, $\dot{\omega}_\alpha$ is the molar rate of production by homogeneous gas reactions and $M_{w,\alpha}$ is the molecular weight of the species α. Such reactions

cannot change the total mass of the gas, but they alter the composition of the gas flowing in the reactor.

The conservation of momentum expresses the balance between the pressure forces, inertia, and viscous drag in the reactor, therefore the equation of conservation of momentum can be expressed as:

$$A\frac{dP}{dx} + \rho u A\frac{du}{dx} + \frac{dF}{dx} = 0 \tag{3-36}$$

where P is the absolute pressure and $F$is the drag force exerted on the gas by the reactor wall. However, in the current study, drag force is assumed to be absent, therefore the equation becomes:

$$\frac{dP}{dx} + \rho u\frac{du}{dx} = 0 \tag{3-37}$$

Since an axial temperature profile for the PFR model is specified as a user-defined linear profile as shown in Figure 3.4, therefore the conservation of energy was not required.

It should be noted that since the heat loss in the combustor is considered in the CFD simulation, the initial temperature of the PFR implemented in Chemkin-PRO is the combustor's outlet temperature obtained from the combustion simulation. The initial flue gas composition used in the model is also based on the results provided from the CFD simulation at different pressures.

The mechanism proposed for the simulation is based on the work of Choudhury et al. [28] The mechanism contains 111 species and 742 reactions, including the SO_x and NO_x reactions in an oxy-fuel combustion environment [27]. To investigate the direct SO_x – NO_x interaction, the reaction subset from reactions for SO_x – NO_x reaction from Glarborg et al. [94] is integrated to the oxy-fuel combustion mechanism. The conversion of SO_3 to H_2SO_4 at in a combustion system also

occurs low temperatures. Therefore, the reaction for SO_3 conversion to H_2SO_4 is also adopted from Leeds mechanism [95] and implemented in the reaction mechanism applied in the current study. The proposed kinetic mechanism is shown in Appendix B.

The objective of the study is to investigate the effect of pressure on the interaction of SO_x and NO_x in the flue gas, as it is cooling down. Another objective is to investigate if these reactions favour the formation of SO_3, as it is more soluble in water and can be removed during condensation.

3.4 Removal of SO_x and NO_x from flue gas

In oxy-fuel combustion process, the flue gas has to be purified to obtained a concentrated CO_2 stream, which occurred in the CO_2CPU. Prior to entering the CO_2CPU, moisture must be removed, as well as SO_x and NO_x in order to minimize the risk of corrosion. The purification system in this study employs the SO_x -NO_x interaction and nitric acid process for the removal of SO_x and NO_x and a reactive absorber column for the removal of moisture, and the acidic species (HNO_3, H_2SO_4) produced.

In this work, simulation of the reactive absorber column was performed on ASPEN Plus V8.8 using rate-based calculations, and the Electrolyte NRTL model was selected for the thermodynamic properties calculations as various electrolytes were considered. The absorber column is modelled using a RADFRAC block in ASPEN Plus to allow the rate based calculations in the column. Figure 3.5 represents the flowsheet of the absorber column implemented for the simulation.

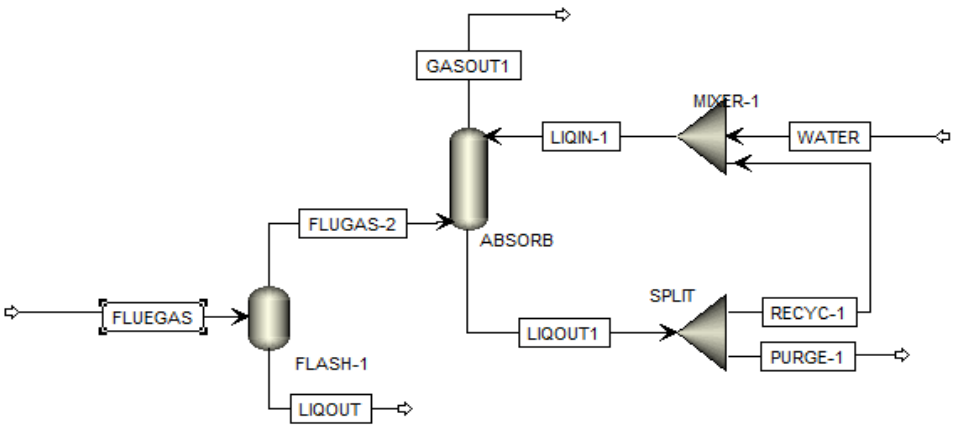

Figure 3.5 Flowsheet for the reactive absorber column in ASPEN Plus

The flue gas then enters the bottom of the absorber ("ABSORB") and flows counter-currently to the aqueous scrubbing liquid (water and dilute acids) ("LIQIN-1"). A splitter ("SPLIT") is used to recycle a part of the liquid flow to the top of the absorber before it is mixed ("MIXER-1") with the make-up water ("WATER"). The washed gas ("GASOUT1") leaves the column from the top for further processing in the CO_2CPU.

Design specifications have been adapted from the Air Product pilot setup [96], ensuring that the adequate hydrodynamic conditions are met (actual velocity to be lower than the threshold for flooding). The parameters used in the model for the design of the reactive absorber column are specified in Table 3-1.

Table 3-1 Design specifications of the reactive absorber column

Design Specification	
Column pressure	15 atm
Number of stages	12
Flue gas feed stage	Bottom
Water feed stage	Top
Column packed height	12 m
Column packing type	IMTP 25 mm
Column diameter	0.15 m

As mentioned earlier, the reactive absorber column is modelled using the RADFRAD block, as it can handle both equilibrium as well as kinetically limited reactions. The complete reaction mechanism implemented in the absorber includes 20 reactions. Table 3-2 presents the reactions considered in the reactive absorber column for the absorption of SO_x and NO_x and the generation of acidic solution. Those reactions could either occur in the gas phase or in the liquid phase, and be considered either as equilibrium or kinetic reactions. If the reaction is available in ASPEN Plus, these data are used, but otherwise, reactions are implemented using literature data or calculated from Gibbs free energies. The solubility of gases in water are calculated by means of Henry's law [97].

Table 3-2 Gas and liquid reaction implemented in the reactive absorber column

	No	Reaction	Type	Phase	Ref
H_2O	1.	$2\,H_2O \rightleftharpoons H_3O^+ + OH^-$	Equilibrium	Liquid	Aspen Plus database
CO_2	2.	$CO_2 + 2\,H_2O \rightleftharpoons HCO_3^- + H_3O^+$	Equilibrium	Liquid	Aspen Plus database
	3.	$HCO_3^- + H_2O \rightleftharpoons CO_3^{2-} + H_3O^+$	Equilibrium	Liquid	Aspen Plus database
NO_x	4.	$2\,NO + O_2 \rightarrow 2\,NO_2$	Kinetic	Gas	[98]
	5.	$2\,NO_2 \rightleftharpoons N_2O_4$	Equilibrium	Gas	[99]
	6.	$NO + NO_2 + H_2O \rightleftharpoons 2\,HNO_2$	Equilibrium	Gas	[99]
	7.	$NO + NO_2 \rightleftharpoons N_2O_3$	Equilibrium	Gas	[100]
	8.	$N_2O_3 + H_2O \rightarrow 2\,HNO_2$	Kinetic	Liquid	[101]
	9.	$N_2O_4 + H_2O \rightarrow HNO_2 + HNO_3$	Kinetic	Liquid	[100]
	10.	$2\,NO_2 + H_2O \rightarrow HNO_2 + HNO_3$	Kinetic	Liquid	[102]
	11.	$3\,HNO_2 \rightarrow NO + HNO_3 + H_2O$	Kinetic	Liquid	[103]
	12.	$HNO_2 + H_2O \rightleftharpoons NO_2^- + H_3O^+$	Equilibrium	Liquid	Aspen Plus database
	13.	$HNO_3 + H_2O \rightleftharpoons NO_3^- + H_3O^+$	Equilibrium	Liquid	Gibbs free energy

SO_x	14.	$SO_2 + 0.5\ O_2 \rightleftharpoons SO_3$	Equilibrium	Gas	Gibbs free energy
	15.	$SO_2 + H_2O \rightleftharpoons HSO_3^- + H_3O^+$	Equilibrium	Liquid	Aspen Plus database
	16.	$HSO_3^- + H_2O \rightleftharpoons SO_3^{2-} + H_3O^+$	Equilibrium	Liquid	Aspen Plus database
	17.	$SO_3 + 2\ H_2O \rightleftharpoons HSO_4^- + H_3O^+$	Equilibrium	Liquid	Gibbs free energy
	18.	$HSO_4^- + H_2O \rightleftharpoons SO_4^{2-} + H_3O^+$	Equilibrium	Liquid	Aspen Plus database
	19.	$H_2SO_4 + H_2O \rightleftharpoons HSO_4^- + H_3O^+$	Equilibrium	Liquid	Aspen Plus database
SO_x/NO_x	20.	$NO_2 + SO_2 \rightarrow SO_3 + NO$	Kinetic	Gas	[104]

4 CFD simulation of pressurized oxy-fuel combustion

In this chapter, a comprehensive CFD modelling study of oxy-fuel combustion was performed at different absolute pressures. The model was validated using experimental measurements at atmospheric pressure (1 atm), and the analysis was performed at three different pressures (1 atm, 5 atm and 15 atm) to gain insight into the effect of pressure into the coal combustion in oxy-fuel environment.

In this chapter, we also focus on the performance of the models used for SO_x and NO_x production from coal combustion, in order to predict the flue gas concentration at different pressures.

4.1 Validation of the CFD simulation at atmospheric pressure

Since no experimental data are available for pressurized coal oxy-fuel combustion, the validation of the CFD model for oxy-fuel combustion was done using the experimental results performed at atmospheric pressure by Andersson et al. [105] and Hjartstam et al. [106]. Those experiments involved the combustion of lignite coal under an O_2/CO_2 oxidizing atmosphere, with an O_2 molar fraction of 29%.

4.1.1 Coal

Lusatian lignite coal with a high heating value (HHV) of 20.9 MJ/kg was used for combustion. Table 4-1 shows the proximate and ultimate analysis of the coal. The size of the coal particle was kept constant in this simulation with a mean diameter of 50 μm.

Table 4-1 Proximate and ultimate analysis of the Lusatian lignite coal

	As received (AR)	Dry	DAF
Proximate Analysis (*wt. %*)			
Moisture	10.20		
Ash	5.00	5.57	
Volatiles	50.37	56.09	59.40
Char	34.43	38.34	40.60
Ultimate Analysis (*wt. %*)			
C	59.28	66.01	69.90
H	4.58	5.10	5.40
O	19.59	21.81	23.10
N	0.51	0.57	0.60
S	0.85	0.94	1.00

4.1.2 Furnace and burner geometry

The furnace geometry modelled in this numerical study is the 100 kW test facility at Chalmers University of Technology, Sweden. The combustor is a down-fired cylindrical refractory lined unit with a height of 2.4 m and inner diameter of 0.8 m, cooled by four water cooled tubes, as shown in Figure 4.1a. The burner configuration has three concentrically separate inlets (Figure 4.1b). The central inlet is used to feed the fuel, which is a mixture of oxidizer (CO_2/O_2) and pulverized coal. The primary and secondary inlets are equipped with swirl producing fins, where the oxidizer gas was injected with a swirl number (SN) of 0.79 and 0.21 respectively.

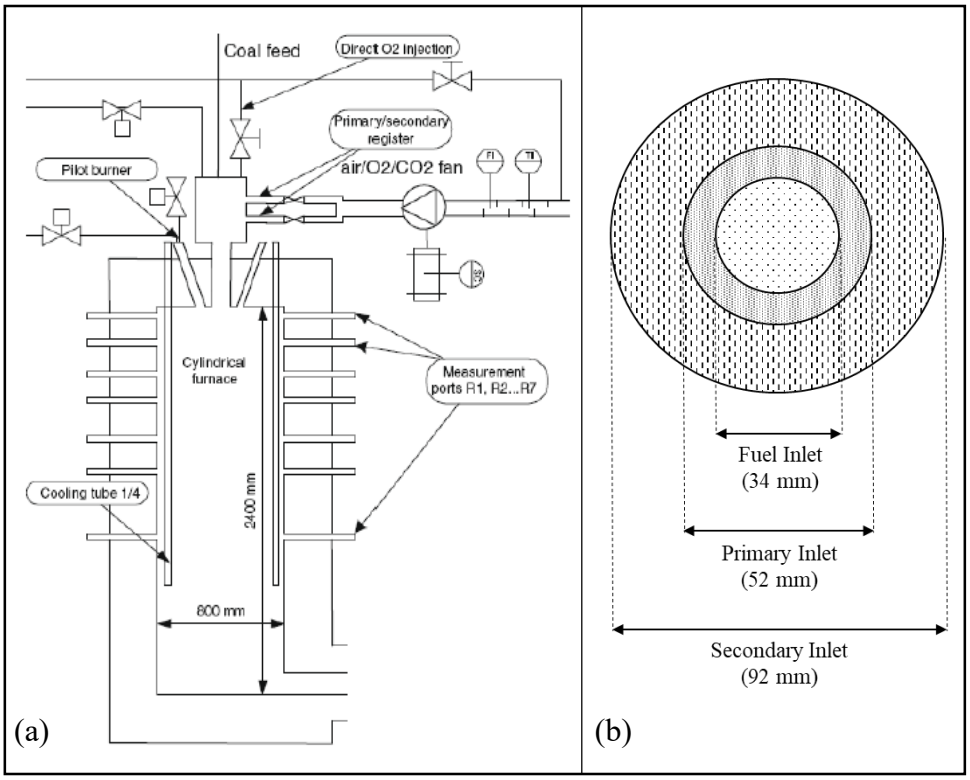

Figure 4.1 (a) Chalmers 100 kW combustor unit [105] (b) Cross section of the burner configuration of the combustor.

It has been suggested that it is possible to obtain good predictions using axisymmetric two-dimensional (2D) domain for oxy-fuel combustion [107], [108]. Gaikwad et al. [107] compared the 2D model for oxy-fuel combustion using $SST\ k-\omega$ turbulence model and suggest that using 2D domain with $SST\ k-\omega$ model, the gas temperature distribution deviated by only 5-15% from the experimental data. This can be improved by increasing the mesh size of the domain, especially near the burner zone to accurately predict the mixing and combustion of coal with the oxidizer.

Based on the burner and furnace geometry, an axisymmetric two-dimensional (2D) model was generated with 40,244 cells. A high mesh concentration was used along the centerline axis of

the furnace in the region between the inlet and the center of the furnace. Figure 4.2 shows the axisymmetric 2D mesh of the combustion chamber.

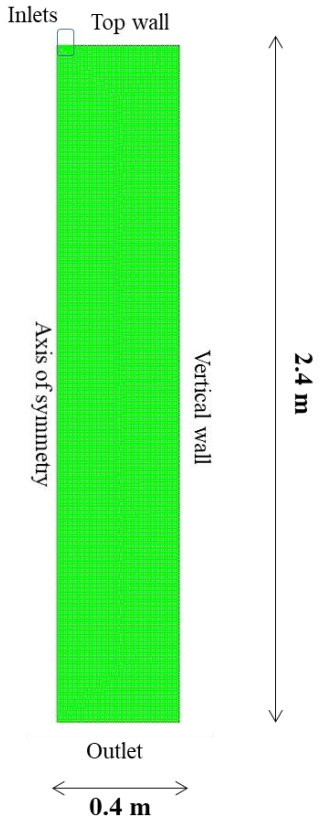

Figure 4.2 Axisymmetric 2D mesh for 100 kW Chalmers vertical combustor

4.1.3 Boundary conditions

In the CFD simulation, the accuracy of the numerical results is dependent on the selection of boundary conditions. The boundary conditions used in the simulation is based on Chalmers oxy-fuel combustion experiments performed by Andersson et al. [105].

The coal mass flow used in the inlet was 13.1 kg/hr, based on a fuel input power of 76 kW. Coal is injected with the help of carrier gas, comprising of 30 vol.% O_2 and 68 vol.% CO_2, in the fuel inlet. The oxygen/fuel ratio described by overall stoichiometric value (λ) , was kept at 1.18, as suggested by Andersson et al. [105]. The rest of the oxidizing gas enters the combustor from

the primary and secondary inlet. The compositions and flow rates for the inlet streams are shown in Table 4-2.

Table 4-2 Operating conditions of the oxy-fuel combustion at 1 atm

	Mass flow rate *kg/h*	**Mean velocity** *m/s*	**O_2** *vol %*	**CO_2** *vol %*	**Temperature** *K*
Fuel carrier gas	3.93	0.74	30	68	300
Primary inlet	40.48	5.63	29	69	300
Secondary inlet	94.44	3.53	29	69	300

The densities of the reactants and products were calculated by the ideal gas law equations, while the other physical properties for the gas such as specific heat, molecular weight, viscosity, thermal conductivity, and diffusion were calculated by the mixing-law, which calculates the properties based on the mass fraction average of the pure species [68].

At the outlet boundary condition of the furnace, the von-Neumann boundary condition, which sets the gradient of the variables in the direction normal to the boundary to a constant values, typically zero.

$$\frac{\partial \emptyset}{dx_j} = 0 \qquad (4\text{-}1)$$

For the precise modelling, the wall of the furnace was divided into two parts, top-wall and vertical-wall. No slip condition was applied for both parts. The boundary conditions for the combustor walls are given in Table 4-3. The walls temperatures are based on the experimental work by Andersson et al. [109], who suggested that temperature at the refractory lined walls have

a temperature about 873 ± 50 K at 1 atm. The emissivity values for the furnace walls were adopted from the work of Al-Abbas et al. [77].

Table 4-3 Boundary conditions at the walls

	Temperature	**Emissivity**
Top wall	873 K	0.52
Vertical wall	923 K	0.52

Since the wall temperature and emissivity at higher pressures is not known, therefore the wall boundary conditions at 1 atm are used for simulations at higher pressures in this study.

4.1.4 Results and discussion

The results of the validation study showed reasonable results, and confirmed that it is possible to obtain good predictions using a 2D model of the combustor. Figure 4.3 shows the temperature profile and the locations of the measurement ports located on the furnace. The ports are located at distances of 0.215 m (port 1), 0.384 m (port 2) and 0.553 m (port 3) from the burner.

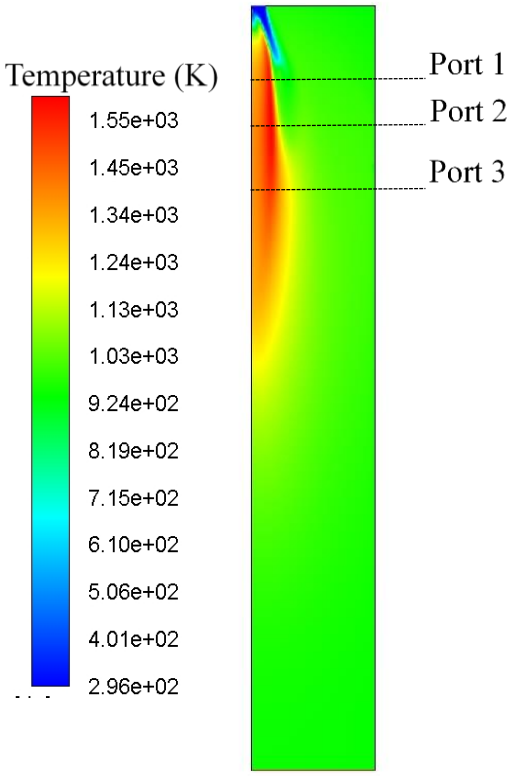

Figure 4.3 Temperature profile of oxy-fuel combustion at 1 atm

Figure 4.4 shows a comparison of the radial temperature profiles obtained from the CFD simulation at 1 atm and the experimental results, obtained by Andersson [105]. It is shown that the temperature profiles conform to the experimental measurements, however there are some areas in the flame that are over-predicted in the simulation. This can be attributed to the two-step global reaction for combustion as described in Equations (3-8) and (3-9), where volatiles combust to form CO, CO_2 and H_2O. However, coal combustion chemistry is complex with multiple finite rate reactions during combustion, and is computationally expensive, which necessitates the use of simpler models to describe its overall behavior. Overall, the results are accurate enough, with regards to the temperature distribution in the combustor, and the model will be used to simulate the combustion at higher pressures.

(a)

(b)

(c)

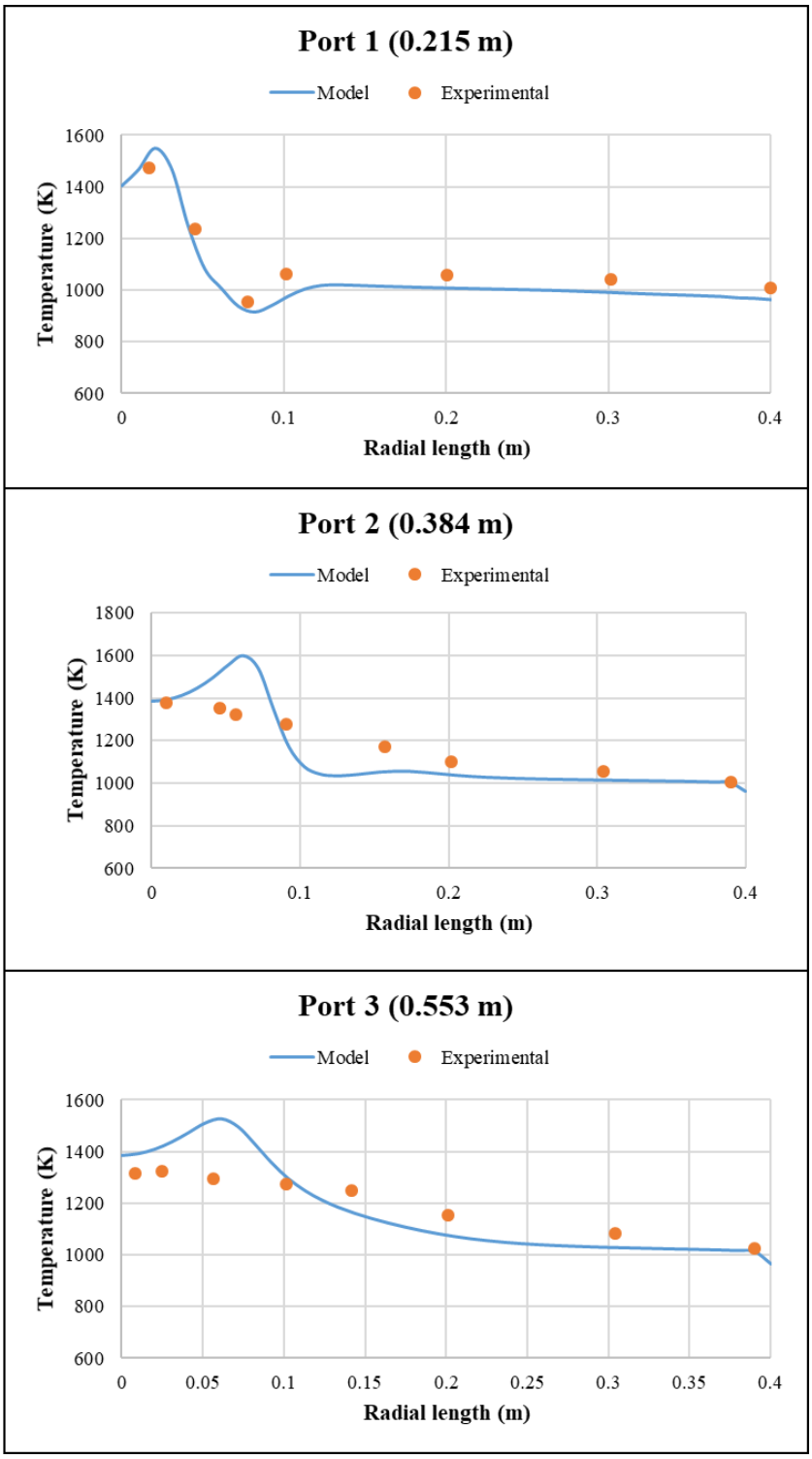

Figure 4.4 Temperature profiles of the model and the experimental data at (a) Port 1 (0.215 m) (b) Port 2 (0.384 m) (c) Port 3 (0.553 m)

4.2 Effect of pressure in oxy-fuel combustion of coal

The objective of this study is to examine the effect of pressure on oxy-fuel combustion characteristics, especially the combustion reactions and the flue gas species, including SO_x and NO_x formation. The validated CFD model developed is used to simulate the oxy-fuel combustion under elevated pressures, with the geometry of the combustor and the boundary conditions similar to the validated CFD model.

In order to analyse the effect of pressure, simulations were performed for the combustor geometry described previously, at constant 76 kW thermal power and constant stoichiometric ratio (λ) of 1.18. Therefore, the mass flowrates of the coal and oxidizer at the inlets were kept constant at the values used in the validated model. However, the increased pressure proportionally increases the gas density, based on ideal gas law, which results in reduced velocity and increased residence time in the combustor. Table 4-4 shows the change in densities and the mean velocities at the inlets.

Table 4-4 Inlet conditions at atmospheric and elevated pressures

Pressure (absolute)			**Fuel inlet**	**Primary inlet**	**Secondary inlet**
1 atm	Mass flow rate	*(kg/h)*	3.93	40.48	94.44
	Density	*(kg/m^3)*	1.64	1.64	1.64
	Mean velocity	*(m/s)*	0.74	5.63	3.53
5 atm	Mass flow rate	*(kg/h)*	3.93	40.48	94.44
	Density	*(kg/m^3)*	8.19	8.22	8.22
	Mean velocity	*(m/s)*	0.15	1.13	0.71
10 atm	Mass flow rate	*(kg/h)*	3.93	40.48	94.44
	Density	*(kg/m^3)*	16.38	16.43	16.43
	Mean velocity	*(m/s)*	0.074	0.56	0.35
15 atm	Mass flow rate	*kg/h*	3.93	40.48	94.44
	Density	*(kg/m^3)*	24.57	24.65	24.65
	Mean velocity	*m/s*	0.05	0.38	0.24

The sub-models used for the devolatilization, char combustion, NO_x and SO_x formation are same as the validated CFD model.

4.2.1 Results and discussion

In this section, the results and discussion of the four different combustion cases (pressures of 1, 5, 10 and 15 atm) are presented. The difference and comparisons for the combustion environment are based on the operating pressure. The mass flow rate of the coal and the oxidizer are kept constant for all the combustion cases, however due to the increase in pressure, the volumetric flow rate and the inlet velocities of the oxidizing gas are different (Table 4-4). The findings of these different combustion environments are analysed and discussed in three different sections: temperature distribution, species concentration, and pollutant (SO_x, NO_x) concentration.

Temperature distribution

Figure 4.5 shows the temperature distribution of oxy-fuel combustion in the axisymmetric furnace. The main purpose of the figure is to visualize the overall flame temperature and its distribution in the furnace.

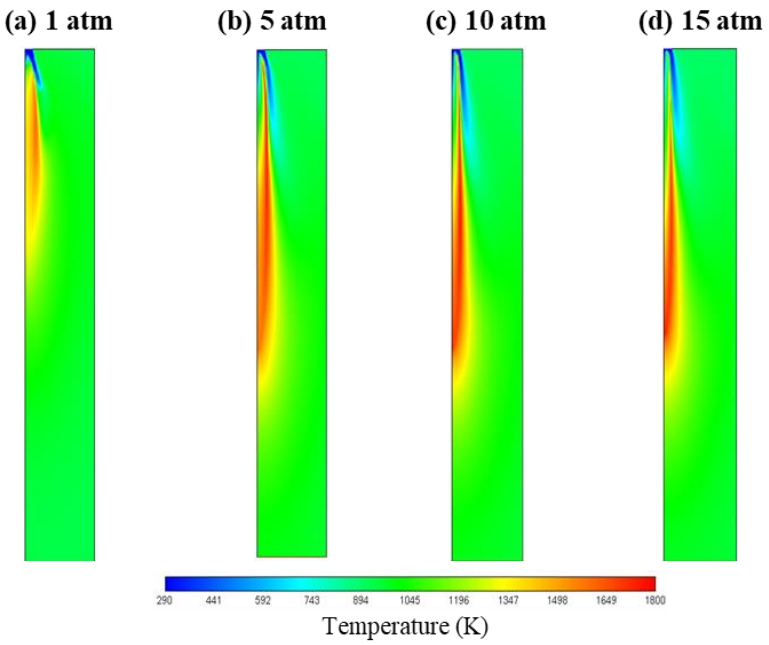

Figure 4.5 Flame temperature distribution in the furnace at (a) 1 atm (b) 5 atm (c) 10 atm (d) 15 atm

For the atmospheric combustion, (Figure 4.5a), the flame starts at the burner and the maximum temperature reached in the flame is around 1600K. Whereas, in the pressurized case (Figure 4.5b-d), the flame length is fairly longer, as the pressure is increased, and the maximum temperature reached in the cases of 5 atm, 10 atm and 15 atm, were 1750 K, 1755 K and 1760 K, respectively. One of the reasons for the longer flame length is due to the pressure's effect on moisture's evaporation. Due to the increased pressure, the evaporation rate of the moisture in the coal is lower, as compared to atmospheric pressure. It can be seen in Figure 4.8 that the concentration of H_2O is higher close to the burner as compared to cases at higher pressure, where the H_2O is released at a slower rate. Due to the nature of the model used in the simulation, the moisture has to be removed, before devolatilization and ignition of the hydrocarbons occur. Secondly, at higher pressures, char oxidation is control by O_2 diffusion into the particle, delaying the char burnout, due to the slow diffusion of O_2 to the char at high pressures.

Figure 4.6 to Figure 4.8 shows the CO_2, O_2 and H_2O distributions in the furnace. It can be seen that the CO_2 concentration is low in the zones near the burner where evaporation and devolatilization occurred.

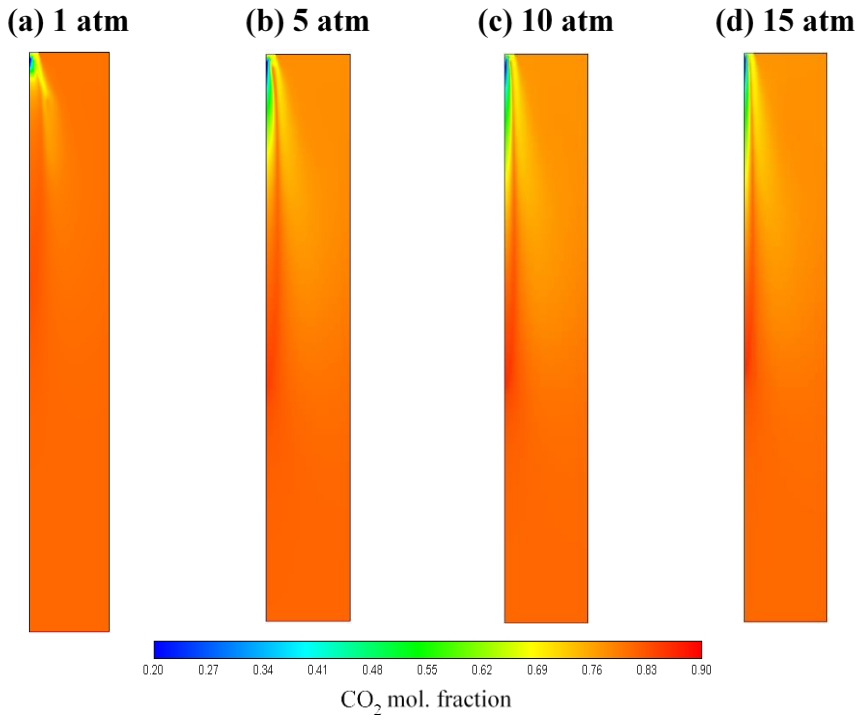

Figure 4.6 Concentration of CO_2 in the furnace at different pressures

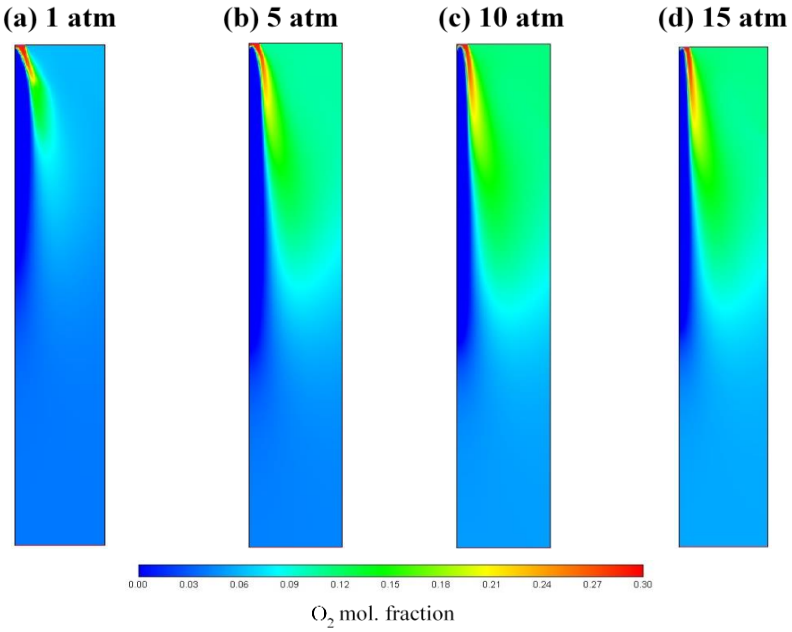

Figure 4.7 Contour for the concentration of O_2 at different pressures

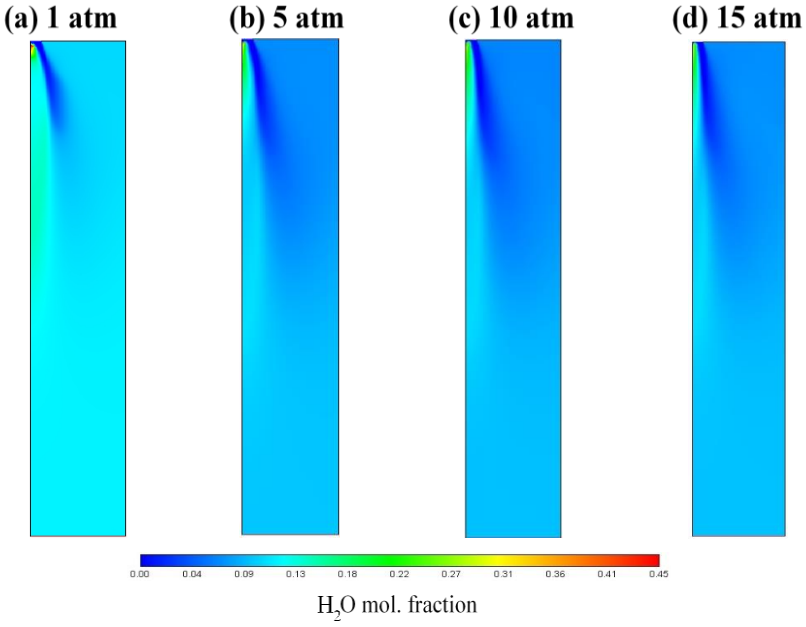

Figure 4.8 Contour for the concentration of H_2O at different pressures

It has been noted that there is no net effect of pressure on the main combustion products and the concentrations are within 0.1% for CO_2, H_2O and O_2 for the exit flue gas. Table 4-5shows the compositions of the flue gas at the furnace exit.

Table 4-5 Composition of the flue gas exiting the furnace

	1 atm	**5 atm**	**10 atm**	**15 atm**
CO_2	0.814	0.816	0.814	0.812
H_2O	0.115	0.1104	0.107	0.107
O_2	0.051	0.053	0.060	0.060
N_2	0.0007	0.0007	0.00068	0.00067
Ar	0.018	0.018	0.018	0.018
SO_2	0.001	0.001	0.001	0.001

The simulation of the NO production was conducted as a post processing task, since NO production do not have a significant effect on the flow fields and the temperature profile. Since the concentration of NO_2 is significantly low at the furnace temperatures, it was not included in the CFD model. Figure 4.9 shows the concentration of NO at the furnace outlet at different pressures.

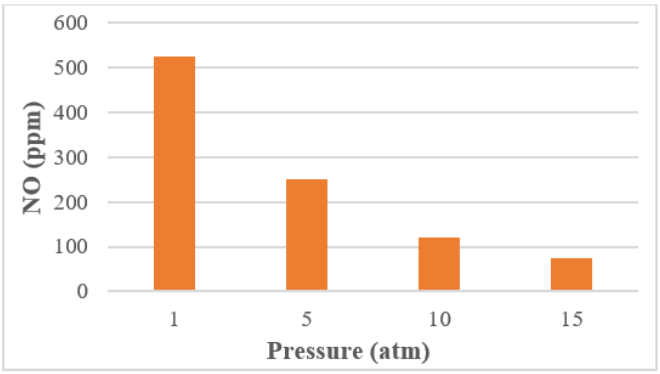

Figure 4.9 NO concentration at the furnace exit at different pressures.

It can be seen from the results that NO concentration decreased with increasing pressure. This is mostly due to the decrease in the O radicals, due to increase in pressure. Since O and OH are This is due to the fact that O_2 diffuses into the char to react with nitrogen present in char, and produces NO_x; and then the NO_x diffuses out and reduces to with carbon, according to Hatano et al. [110]. Secondly, NO formed may be reduced to N_2 over the residual char due to its catalytic effect at high pressures according to De Soete et al. [86].

Figure 4.10 shows the SO_2 formation at different pressures.

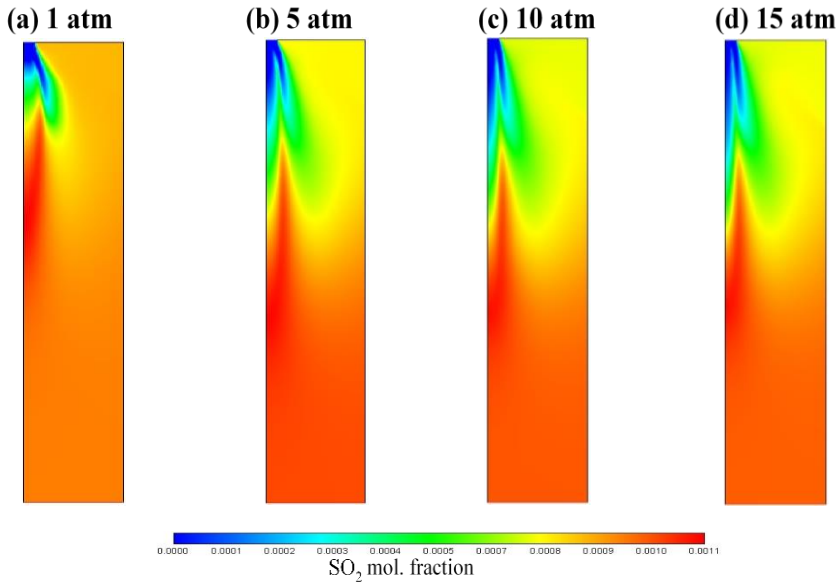

Figure 4.10 Contour of SO_2 concentration at different pressures.

It is worth noting that although the rate of SO_x formation is affected by increasing pressure, the SO_2 leaving the outlet of the furnace is between 900 to 1000 ppm for all the cases. This suggests that all the sulfur in the coal was oxidized to SO_2. It was also observed that SO_3 formation was increased at higher pressures, as O radicals are pre-dominant at higher pressures leading to the formation of SO_3 via reaction (3-32). Figure 4.11 shows the concentration of SO_x leaving the combustor.

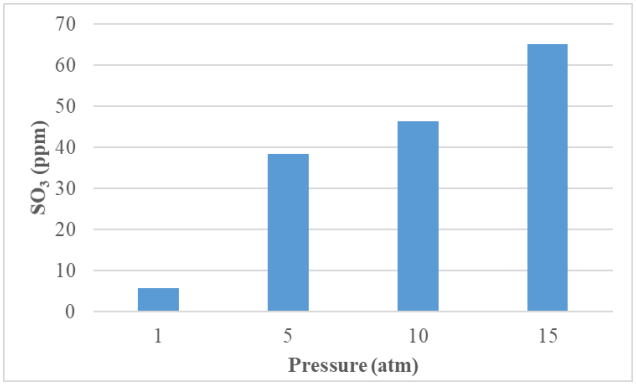

Figure 4.11 SO_3 concentration at the outlet of combustor at different pressures.

In summary, the CFD simulation showed that due to the pressure increase, the maximum temperature of the flame has increased by 150 K between 1 atm and 5 atm but increased slightly between 5 atm and 15 atm. There was no change on the composition of the main species in the flue gas when the pressure was increased, however significant decrease in NO was observed as pressure was increased, suggesting that high pressure combustion effectively reduces NO formation.

5 Effect of pressure on NO_x and SO_x concentrations in the flue gas

It is well established that one of the drawbacks of oxy-fuel combustion is the higher concentration of SO_x in the flue gas [21], [22], [37], [56], [58]. The increased levels of SO_x, especially SO_3, can cause severe corrosion to the boiler and the processes downstream to the boiler at lower temperatures [21]. Therefore, it is important to understand the sulphur chemistry in the flue gas, in order to remove SO_x from the flue gas before it is further processed in the CO_2CPU.

In this chapter, a comprehensive kinetic modelling study of the flue gas exiting the combustor is performed. The main objective is to understand and identify the fate of SO_x and NO_x in the flue gas in oxy-fuel environment, as the flue gas is cooling down in the boiler of the oxy-fuel combustion power plant at different pressures.

SO_x reactions:

In the combustion process, SO_3 is formed in the boiler where O_2 is in excess. Equilibrium calculations for high temperature reactions show that under O_2-rich conditions, the major SO_x species produced is SO_2 and low levels of SO_3[22], [56], [111], [112].

$$SO_2 + 0.5\,O_2 \rightleftharpoons SO_3 \qquad (5\text{-}1)$$

Since reaction (5-1) is an exothermic reaction, the equilibrium shifts towards SO_3 formation at low temperatures, but the reaction rate slows down as the flue gas is cooled. As a result, the reported conversion of SO_2 to SO_3 under oxy-fuel combustion conditions ranges from 0.1% to 5% [8], [113]–[115] . However, according to Fleig et al. [24], SO_3 formation is kinetically controlled, therefore the equilibrium assumption cannot be used to predict the SO_3 formation in the post flame region (<1400 K). Hindiyarti et al. [59] proposed the following reactions as the most important reactions in SO_3 formation:

$$SO_2 + O\ (+M) \rightleftharpoons\ SO_3\ (+M) \quad (5\text{-}2)$$

$$SO_2 + OH\ (+M) \rightleftharpoons\ HOSO_2\ (+M) \quad (5\text{-}3)$$

$$HOSO_2 +\ O_2 \rightleftharpoons\ SO_3 +\ HO_2 \quad (5\text{-}4)$$

The formation of SO_3 via reaction (5-2) is important at temperatures above 1150 K due to the availability of O radicals , whereas the formation of SO_3 via reactions (5-3) and (5-4) is active at lower temperatures (<1150 K) [59]. Therefore, reaction (5-2) is not important for temperatures below 1150 K. At flue gas temperatures below 800 K, H_2SO_4 starts to form via reaction (5-5), if H_2O is present in the flue gas [116].

$$SO_3 +\ H_2O \rightleftharpoons\ H_2SO_4 \quad (5\text{-}5)$$

<u>NO_x reactions:</u>

Oxy-fuel combustion has shown promises in reducing NO_x emissions, due to the inhibition of thermal NO_x. The primary source of NO_x is oxidation of nitrogen content in the fuel. Equilibrium dictates that NO is favoured as compared to NO_2 at high temperature, whereas NO_2 production is favourable at lower temperatures, as shown in reaction (5-6) [117]:

$$NO + 0.5\ O_2\ \rightleftharpoons\ NO_2 \quad (5\text{-}6)$$

According to the experiments performed by Tsukahara et al. [53], the reaction rate for NO oxidation is likely to become significant at higher pressures and lower temperatures. NO_2 is preferable over NO in the flue gas, as NO_2 is more soluble in H_2O as compared to NO, and more likely to be removed through condensation of H_2O.

In addition to the SO_2 and NO oxidation at lower temperatures, studies have revealed a synergistic effect between SO_x and NO_x species in the post flame region, where the presence of NO_2 favours the formation of SO_3 via reaction (5-7) [61], [62]:

$$SO_2 + NO_2 \rightleftharpoons SO_3 + NO \quad (5\text{-}7)$$

Reactions (5-4) and (5-7) provide a pathway for SO_x to be removed as H_2SO_4, as the flue gas is cooled down and processed via reactive distillation.

5.1 Gas phase kinetic model

In chapter 4, CFD modelling was performed to predict the NO_x and SO_x formation in the flame zone. In order to remove SO_x and NO_x, it is important to understand the evolution of SO_x and NO_x as the flue gas is cooling down in the boiler and subsequent pipes.

In this chapter, a plug flow reactor (PFR) is modelled to simulate the reactions occurring in the flue gas. The model is simulated in Chemkin-PRO [69] software at different pressures to understand the pathway and identify the reactions that are favoured at the post flame temperatures. The kinetic mechanism used for the simulation is based on the work of Gimenez Lopez [27], and is further modified to include the SO_x – NO_x interaction [94] and formation of H_2SO_4 [95]. The detailed kinetic mechanism is shown in Appendix B.

The mass flow rate and the temperature at the inlet were kept identical to the values obtained from the CFD simulation in Chapter 4. The inlet mass flow rate and temperature used were 0.038 kg. s^{-1} and 1000 K, respectively for all the cases. Table 5-1 shows the composition (mole fraction) of the inlet flue gas at different pressures, obtained from the simulation results in Chapter 4.

Table 5-1 Flue gas composition (molar basis) at the PFR inlet at different pressures

		1 atm	5 atm	10 atm	15 atm
CO_2	mol. fr.	0.82	0.82	0.82	0.82
H_2O	mol. fr.	0.11	0.11	0.11	0.11
O_2	mol. fr.	0.05	0.05	0.05	0.05
Ar	mol. fr.	0.018	0.018	0.018	0.018
N_2	ppm	437	574	640	663
SO_2	ppm	994.25	960	953.75	934.80
NO	ppm	526	251	121	73.6
SO_3	ppm	5.75	38.3	46.2	65.2

To fully understand the behaviour of flue gas reactions, the PFR was subjected to a temperature profile (Figure 5.1), similar to that of a coal power plant [93]. It should be noted that the temperature profile applied to the PFR is shown in Figure 5.1a as a dashed line, as the high temperature analysis has been performed in the CFD model in Chapter 4. The inlet temperature is 1000 K, and the outlet temperature is around 430 K.

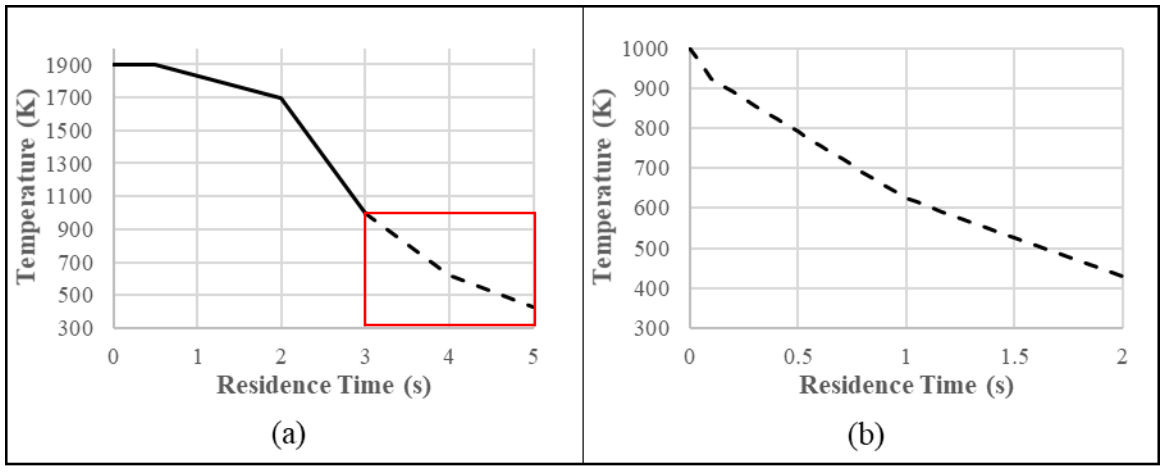

Figure 5.1 (a) represents the temperature profile of flue gas in a typical coal power plant (b) represents the enlarged view of the dashed portion of Figure 1.1 (a)

The simulations are performed in two scenarios, in order to study the effect of pressure and temperature on the reaction kinetics:

1. Fixed geometry: The dimensions of the PFR model were kept the same at all pressures, resulting in reduced volumetric flow rate and increased residence time.
2. Constant residence time: The residence time in the PFR model was kept constant at 2 s; this was achieved by reducing the diameter of the PFR and by increasing the volumetric flow rate, accordingly.

5.2 Results and discussion

5.2.1 Fixed geometry

Since the geometry for the PFR is fixed, as the pressure increases, the volumetric flow rate of the flue gas is reduced, and thus the residence time increases. Figure 5.2 shows the concentration of NO_2 across the PFR as a function of residence time at different pressures. The residence time for 1 atm was 2 s (Figure 5.1(b)). However, simulations performed at 5 atm, 10 atm and 15 atm, the residence time increased to 10 s, 20 s and 30 s, respectively, allowing for a reduced temperature gradient across the PFR as the pressure increases.

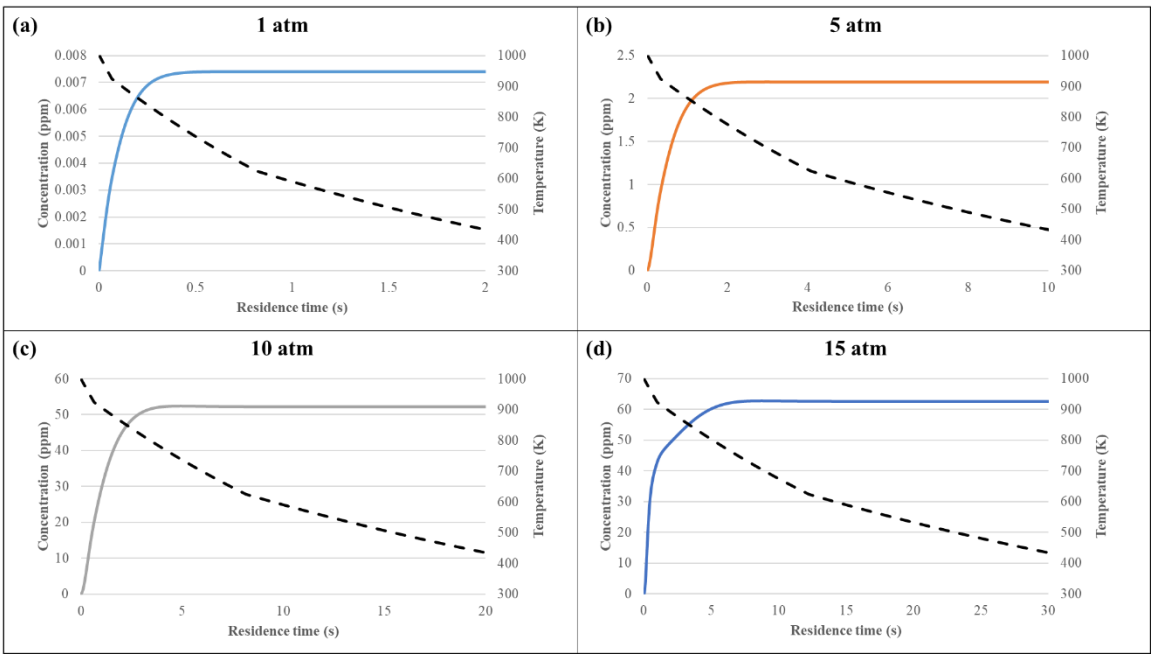

Figure 5.2 NO_2 concentration across the PFR at (a) 1 atm (b) 5 atm (c) 10 atm (d) 15 atm. The dashed line represents the temperature in K.

It is observed that NO_2 concentration increases at higher pressures, and reaches their final value at around 800 K for all pressures. It is worth noting that although the inlet NO concentrations decrease with increasing pressure (Table 5-1), NO_2 formation is favoured as pressure is increased. This highlight the major effect of pressure in the conversion of NO to NO_2, primarily due to the slower rate of temperature decrease across the PFR. Figure 5.3 shows the rate of production of NO2 at different pressures; only the reactions with non-negligible rate of formation are shown.

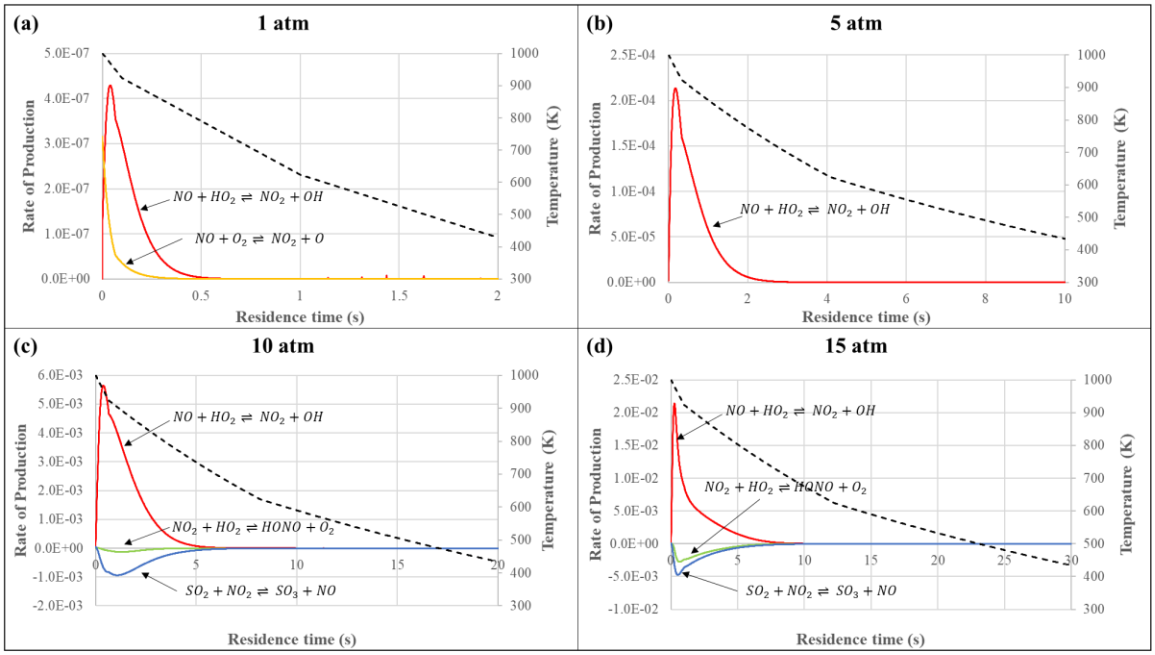

Figure 5.3 Rate of reactions (mol.m^{-3}.s^{-1}) for the production of NO_2 at (a) 1 atm (b) 5 atm (c) 10 atm (d) 15 atm. The dashed line represents temperature profile in K.

At 1 atm, it is observed (Figure 5.3a) that NO is oxidized by O_2 and HO_2 radicals at temperatures above 700 K via reactions (5-8) and (5-9). However, it is insignificant as a maximum of 0.0073 ppm NO_2 is formed, as shown in Figure 5.2(a)

$$NO + HO_2 \rightleftharpoons NO_2 + OH \quad (5\text{-}8)$$

$$NO + O_2 \rightleftharpoons NO_2 + O \quad (5\text{-}9)$$

At high pressure (Figure 5.3b-d), NO oxidation is predominately increased by reaction (5-8), Also, at high pressure NO_2 reduction to NO occurs via reactions (5-10) and (5-11)

$$NO_2 + HO_2 \rightleftharpoons HONO + O_2 \quad (5\text{-}10)$$

$$HONO\ (+M) \rightleftharpoons NO + OH\ (+M) \quad (5\text{-}11)$$

This suggests that the major pathway for NO oxidation to NO_2 is via reaction (5-8), but consumption of NO_2 by HO_2 (reaction (5-10)) increases as pressure increases (Figure 5.3c-d) [63]. The effect of synergistic interaction of SO_x and NO_x increases a pressure increase, as NO_2 is reduced to NO by reacting with SO_3 via reaction (5-7). Overall, NO oxidation is favoured as pressure is increased and almost 85% of the NO was converted to NO_2 at 15 atm.

SO_2 oxidation to SO_3 is also observed at all pressures, as shown in Figure 5.4. It was also observed that pressure has a positive effect on the production of SO_3, as SO3 concentration increased with increase in pressure. The concentration of SO_3 reached the maximum value around 800 K, before SO_3 started to react with H_2O to form H_2SO_4.

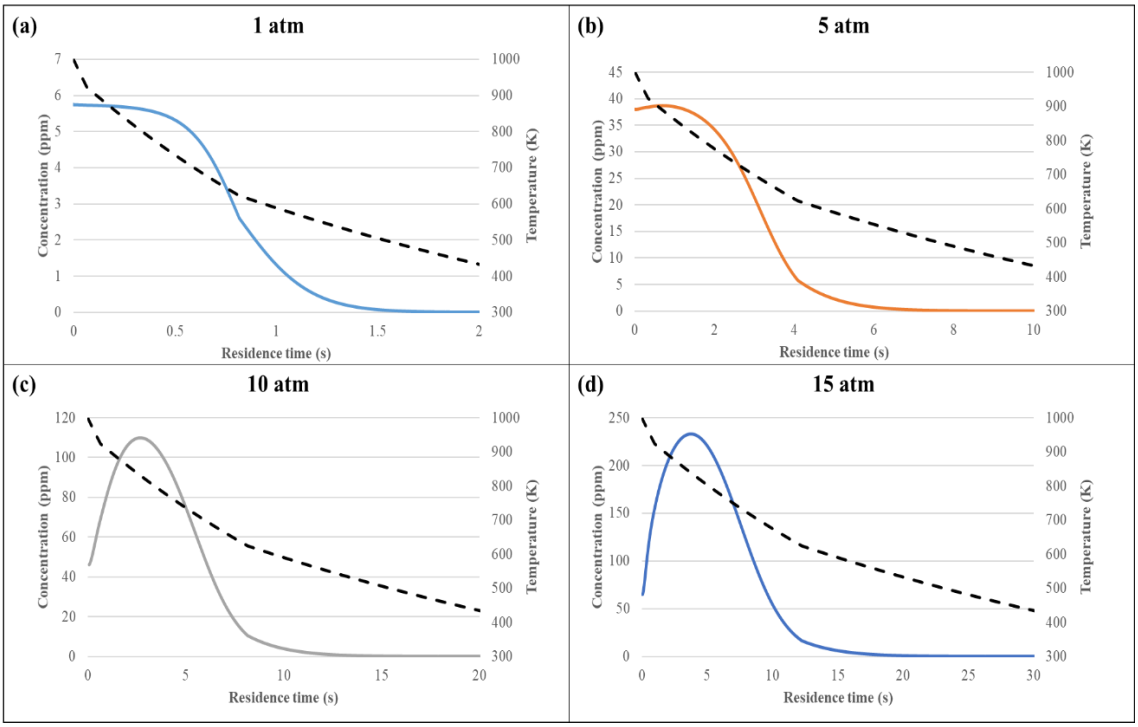

Figure 5.4 SO_3 concentration across the PFR at (a) 1 atm (b) 5 atm (c) 10 atm (d) 15 atm. The dashed line represents the temperature in K.

It was observed in Figure 5.5 that SO_3 formation is formed via reaction (5-2) above 900 K only, due to the availability of O radicals at high temperatures, but has no impact at lower temperatures. In the cooling zone, the dominant pathways for SO_3 formation is mostly through the intermediate $HOSO_2$ at temperatures between 700 K to 1000 K, via reaction (5-3) and (5-4). This is in agreement with the experiments done by Hindiyarti et al. [59], suggesting that the major pathway for SO_2 oxidation in the intermediate temperature zone is via $HOSO_2$.

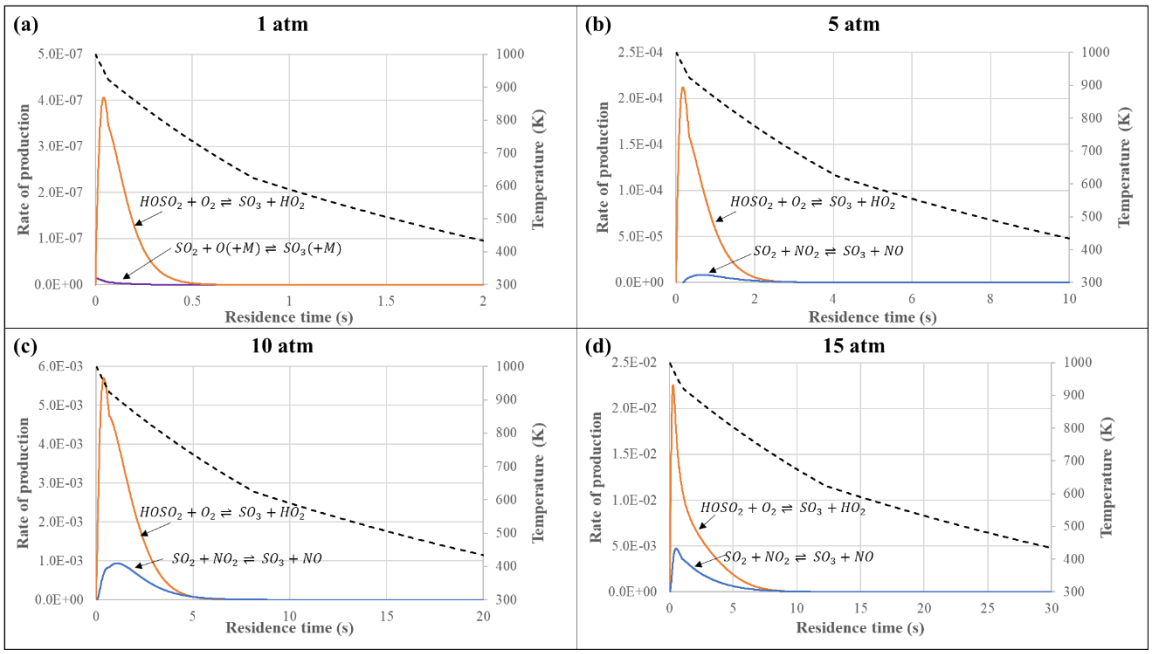

Figure 5.5 Rate of reactions (mol.m^{-3}.s^{-1}) for the production of SO_3 at (a) 1 atm (b) 5 atm (c) 10 atm (d) 15 atm. The dashed line represents temperature profile in K.

It was also observed that the rate of SO_3 formation increased with increasing pressure. As mentioned above, SO_3 formation from SO_x-NO_x interaction, reaction (5-7) increases at higher pressures, and at temperature between 1000 K to 700 K. Due to the increased pressure, the rate of formation of SO_3 is much higher between 1000 K to 700 K as compared to the rate of consumption to form H_2SO_4. This is observed only at higher pressures (10 atm, 15 atm), since at lower pressures,

the rate of consumption of SO_3 to H_2SO_4 is more dominant than the SO_2 oxidation. Below 700 K, the rate of consumption of SO_3 is dominated via reaction (5-4) to form H_2SO_4 for all the cases (Figure 5.4), and all of the SO_3 has reacted to form H_2SO_4 at low temperatures, and no SO_3 was observed at temperatures below 500 K for all the pressures.

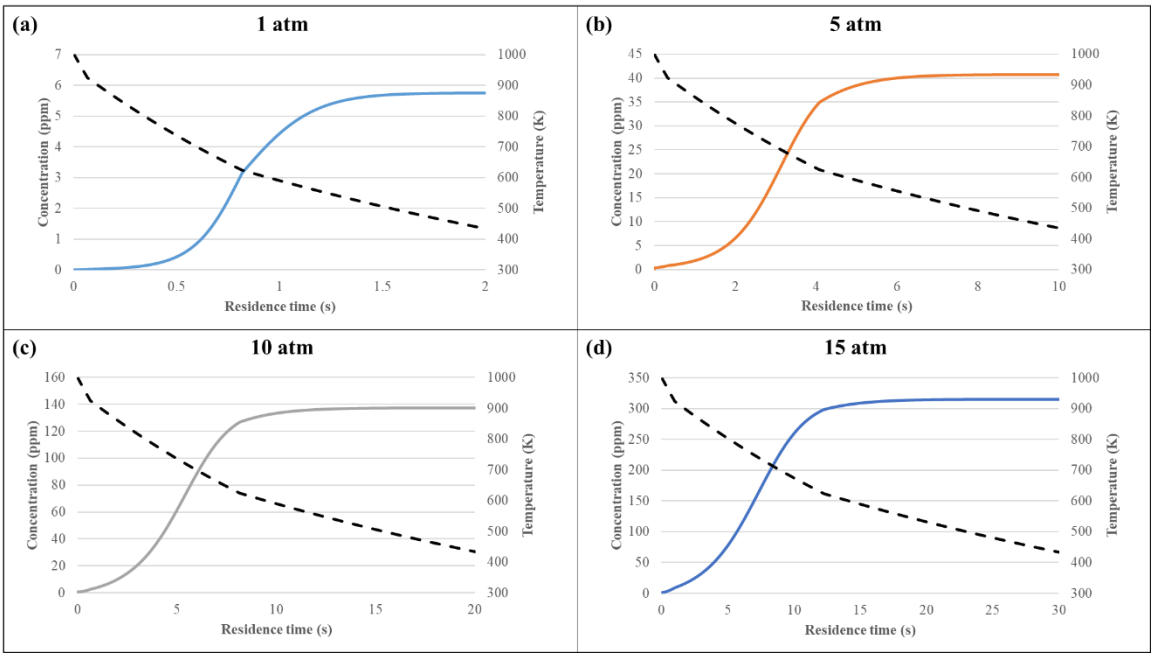

Figure 5.6 H_2SO_4 concentration across the PFR at (a) 1 atm (b) 5 atm (c) 10 atm (d) 15 atm. The dashed line represents the temperature in K

Overall, SO_2 oxidation is favoured at higher pressures as 26.7% of SO_2 is converted to SO_3/H_2SO_4 at 15 atm, as compared to less than 0.5% at 1 atm. It was also observed that almost all of the SO_3 was converted to H_2SO_4 at the outlet of PFR in all the cases. It should be noted that the acid dew point (ADP) is dependent on the concentration of H_2SO_4 and pressure, therefore increasing these properties would lead to the production of acid mist at higher temperatures. It is essential to identify the acid dew point, since there is a risk of corrosion in the equipment, due to the condensation on the walls. The ADP calculated, based on the work on Verhoff et al. [118], is

given in Table 5-2 along with the inlet and outlet concentrations, and conversions of the inlet species.

Table 5-2 Inlet and Outlet concentrations of SO_x, NO_x and H_2SO_4.

		1 atm	**5 atm**	**10 atm**	**15 atm**
NO	Inlet (ppm)	526	251	121	74
	Outlet (ppm)	526	249	69	11
	% Conversion	0.0	0.9	43.3	85.1
SO_2	Inlet (ppm)	994	972	954	935
	Outlet (ppm)	994	959	863	685
	% Conversion	0.00	1.34	9.55	26.73
SO_3	Inlet (ppm)	6	28	46	65
	Outlet (ppm)	0.001	0.002	0.003	0.005
	% Conversion	99.98	99.99	99.99	99.99
NO_2	Outlet (ppm)	0	2	52	63
H_2SO_4	Outlet (ppm)	6	41	138	315
Acid dew point	K	387.6	443.86	472.83	491.06

5.2.2 Constant residence time

As mentioned earlier, the increase in pressure reduces the volumetric flow rate, causing the flue gas to have more residence time in the reactor. In a conventional power plant, the flue gas temperature drops from 1000 K to 423 K within 2 seconds (Figure 5.1). So, to avoid the effect of residence time on the flue gas reactions, the diameter of the PFR is reduced, such that the residence time remains constant at 2 s for all the pressure conditions. The inlet mass flow rate was 0.038 $kg.s^{-1}$ and the composition of the flue gas used are given in Table 5-1. The dimensions of the PFR at different pressures are given in Table 5-3.

Table 5-3 Dimensions used for the PFR model at different pressures

		1 atm	**5 atm**	**10 atm**	**15 atm**
Residence time	*(s)*	2	2	2	2
Length	*(m)*	2	2	2	2
Diameter	*(m)*	0.25	0.112	0.078	0.064
Reduction	*(% vol.)*	-	80%	90%	93%

Figure 5.7 shows the concentration of NO_2 across PFR. It was observed that reducing the residence time at higher pressures have resulted in negligible oxidation of NO to NO_2. At a given residence time, the temperature dropped rapidly, resulting in the low oxidation of NO to NO_2,at temperatures between 800 K – 1000 K. NO_2 concentrations plateaued below 800 K, suggesting no more reaction occurred. Although there is an increase in the NO_2 formation as pressure increased, it was not significant to remove NO from the flue gas.

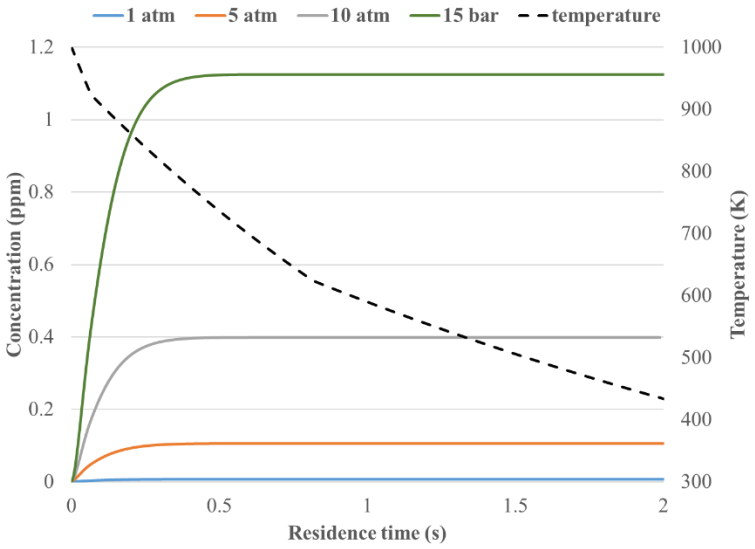

Figure 5.7 NO_2 concentration in the PFR at different pressures

Figure 5.8 shows the SO_3 and H_2SO_4 concentration at different pressures. It was observed that there was no net increase in the SO_3 concentration, suggesting that there was insignificant SO_2 oxidation, as the rate of production of SO_3 was significantly lower than the rate of consumption of SO_3 to H_2SO_4 via reaction (5-5). SO_3 gradually reacts to form H_2SO_4, as this reaction is favourable at lower temperatures via reaction (5-5).

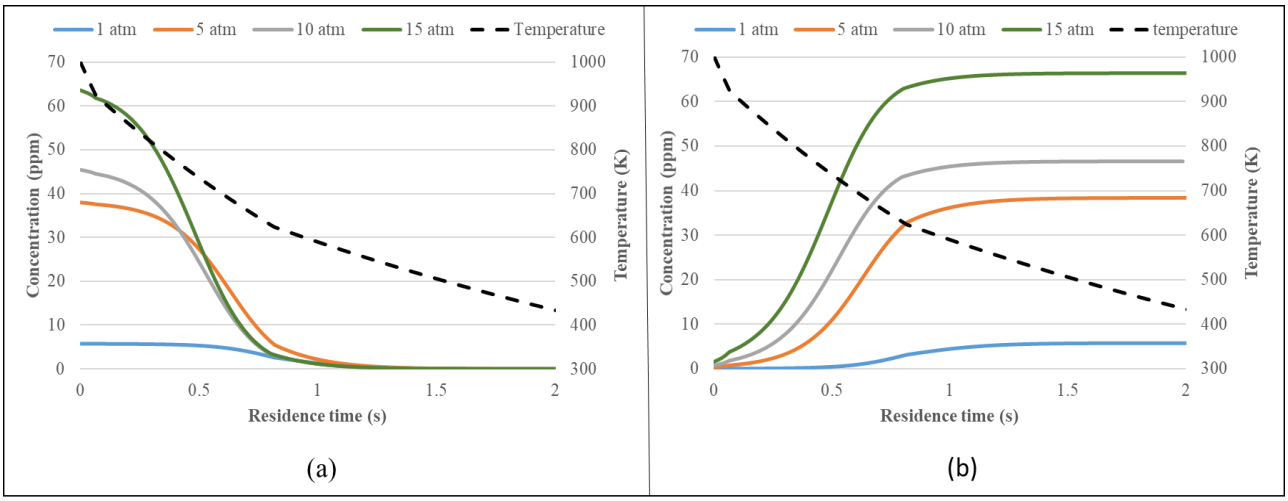

Figure 5.8 (a) SO_3 concentration and (b) H_2SO_4 concentration in the PFR at different pressures.

In this study, it was observed that increased pressures and a residence time of 2 s, has insignificant effect on the SO_2 and NO conversion to SO_3 and NO_2. The only significant reaction that takes place in this domain is the formation of sulphuric acid due to the reaction between SO_3 and H_2O as the flue gas is cooling down. The concentration of H_2SO_4 plateaued around 550 K, suggesting that almost all of the SO_3 in the flue gas has converted to H_2SO_4, irrespectively of pressure. Table 5-4 shows the concentrations of NO_x, SO_x and H_2SO_4 at the inlet and outlet of the PFR.

Table 5-4 Inlet/Outlet concentrations of SO_x, NO_x and H_2SO_4.

		1 atm	**5 atm**	**10 atm**	**15 atm**
NO	Inlet (ppm)	526.0	251.1	121.0	73.6
	Outlet (ppm)	526.0	251.0	120.6	72.5
	% Conversion	**0.00**	**0.04**	**0.33**	**1.50**
SO_2	Inlet (ppm)	994.3	972.4	953.8	934.8
	Outlet (ppm)	994.3	972.1	953.5	933.7
	% Conversion	**0.00**	**0.03**	**0.03**	**0.12**
SO_3	Inlet (ppm)	5.8	38.0	46.2	65.2
	Outlet (ppm)	0.00	0.00	0.00	0.00
	% Conversion	**100.0**	**100.0**	**100.0**	**100.0**
NO_2	Outlet (ppm)	0.01	0.11	0.40	1.12
H_2SO_4	Outlet (ppm)	5.8	38.4	46.6	66.4
ADP	K	387.6	443.1	461.2	474.2

In conclusion, this study shows that elevated pressures enhance the SO_2 and NO oxidation to SO_3 and NO_2 in the flue gas as it is cooling down. It was also found out that these reactions are highly dependent on the rate of change of temperature (cooling rate across the PFR). At constant residence time, the effect of pressure on SO_2 and NO oxidation becomes insignificant, since the temperature dropped rapidly, prohibiting the oxidation of NO and SO_2 at high temperature. Therefore, it is important that more focus should be given to develop a boiler for pressurized oxy-fuel combustion, that allows residence time for SO_2 and NO oxidation in the flue gas.

6 Removal of SO_x and NO_x in the absorber column

The main motivation behind using oxy-fuel technology is to maximize the CO_2 content in the flue gas for easy separation and to eliminate complex post-combustion processes (such as amine scrubbing, etc.). However, the flue gas from oxy-fuel combustion contains several impurities and at different levels, depending on the fuel, and therefore additional purification steps are needed to achieve the final specification of CO_2 stream for transportation [119].

In oxy-fuel combustion of coal, the impurities in the flue gas consists of moisture, SO_x, NO_x and non-condensable gases such as N_2, O_2 and argon. The removal of moisture can be achieved by cooling and compression, along with adsorption stage to achieve the desired level of moisture in the flue gas prior to cryogenic process. The non-condensable gases are removed by liquefaction and phase separation of flue gas in the cryogenic process.

Traditionally, SO_x and NO_x removal has been achieved in the power industry through flue gas desulphurization (FGD) and selective catalytic reduction (SCR), respectively. The main drawback of these technologies is the additional cost of the equipment and raw material. Therefore, a novel method has been proposed to remove NO_x and SO_x from the flue gas as acid during CO_2 compression [120].

The removal of SO_x and NO_x via absorption, also known as sour-compression method, in oxy-fuel plant has been investigated [29], [65], [67], [121], [122], and compared with conventional primary and secondary removal methods [117]. The process allows the removal of SO_x and NO_x by the means of reactive and pressurized absorption of water and represents a pathway for SO_x to be removed as H_2SO_4, whereas NO_x can be removed as HNO_3 dissolved in water.

In all the studies published on the removal of SO_x and NO_x via absorption, the flue gas from the combustion is at atmospheric pressure, which requires compression in order to be at the required operating pressure of the absorber. Since, pressurized oxy-fuel combustion is already at elevated pressure, the cost for compression can be reduced or even eliminated.

This chapter evaluates the integrated removal of SO_x and NO_x from flue gases of pressurized oxy-fuel combustion using a sour compression unit (SCU).

6.1 Design specifications

In this study, the design specifications have been adapted from Air Product [96], ensuring the adequate hydrodynamic conditions are met. The parameters used in the model for the absorber column are specified in Table 3-1. The reaction mechanism utilized (Table 3-2) for the gas and liquid reactions is based on the work of Meunier et al. [29].

In this study, the flue gas composition and conditions are based on the results in Chapter 5 for pressurized oxy-fuel combustion at 15 atm. It is important to note that the flue gas temperature should be kept above the acid dew point temperature at the given composition and pressure. Therefore, a conservative temperature of 533K was chosen to prevent acid condensation in the flue gas ducts and piping [17]. Since, in the case for combustion at 15 atm, no compression is required, therefore the risk of acid condensation in the compressor is also eliminated.

Given the lack of consensus amongst experts on the required specifications of SO_x and NO_x in the flue gas for CO_2 transportation in pipeline, the purification model in this study utilizes recommended maximum values of 100 ppm for both SO_x and NO_x as suggested by Visser et al. [123]. Since NO_x concentration at 15 atm is already below 100 ppm in the flue gas, the aim is to reduce the concentration of SO_x in order to meet the pipeline specifications.

To simulate the model, ASPEN Plus process simulator was used [70]. The details on methodology for this process are mentioned in Chapter 3, including the blocks and the equation of state (EOS) utilized for the simulations.

The base model used for this study is a single column absorber at 15 atm based on Air Liquid [96]. The liquid to gas ratio (per mass basis) of 3 was maintained in the column. The product from the liquid stream from the outlet of the absorber is mixed with fresh water at 298 K and recycled back to the absorber.

6.2 Results and Discussion

For the base model, with liquid recycle of 90%, the results of the outlets are shown in Table 6-1.

Table 6-1 Composition (molar basis) of the inlet and outlet products in the absorber column

		Gas Inlet	**Gas Outlet**	**Liquid Outlet**
Temperature (K)		533	391.4	401.97
Temperature (°C)		260	118.4	128.97
Major species	CO_2	0.82	0.799	0.001
	H_2O	0.11	0.134	0.99
	O_2	0.05	0.049	9 ppm
	Ar	0.018	0.017	181 ppm
	N_2	663 ppm	647 ppm	78.5 ppb
SO_x **species**	SO_2	934 ppm	traces	traces
	SO_3	0	traces	traces
	H_2SO_4	66.4 ppm	traces	traces
	SO_4^{2-}			24 ppm
	HSO_4^-			0.0015
NO_x **species**	NO	73 ppm	50.6 ppm	16.3 ppb
	NO_2	1 ppm	2.6 ppb	traces
	HNO_3		traces	31 ppm
	HNO_2		92.4 ppb	1 ppm
	NO_3^-			1.3 ppm

*Traces refer to concentrations below 1 ppb.

It should be noted from the results that there has been 100% SO_x removal in the gas leaving the absorber. Most of the SO_x has converted to acids in the liquid phase, mainly H_2SO_4 in its ionic form, SO_4^{2-} and HSO_4^-. This suggests that SO_2 conversion to SO_3 has occurred in the absorber, mainly through SO_2 oxidation via reacting with O_2 and also with NO_2.

For NO_x, removal, it was observed that only 29% of the NO was removed, whereas almost 99% of NO_2 was removed in the outlet, with less than 3 ppb of NO_2 present in the outlet. It should be noted that there was an insignificant amount of N_2O_3 and N_2O_4 that remained in the gas phase. This suggests that under these conditions the oxidation of NO to NO_2 in the gas phase has little impact the reduction of NO. in the liquid phase, the major NO_x species were HNO_2, HNO_3 and NO_3^{2-}, suggesting that most of the NO_2, and N_2O_4 dissolved in the liquid converted to form acids.

As the flue gas introduced in the absorber was at 533 K, the overall temperature in the absorber was much higher. It can be seen that the moisture content in the outlet has increased to 13% due to the high temperature in the absorber. The moisture can be removed from the exiting flue gas by a condenser before sending it for further purification, since there is no risk of corrosion in the condenser due to the absence of SO_x species. Secondly, since most of the NO_x reactions involved are exothermic, higher temperatures reduce the conversion significantly in this case.

Overall, SO_x emissions were curtailed, and the NO_x emissions have reduced down to 50 ppm. However, the overall conversion of NO_x to be removed as acids was lower, primarily due to the high absorber recycle stream of 90%.

6.3 Effect of recycle ratio on NO_x and SO_x removal

In the SO_x and NO_x absorption, one of the important factor that needs to be considered is the liquid re-use of the liquid product for absorption. The liquid in the absorber, primarily works as a solvent for the impurities, and also helps reduce the temperature of the flue gas.

A sensitivity analysis was performed on the recycle ratio of the absorber to understand the effect of recycle ratio on the removal of SO_x and NO_x from the flue gas. It was observed that almost all of the gaseous SO_x was removed from the flue gas in all cases. However, NO_x removal was found to be dependent on the recycle ratio. Figure 6.1 shows the results for NO_x removal at different recycle ratios.

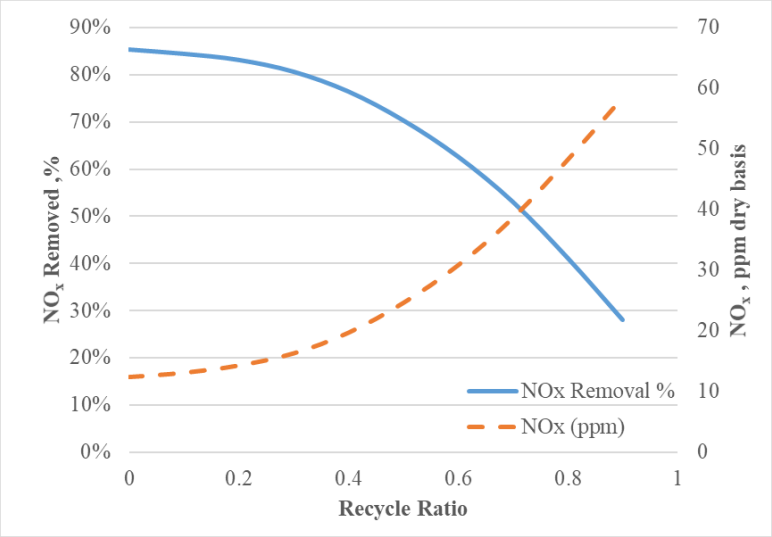

Figure 6.1 NO_x removal and NO_x concentration in the flue gas at different recycle ratio

It can be observed that increasing the recycle ratio decreases the removal of NO_x from the flue gas. It is observed that the maximum removal achieved for NO_x is around 85% and can be achieved when the liquid stream in the absorber is comprised of only fresh water. A significant decrease in the removal was observed when the recycle ratio is higher than 50%. As more liquid

is recycled back into the absorber, the temperature in the absorber was also increased. Figure 6.2 shows the temperature profile of the liquid and gas at the absorber outlet.

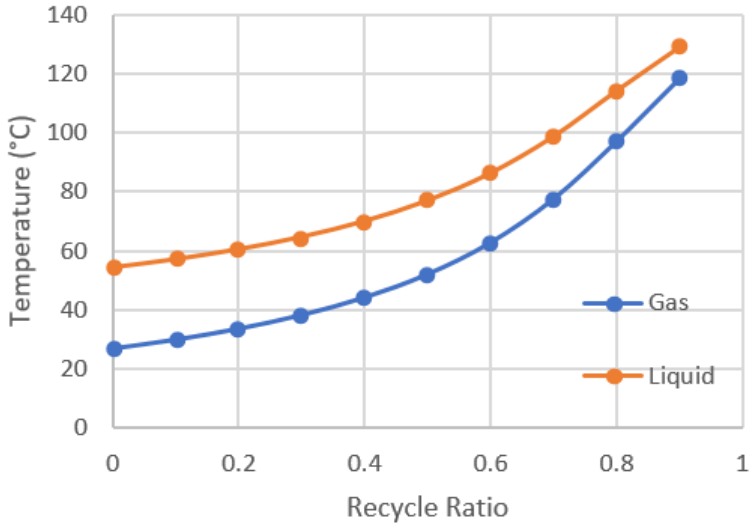

Figure 6.2 Temperature profiles of gas and liquid in the absorber at different recycle ratio

The analysis suggests that NO_x conversion to acids is highly dependent on the temperature in the absorber. As seen in Figure 6.1 and Figure 6.2, NO_x is removed from the flue gas more effectively when the temperature in the absorber is less. This is important in cases when NO_x concentration in the flue gas are higher than 100 ppm, then it would be necessarily to remove NO_x to meet the specifications for NO_x for transport and storage.

In this study, the main aim was to utilize an existing design of the absorber to remove SO_x and NO_x from pressurized oxy-fuel combustion, without any modification to the existing design. It can be seen that the objective of SO_x and NO_x reduction to pipeline specifications was achieved. NO_x removal is dependent on the temperature in the absorber. An increase in the removal of NO_x can be achieved by decreasing the recycle ratio of the liquid, as shown in the analysis. The method is also highly inefficient in terms of heat transfer as the hot flue gas enters the absorber at

approximately 533 K, to avoid acid dew point, and higher quantity of water is needed to cool down the flue gas in the absorber for increased NO_x removal. Therefore, a better design of the absorber column is needed to avoid material and heat losses in the process.

7 Conclusions and recommendations

7.1 Conclusions

This thesis focused on coal combustion in pressurized oxy-fuel environment and the effect of pressure on the formation of SO_x and NO_x and their removal from the flue gas to meet the pipeline specifications for CO_2 transport. In order to understand the impact of pressure on SO_x and NO_x formation and removal, the investigation was divided into three main tasks:

i. Combustion of coal in oxy-fuel environment, to understand the formation of SO_x and NO_x in the flame zone at different pressures,
ii. Reactions in the flue gas as its temperature decreases from 1000 K (post-combustion) to 423 K (boiler exit), using detailed kinetic mechanism in a plug flow reactor,
iii. Removal of SO_x and NO_x from the flue gas via water absorption, to meet the SO_x and NO_x concentration requirements for pipeline transportation.

A numerical model for oxy-combustion was developed in ANSYS Fluent CFD [68] to study the effect of pressure on the coal combustion and the production of SO_x and NO_x at pressures up to 15 atm. The model was validated by simulating the oxy-fuel combustion of lignite coal at atmospheric pressure and comparing the experimental results from Andersson et al.[109]. After validation, the oxy-fuel combustion of coal was simulated using the same thermal input but at elevated pressures of 5, 10 and 15 atm. It was observed that overall SO_x emissions remain the same, when O_2 was in excess in the flue gas. However, as the pressure increased in the combustor, the concentration of SO_3 increased as well, suggesting that more SO_2 converted to SO_3 at higher pressures. On the other hand, NO_x emissions were noticeably reduced by 85% at 15 atm, as

compared to atmospheric pressure. At 15 atm, NO_x was well below the maximum allowed concentration of 100 ppm in the flue gas for pipeline transportation. The reduction of NO_x with increasing pressure is found to be related to the reduction in equilibrium concentration of O radicals during combustion.

The flue gas from the combustor is used to heat the steam in a thermal power plant, where the heat from the flue gas is extracted. In order to mimic these conditions, a plug flow reactor with a temperature profile similar to that of a real coal power plant [93] was modelled as a one-dimensional plug flow reactor in Chemkin-PRO [69], using the reaction mechanism based on the work of Gimenez-Lopez [124]. The effect of pressure on the conversion of SO_x and NO_x were investigated under reducing temperature profile. In the case when a constant geometry was used for all pressures, the results showed that at higher pressure, the temperature was reduced along the reactor at a lower rate, giving more time for the reactions to occur at higher temperatures. As the pressure was increased, there was higher conversion of SO_2 and NO to SO_3 and NO_2, respectively. It was also seen that almost all of the SO_3 was converted to H_2SO_4 below 550 K in the gas phase. A more realistic model with a constant residence time of 2 s at all pressures was simulated to observe the effect of pressure on SO_x and NO_x. At constant residence time, the rate of temperature drop for all pressure cases remained the same. It was observed that there is small amount of oxidation of SO_2 (1.5%) and NO (0.12%) at 15 atm. This suggests that the major influence on the oxidation of SO_2 and NO to SO_3 and NO_2 in the flue gas is due to the rate of temperature drop in the reactor, as compared to pressure. In addition to this, the increased amount of SO_3 in the flue gas at higher pressures resulted in an increase in acid dew point temperature of the flue gas, 388 K at 1 atm to 475 K at 15 atm, which can increase the risk of corrosion. Therefore, the temperature

in the process has to be kept above the acid dew point temperature to avoid condensation, which could in turn result in energy losses.

The study finally discussed the removal of SO_x and NO_x using reactive absorption. The model for the absorber was based on the work of Meunier et al. [29], using water to remove the SO_x and NO_x from the flue gas at 15 atm. The inlet temperature of the flue gas was kept at 533 K, to avoid the risk of acid condensation in the flue gas. The results showed complete removal of SO_2 and H_2SO_4 during the process converting them into H_2SO_4, HSO_4^- and SO_4^{2-}. NO_x, however, was not completely removed but the level of NO_x was already 100 ppm at 15 atm, which is acceptable for pipeline specifications for CO_2 transportation. The sensitivity analysis for the recycled ratio of the liquid for absorption showed that the efficiency of NO_x removal can be increased by reducing the recycle ratio, mainly to decrease the temperature in the absorber, which could improve the reactions of NO_x in the liquid phase.

Overall, the results showed that pressurized oxy-fuel combustion is an effective method of combustion for CCS, as increasing the pressure resulted in a flue gas, that can be processed and purified utilizing a simple method of NO_x and SO_x removal in the downstream processes. A downside of pressurized oxy-fuel combustion is the higher concentration of SO_3 and the increased acid dew point, that could result in energy loss, as the flue gas needs to be maintained above a higher acid dew-point temperature in the process.

7.2 Recommendations

Pressurized oxy-fuel combustion for coal combustion has recently gained attention of the researchers due to its potential in carbon capture and sequestration. Therefore, there has not been much experimental work done on this subject. Experiments on coal combustion under oxy-fuel environment at elevated pressures can provide insight into the effect of devolatilization rate and flame propagation. It is of great importance to understand these variables, and the ignition characteristics of coal ignition in pressurized oxy-fuel combustion as they are essential for an effective design of the combustor. Due to the limitation in the computational cost, simplified combustion models was used for the simulations. Further work can be done to improve the combustion model by integrating a more complex combustion model, such as Eddy Dissipation Concept (EDC) model to incorporate detailed chemistry for combustion and SO_x-NO_x formation in the CFD model.

In addition, higher pressure in oxy-fuel combustion can allow reduction in the size of the combustor, due to lower volume in the combustor. A sensitivity analysis on the sizing of the combustion can identify the optimum size of the combustor for better performance and also allow small size reactors for power generation.

As it was discussed, NO_x and SO_x oxidation reactions in the flue gas are more influenced by the rate of temperature decrease, rather than pressure, therefore it is worth looking to improve the rate of temperature decrease that can increase the performance of the NO oxidation to NO_2, since NO_2 can be removed via absorption using less energy. However, slower rate of temperature decrease could affect the thermal efficiency of the boiler, therefore an optimization analysis should be performed that can improve the overall performance of the oxy-fuel combustion power plant.

Since it was found that at higher pressures, SO_3 production is more favourable and the acid dew point temperature is much higher in the flue gas, therefore, materials for the piping and equipment should be taken into consideration that are less prone to corrosion at the given temperatures. Secondly, energy losses are incurred due to the higher temperature (above acid dew point temperature) in the flue gas to avoid condensation of H_2SO_4. Therefore, process intensification through indirect heat exchangers for flue gas latent heat recovery can increase the plant efficiency by recuperating the heat from condensation before the flue gas is processed for SO_x and NO_x removal in the absorption column.

References

[1] British Petroleum Company, “BP Statistical Review of World Energy,” London, 2018.

[2] IEA, “CO2 Emissions from Fuel Combustion 2017,” Paris, 2017.

[3] IPCC, “Climate Change 2014: Synthesis Report. Contribution of Working Groups I, II and III to the Fifth Assessment Report of the Intergovernmental Panel on Climate Change,” Geneva, Switzerland, 2014.

[4] S. Ansolabehere, “The Future of Coal: Options for a Carbon-Constrained World,” Cambridge, 2007.

[5] B. Metz, O. Davidson, H. de Coninck, M. Loos, and L. Meyer, “IPCC Special Report on Carbon Dioxide Capture and Storage,” Cambridge, UK, 2010.

[6] IEA, “World Energy Outlook 2018,” Paris, 2018.

[7] T. F. Wall, “Combustion processes for carbon capture,” *Proc. Combust. Inst.*, vol. 31, no. 1, pp. 31–47, 2007.

[8] L. Zheng, *Oxy-fuel combustion for power generation and carbon dioxide (CO2) capture*. Oxford: Woodhead Publishing, 2011.

[9] B. M. Abraham, J. G. Asbury, E. P. Lynch, and A. P. S. Teotia, “Coal-oxygen process provides CO2 for enhanced recovery,” *Oil Gas J.*, vol. 80, no. 11, pp. 68–70, 1982.

[10] F. L. Horn and M. Steinberg, “Control of carbon dioxide emissions from a power plant (and use in enhanced oil recovery),” *Fuel*, vol. 61, no. 5, pp. 415–422, 1982.

[11] C. Breidenich, D. Magraw, A. Rowley, and J. W. Rubin, “The Kyoto Protocol to the United Nations Framework Convention on Climate Change,” *Am. J. Int. Law*, vol. 92, no. 2, pp. 315–331, 1998.

[12] M. B. Toftegaard, J. Brix, P. A. Jensen, P. Glarborg, and A. D. Jensen, “Oxy-fuel combustion of solid fuels,” *Prog. Energy Combust. Sci.*, vol. 36, no. 5, pp. 581–625, 2010.

[13] B. J. P. Buhre, L. K. Elliott, C. D. Sheng, R. P. Gupta, and T. F. Wall, “Oxy-fuel combustion technology for coal-fired power generation,” *Prog. Energy Combust. Sci.*, vol. 31, no. 4, pp.

283–307, 2005.

[14] H. Hagi, M. Nemer, Y. Le Moullec, and C. Bouallou, “Towards second generation oxy-pulverized coal power plants: Energy penalty reduction potential of pressurized oxy-combustion systems,” *Energy Procedia*, vol. 63, pp. 431–439, 2014.

[15] A. Gopan, B. M. Kumfer, and R. L. Axelbaum, “Effect of operating pressure and fuel moisture on net plant efficiency of a staged, pressurized oxy-combustion power plant,” *Int. J. Greenh. Gas Control*, vol. 39, pp. 390–396, 2015.

[16] R. Soundararajan and T. Gundersen, “Coal based power plants using oxy-combustion for CO2 capture: Pressurized coal combustion to reduce capture penalty,” *Appl. Therm. Eng.*, vol. 61, no. 1, pp. 115–122, 2013.

[17] J. Hong, R. Field, M. Gazzino, and A. F. Ghoniem, “Operating pressure dependence of the pressurized oxy-fuel combustion power cycle,” *Energy*, vol. 35, no. 12, pp. 5391–5399, 2010.

[18] J. Hong, G. Chaudhry, J. G. Brisson, R. Field, M. Gazzino, and A. F. Ghoniem, “Analysis of oxy-fuel combustion power cycle utilizing a pressurized coal combustor,” *Energy*, vol. 34, no. 9, pp. 1332–1340, 2009.

[19] A. Gopan, B. M. Kumfer, and R. L. Axelbaum, “Effect of operating pressure and fuel moisture on net plant efficiency of a staged, pressurized oxy-combustion power plant,” *Int. J. Greenh. Gas Control*, vol. 39, pp. 390–396, 2015.

[20] J. Hong, A. F. Ghoniem, R. Field, and M. Gazzino, “Techno-economic evaluation of pressurized oxy-fuel combustion systems,” in *International Mechanical Engineering Congress and Exposition, IMECE 2010*, 2010, pp. 577–585.

[21] R. Stanger and T. Wall, “Sulphur impacts during pulverised coal combustion in oxy-fuel technology for carbon capture and storage,” *Prog. Energy Combust. Sci.*, vol. 37, no. 1, pp. 69–88, 2011.

[22] E. Croiset and K. V. Thambimuthu, “NOx and SO2 emissions from O2/CO2 recycle coal combustion,” *Fuel*, vol. 80, no. 14, pp. 2117–2121, 2001.

[23] L. T. Murciano, V. White, F. Petrocelli, and D. Chadwick, “Sour compression process for the removal of SOx and NOx from oxyfuel-derived CO2,” *Energy Procedia*, vol. 4, pp. 908–916, 2011.

[24] D. Fleig, K. Andersson, F. Normann, and F. Johnsson, “SO3 Formation under oxyfuel combustion conditions,” *Ind. Eng. Chem. Res.*, vol. 50, no. 14, pp. 8505–8514, 2011.

[25] L. Chen, S. Z. Yong, and A. F. Ghoniem, “Modeling the slag behavior in three dimensional CFD simulation of a vertically-oriented oxy-coal combustor,” *Fuel Process. Technol.*, vol. 112, pp. 106–117, 2013.

[26] F. Xia, Z. Yang, A. Adeosun, A. Gopan, B. M. Kumfer, and R. L. Axelbaum, “Pressurized oxy-combustion with low flue gas recycle: Computational fluid dynamic simulations of radiant boilers,” *Fuel*, vol. 181, pp. 1170–1178, 2016.

[27] J. Giménez-López, M. Martínez, A. Millera, R. Bilbao, and M. U. Alzueta, “SO2effects on CO oxidation in a CO2atmosphere, characteristic of oxy-fuel conditions,” *Combust. Flame*, 2011.

[28] N. N. Choudhury and B. Padak, “A comprehensive experimental and modeling study of sulfur trioxide formation in oxy-fuel combustion,” *Int. J. Greenh. Gas Control*, vol. 51, pp. 165–175, 2016.

[29] N. Meunier, S. Laribi, L. Dubois, D. Thomas, and G. De Weireld, “CO2capture in cement production and re-use: First step for the optimization of the overall process,” *Energy Procedia*, vol. 63, pp. 6492–6503, 2014.

[30] R. H. Essenhigh, M. K. Misra, and D. W. Shaw, “Ignition of coal particles: A review,” *Combust. Flame*, vol. 77, no. 1, pp. 3–30, 1989.

[31] K. Andersson, R. Johansson, S. Hjärtstam, F. Johnsson, and B. Leckner, “Radiation intensity of lignite-fired oxy-fuel flames,” *Exp. Therm. Fluid Sci.*, vol. 33, no. 1, pp. 67–76, 2008.

[32] G. Krishnamoorthy, M. Sami, S. Orsino, A. Perera, M. Shahnam, and E. D. Huckaby, “Radiation modelling in oxy-fuel combustion scenarios,” *Int. J. Comut. Fluid Dyn.*, vol. 24, no. 3–4, pp. 69–82, 2010.

[33] K. Andersson and F. Johnsson, “Flame and radiation characteristics of gas-fired O2/CO2 combustion,” *Fuel*, vol. 86, no. 5–6, pp. 656–668, 2007.

[34] E. Croiset, K. Thambimuthu, and A. Palmer, “Coal combustion in O2/CO2 mixtures compared with air,” *Can. J. Chem. Eng.*, vol. 78, no. 2, pp. 402–407, 2000.

[35] L. Chen, S. Z. Yong, and A. F. Ghoniem, “Oxy-fuel combustion of pulverized coal: Characterization, fundamentals, stabilization and CFD modeling,” *Prog. Energy Combust. Sci.*, vol. 38, no. 2, pp. 156–214, 2012.

[36] R. Stanger *et al.*, “Oxyfuel combustion for CO2 capture in power plants,” *Int. J. Greenh. Gas Control*, vol. 40, pp. 55–125, 2015.

[37] T. Wall, R. Stanger, and S. Santos, “Demonstrations of coal-fired oxy-fuel technology for carbon capture and storage and issues with commercial deployment,” *Int. J. Greenh. Gas Control*, vol. 5, pp. S5–S15, 2011.

[38] C. Yin and J. Yan, “Oxy-fuel combustion of pulverized fuels: Combustion fundamentals and modeling,” *Appl. Energy*, vol. 162, pp. 742–762, 2016.

[39] P. Edge *et al.*, “Combustion modelling opportunities and challenges for oxy-coal carbon capture technology,” *Chem. Eng. Res. Des.*, vol. 89, no. 9, pp. 1470–1493, 2011.

[40] L. Chen and A. F. Ghoniem, “Simulation of oxy-coal combustion in a 100 kW test facility using RANS and LES: A validation study,” *Energy and Fuels*, vol. 26, pp. 4783–4798, 2012.

[41] D. Toporov *et al.*, “Detailed investigation of a pulverized fuel swirl flame in CO2/O2 atmosphere,” *Combust. Flame*, vol. 155, no. 4, pp. 605–618, 2008.

[42] A. H. Al-Abbas and J. Naser, “Effect of chemical reaction mechanisms and NOx modeling on air-fired and oxy-fuel combustion of lignite in a 100-kW furnace,” *Energy and Fuels*, vol. 26, no. 6, pp. 3329–3348, 2012.

[43] L. Chen, M. Gazzino, and A. F. Ghoniem, “Characteristics of Pressurized Oxy-Coal Combustion Under Increasing Swirl Number,” in *35th International Technical Conference on Coal Utilization & Fuel Systems*, 2010, pp. 161–172.

[44] L. Chen, “Computational fluid dynamics simulations of oxy-coal combustion for carbon capture at atmospheric and elevated pressures,” 2013.

[45] A. Gopan, B. M. Kumfer, J. Phillips, D. Thimsen, R. Smith, and R. L. Axelbaum, “Process design and performance analysis of a Staged, Pressurized Oxy-Combustion (SPOC) power plant for carbon capture,” *Appl. Energy*, vol. 125, pp. 179–188, 2014.

[46] F. Xia, Z. Yang, A. Adeosun, A. Gopan, B. M. Kumfer, and R. L. Axelbaum, “Pressurized oxy-combustion with low flue gas recycle: Computational fluid dynamic simulations of radiant boilers,” *Fuel*, vol. 181, pp. 1170–1178, 2016.

[47] G. S. B Dhungel, P Mönckert, J Maier, “Investigation of oxy-coal combustion in semi-technical test facilities,” *Third Int. Conf. Clean Coal Technol. our Futur.*, vol. 5, pp. 15–17, 2007.

[48] Y. B. Zeldovich, “The Oxidation of Nitrogen in Combustion and Explosions,” *Acta Physicochim. U.S.S.R*, vol. 21, pp. 577–628, 1946.

[49] G. G. De Soete, E. Croiset, and J.-R. Richard, “Heterogeneous formation of nitrous oxide from char-bound nitrogen,” *Combust. Flame*, vol. 117, no. 1–2, pp. 140–154, 1999.

[50] Y. Q. Hu, N. Kobayashi, and M. Hasatani, “The reduction of recycled-NOx in coal combustion with O2/recycled flue gas under low recycling ratio,” *Fuel*, vol. 80, no. 13, pp. 1851–1855, 2001.

[51] H. Cao, S. Sun, Y. Liu, and T. F. Wall, “Computational fluid dynamics modeling of NOx reduction mechanism in oxy-fuel combustion,” *Energy and Fuels*, vol. 24, no. 1, pp. 131–135, 2010.

[52] L. Álvarez *et al.*, “CFD modeling of oxy-coal combustion: Prediction of burnout, volatile and NO precursors release,” *Appl. Energy*, vol. 104, pp. 653–665, 2013.

[53] H. Tsukahara, T. Ishida, and M. Mayumi, “Gas-Phase Oxidation of Nitric Oxide: Chemical Kinetics and Rate Constant,” *Nitric Oxide*, vol. 3, no. 3, pp. 191–198, 1999.

[54] M. Thiemann, E. Scheibler, and K. W. Wiegand, “Nitric Acid, Nitrous Acid, and Nitrogen Oxides,” in *Ullmann’s Encyclopedia of Industrial Chemistry*, Amsterdam, Netherland:

Wiley-VCH, 2000.

[55] P. Adolphi, M. Störr, P. G. Mahlberg, H. H. Murray, and E. M. Ripley, “Sulfur sources and sulfur bonding of some central European attrital brown coals,” *Int. J. Coal Geol.*, vol. 16, no. 1–3, pp. 185–188, 1990.

[56] Y. Tan, E. Croiset, M. A. Douglas, and K. V. Thambimuthu, “Combustion characteristics of coal in a mixture of oxygen and recycled flue gas,” *Fuel*, vol. 85, no. 4, pp. 507–512, 2006.

[57] R. A. Durie, C. J. Matthews, and M. Y. Smith, “The catalytic formation of sulfur trioxide in fuel-rich propane-air flames,” *Combust. Flame*, vol. 15, no. 2, pp. 157–165, 1970.

[58] D. Fleig, K. Andersson, and F. Johnsson, “Influence of operating conditions on SO3formation during air and oxy-fuel combustion,” *Ind. Eng. Chem. Res.*, vol. 51, no. 28, pp. 9483–9491, 2012.

[59] L. Hindiyarti, P. Glarborg, and P. Marshall, “Reactions of SO3 with the O/H radical pool under combustion conditions,” *J. Phys. Chem. A*, vol. 111, no. 19, pp. 3984–3991, 2007.

[60] M. Müller, U. Schnell, and G. Scheffknecht, “Modelling the fate of sulphur during pulverized coal combustion under conventional and oxy-fuel conditions,” *Energy Procedia*, vol. 37, pp. 1377–1388, 2013.

[61] J. W. Armitage and C. F. Cullis, “Studies of the reaction between nitrogen dioxide and sulfur dioxide,” *Combust. Flame*, vol. 16, no. 2, pp. 125–130, 1971.

[62] J. O. L. Wendt and C. V. Sternling, “Catalysis of SO2 oxidation by nitrogen oxides,” *Combust. Flame*, vol. 21, no. 3, pp. 387–390, 1973.

[63] M. A. Mueller, R. A. Yetter, and F. L. Dryer, “Kinetic modeling of the CO/ H2O/O2/NO/SO2system: Implications for high-pressure fall-off in the SO2+ O(+M) = SO3(+M) reaction,” *Int. J. Chem. Kinet.*, vol. 32, no. 6, pp. 317–339, 2000.

[64] K. E. Zanganeh, A. Shafeen, C. Salvador, A. Beigzadeh, and M. Abbassi, “CO2processing and multi-pollutant control for oxy-fuel combustion systems using an advanced CO2capture and compression unit (CO2CCU),” *Energy Procedia*, vol. 4, pp. 1018–1025, 2011.

[65] C. Iloeje, R. Field, and A. F. Ghoniem, “Modeling and parametric analysis of nitrogen and sulfur oxide removal from oxy-combustion flue gas using a single column absorber,” *Fuel*, vol. 160, pp. 178–188, 2015.

[66] V. White, L. Torrente-Murciano, D. Sturgeon, and D. Chadwick, “Purification of oxyfuel-derived CO2,” *Energy Procedia*, vol. 1, no. 1, pp. 399–406, 2009.

[67] S. Ajdari, F. Normann, K. Andersson, and F. Johnsson, “Gas phase oxidation of SO2 by NO2 in pressurized flue gas systems - an experimental investigation,” *Energy Procedia*, vol. 46, no. 2, pp. 2011–2013, 2013.

[68] Inc. ANSYS, “ANSYS FLUENT Theory Guide,” *Release 18.2*, 2013.

[69] *ANSYS Chemkin Theory Manual 17.0 (15151)*. San Diago, CA, USA, 2015.

[70] M. L. T. Cossio *et al.*, “Getting started with Aspen plus V8,” *Aspen Technol. Inc.*, 2012.

[71] V. D. A. David Migdal, “A Source Flow Model for Continuum Gas-Particle Flow,” *J. Appl. Mech.*, vol. 34, no. 4, pp. 860–865, 1967.

[72] D. B. Spalding, “Mixing and chemical reaction in steady confined turbulent flames,” *Symp. Combust.*, vol. 13, no. 1, pp. 649–657, 1971.

[73] B. F. Magnussen and B. H. Hjertager, “On mathematical modeling of turbulent combustion with special emphasis on soot formation and combustion,” *Symp. Combust.*, vol. 16, no. 1, pp. 719–729, 1977.

[74] F. L. Dryer and C. K. Westbrook, “Simplified Reaction Mechanisms for the Oxidation of Hydrocarbon Fuels in Flames,” *Combust. Sci. Technol.*, vol. 27, no. 1–2, pp. 31–43, 1981.

[75] Inc. ANSYS, “Turbluent Dispersion of Particles,” in *ANSYS FLUENT 18.2, Theory Guide*, 2013, pp. 373–464.

[76] S. Badzioch and P. G. W. Hawksley, “Kinetics of Thermal Decomposition of Pulverized Coal Particles,” *Ind. Eng. Chem. Process Des. Dev.*, vol. 9, no. 4, pp. 521–530, 1970.

[77] A. H. Al-Abbas, J. Naser, and D. Dodds, “CFD modelling of air-fired and oxy-fuel combustion of lignite in a 100 KW furnace,” *Fuel*, vol. 90, no. 5, pp. 1778–1795, 2011.

[78] G. D. Raithby and E. H. Chui, “A Finite-Volume Method for Predicting a Radiant Heat Transfer in Enclosures With Participating Media,” *J. Heat Transfer*, vol. 112, no. 2, pp. 415–423, 1990.

[79] T. F. Smith, Z. F. Shen, and J. N. Friedman, “Evaluation of Coefficients for the Weighted Sum of Gray Gases Model,” *J. Heat Transfer*, vol. 104, no. 4, pp. 602–608, 1982.

[80] L. I. Díez, C. Cortés, and J. Pallarés, “Numerical investigation of NOxemissions from a tangentially-fired utility boiler under conventional and overfire air operation,” *Fuel*, vol. 87, no. 7, pp. 1259–1269, 2008.

[81] U. Maas and S. B. Pope, “Simplifying chemical kinetics: Intrinsic low-dimensional manifolds in composition space,” *Combust. Flame*, vol. 88, no. 3–4, pp. 239–264, 1992.

[82] R. K. Hanson and S. Salimian, “Survey of Rate Constants in the N/H/O System,” in *Combustion Chemistry*, W. C. Gardiner, Ed. New York, NY, USA: Springer, 1984, pp. 361–421.

[83] K. Andersson, F. Normann, F. Johnsson, and B. Leckner, “NO emission during oxy-fuel combustion of lignite,” *Ind. Eng. Chem. Res.*, vol. 47, no. 6, pp. 1835–1845, 2008.

[84] C. K. Westbrook and F. L. Dryer, “Chemical kinetic modeling of hydrocarbon combustion,” *Prog. Energy Combust. Sci.*, vol. 10, no. 1, pp. 1–57, 1984.

[85] N. Nikolopoulos, A. Nikolopoulos, E. Karampinis, P. Grammelis, and E. Kakaras, “Numerical investigation of the oxy-fuel combustion in large scale boilers adopting the ECO-Scrub technology,” *Fuel*, vol. 90, no. 1, pp. 198–214, 2011.

[86] G. G. De Soete, “Overall reaction rates of NO and N2 formation from fuel nitrogen,” *Symp. Combust.*, vol. 15, no. 1, pp. 1093–1102, 1975.

[87] W. H. Calkins, “The chemical forms of sulfur in coal: a review,” *Fuel*, vol. 73, no. 4, pp. 475–484, 1994.

[88] R. Bassilakis, Y. Zhao, P. R. Solomon, and M. A. Serio, “Sulfur and Nitrogen Evolution in the Argonne Coals: Experiment and Modeling,” *Energy and Fuels*, vol. 7, no. 6, pp. 710–720, 1993.

[89] F. García-Labiano, E. Hampartsoumian, and A. Williams, “Determination of sulfur release and its kinetics in rapid pyrolysis of coal,” *Fuel*, vol. 74, no. 7, pp. 1072–1079, 1995.

[90] X. Han, U. Schnell, and K. R. G. Hein, “Applying Eulerian and Lagrangian approaches to the modelling of dry desulfunzation process in pulverized coal furnaces,” *Energy and Fuels*, vol. 15, no. 5, pp. 1069–1076, 2001.

[91] J. C. Kramlich, P. C. Malte, and W. L. Grosshandler, “The reaction of fuel-sulfur in hydrocarbon combustion,” *Symp. Combust.*, vol. 18, no. 1, pp. 151–161, 1981.

[92] S. C. Hunter, “Formation of SO3 in gas turbines,” *Trans. ASME*, vol. 104, pp. 44–51, 1982.

[93] C. L. Senior, A. F. Sarofim, T. Zeng, J. J. Helble, and R. Mamani-Paco, “Gas-phase transformations of mercury in coal-fired power plants,” *Fuel Process. Technol.*, vol. 63, no. 2–3, pp. 197–213, 2000.

[94] P. Glarborg, D. Kubel, K. Dam-Johansen, H.-M. Chiang, and J. W. Bozzelli, “Impact of SO2 and NO on CO oxidation under post-flame conditions,” *Int J Chem Kinet*, vol. 28, no. 10, pp. 773–790, 1996.

[95] K. J. Hughes, T. Turányi, A. R. Clague, and M. J. Pilling, “Development and testing of a comprehensive chemical mechanism for the oxidation of methane,” *Int. J. Chem. Kinet.*, vol. 33, no. 9, pp. 513–538, 2001.

[96] V. White, A. Wright, S. Tappe, and J. Yan, “The Air Products Vattenfall oxyfuel CO2 compression and purification pilot plant at Schwarze Pumpe,” *Energy Procedia*, vol. 37, pp. 1490–1499, 2013.

[97] R. Sander, “Compilation of Henry’s law constants (version 4.0) for water as solvent,” *Atmos. Chem. Phys.*, vol. 15, no. 8, pp. 4399–4981, 2015.

[98] C. England and W. H. Corcoran, “The Rate and Mechanism of the Air Oxidation of Parts-per-Million Concentrations of Nitric Oxide in the Presence of Water Vapor,” *Ind. Eng. Chem. Fundam.*, vol. 14, no. 1, pp. 55–63, 1975.

[99] H. Holma and J. Sohlo, “A mathematical model of an absorption tower of nitrogen oxides in nitric acid production,” *Comput. Chem. Eng.*, vol. 3, no. 1, pp. 135–141, 1979.

[100] P. J. Hoftyzer and J. G. Kwanten, “Absorption of nitrous gases,” in *Gas Purification Processes for air pollution control*, 2nd editio., London: Nonhebel G, Newnes, 1972.

[101] C. E. Corriveau, “The Absorption of N2O3 Into Water,” University of California, Berkeley, 1971.

[102] J. Y. Park and Y. N. Lee, “Solubility and decomposition kinetics of nitrous acid in aqueous solution,” *J. Phys. Chem.*, vol. 92, no. 22, pp. 6294–6302, 1988.

[103] M. S. Rayson, J. C. Mackie, E. M. Kennedy, and B. Z. Dlugogorski, “Accurate Rate Constants for Decomposition of Aqueous Nitrous Acid,” *Inorg. Chem.*, vol. 51, no. 4, pp. 2178–2185, 2012.

[104] S. Jaffe and F. S. Klein, “Photolysis of NO2 in the presence of SO2 at 3660 Å,” *Trans. Faraday Soc.*, vol. 62, no. 0, pp. 2150–2157, 1966.

[105] K. Andersson, “Characterization of Oxy-Fuel Flames - Their Composition, Temperature and Radiation,” Chalmers Unversity of Technology, 2007.

[106] S. Hjärtstam, K. Andersson, F. Johnsson, and B. Leckner, “Combustion characteristics of lignite-fired oxy-fuel flames,” *Fuel*, vol. 88, no. 11, pp. 2216–2224, 2009.

[107] P. Gaikwad, H. Kulkarni, and S. Sreedhara, “Simplified numerical modelling of oxy-fuel combustion of pulverized coal in a swirl burner,” *Appl. Therm. Eng.*, vol. 124, pp. 734–745, 2017.

[108] A. Gutiérrez, A. Posada, and I. Celik, “CFD study of oxy coal combustion in a 100KW downfired furnace,” in *29th Annual International Pittsburgh Coal Conference 2012, PCC 2012*, 2012, vol. 1, pp. 244–259.

[109] K. Andersson, R. Johansson, S. Hjärtstam, F. Johnsson, and B. Leckner, “Radiation intensity of lignite-fired oxy-fuel flames,” *Exp. Therm. Fluid Sci.*, vol. 33, no. 1, pp. 67–76, 2008.

[110] S. Lin, Y. Suzuki, and H. Hatano, “Effect of pressure on NOx emission from char particle combustion,” *Energy and Fuels*, vol. 16, no. 3, pp. 634–639, 2002.

[111] D. Fleig, K. Andersson, F. Johnsson, and B. Leckner, “Conversion of sulfur during

pulverized oxy-coal combustion," *Energy and Fuels*, vol. 25, no. 2, pp. 647–655, 2011.

[112] R. Stanger and T. Wall, "Sulphur impacts during pulverised coal combustion in oxy-fuel technology for carbon capture and storage," *Prog. Energy Combust. Sci.*, vol. 37, no. 1, pp. 69–88, 2011.

[113] D. Fleig, F. Normann, K. Andersson, F. Johnsson, and B. Leckner, "The fate of sulphur during oxy-fuel combustion of lignite," *Energy Procedia*, vol. 1, no. 1, pp. 383–390, 2009.

[114] A. Levy, "Unresolved problems in SOx, NOx, soot control in combustion," *Symp. Combust.*, vol. 19, no. 1, pp. 1223–1242, 1982.

[115] Y. Mitsui, N. Imada, H. Kikkawa, and A. Katagawa, "Study of Hg and SO3 behavior in flue gas of oxy-fuel combustion system," *Int. J. Greenh. Gas Control*, vol. 5, pp. S143–S150, 2011.

[116] R. K. Srivastava, C. A. Miller, C. Erickson, and R. Jambhekar, "Emissions of sulfur trioxide from coal-fired power plants," *J. Air Waste Manag. Assoc.*, vol. 54, no. 6, pp. 750–762, 2004.

[117] F. Normann, K. Andersson, B. Leckner, and F. Johnsson, "Emission control of nitrogen oxides in the oxy-fuel process," *Prog. Energy Combust. Sci.*, vol. 35, no. 5, pp. 385–397, 2009.

[118] F. H. Verhoff and T. Banchero, "Predicting Dew Points of Flue Gases," *Chem. Eng. Prog.*, vol. 70, no. 8, pp. 71–72, 1974.

[119] J. Yan *et al.*, "Flue gas cleaning for CO2 capture from coal-fired oxyfuel combustion power generation," *Energy Procedia*, vol. 4, pp. 900–907, 2011.

[120] V. White, R. Allam, and E. Miller, "Purification of Oxyfuel-Derived CO2 for Sequestration or EOR," in *8th international conference on greenhouse gas control technologies*, 2006, pp. 19–22.

[121] T. Z. Tumsa, S. H. Lee, F. Normann, K. Andersson, S. Ajdari, and W. Yang, "Concomitant removal of NOx and SOx from a pressurized oxy-fuel combustion process using a direct contact column," *Chem. Eng. Res. Des.*, vol. 131, pp. 626–634, 2018.

[122] S. Laribi, L. Dubois, G. De Weireld, and D. Thomas, “Optimization of the Sour Compression Unit (SCU) process for CO2 Purification Applied to Flue Gases Coming from Oxy-combustion Cement Industries,” *Energy Procedia*, vol. 114, pp. 458–470, 2017.

[123] E. de Visser *et al.*, “Dynamis CO2 quality recommendations,” *Int. J. Greenh. Gas Control*, vol. 2, no. 4, pp. 478–484, 2008.

[124] J. Giménez-López, M. Martínez, A. Millera, R. Bilbao, and M. U. Alzueta, “SO2 effects on CO oxidation in a CO2 atmosphere, characteristic of oxy-fuel conditions,” *Combust. Flame*, vol. 158, no. 1, pp. 48–56, 2011.

Appendix A Gas phase reactions for sulphur in ANSYS Fluent

The reduced kinetic data used in ANSYS Fluent for the gas phase reactions for sulphur based on the work of Kramlich et al.[91]. The rate coefficient is expressed by the three-parameter empirical Arrhenius form:

$$k(T) = AT^{b} \exp(\frac{E}{RT}) \quad \text{(A-1)}$$

The pre-exponent factor A is given in units m^3. $(mol\text{-}s)^{-1}$. The temperature T is the temperature is given in K. The temperature exponent b is dimensionless. The activation energy E is given in units of J/mol.

Table A-1 Reduced mechanism for sulphur reaction in ANSYS Fluent

Reaction	A	b	E
$H_2S + H \rightarrow SH + H_2$	1.819702E+07	0.0E+00	7.484300E+03
$SH + H_2 \rightarrow H_2S + H$	9.375623E+06	0.0E+00	6.253660E+04
$H_2S + OH \rightarrow SH + H_2O$	1.380385E+02	0.0E+00	3.742150E+03
$SH + H_2O \rightarrow H_2S + OH$	3.104557E+07	0.0E+00	1.218543E+05
$H_2S + O \rightarrow SH + OH$	4.365162E+03	0.0E+00	1.380493E+04
$SH + OH \rightarrow H_2S + O$	9.885528E+08	0.0E+00	6.035996E+04
$H_2S + M \rightarrow SH + H + M$	8.669613E+14	0.0E+00	3.819463E+05
$SH + H + M \rightarrow H_2S + M$	1.096478E+03	0.0E+00	0.000000E+00
$SH + O \rightarrow SO + H$	3.548135E+08	0.0E+00	2.687316E+03
$SO + H \rightarrow SH + O$	2.985385E+09	0.0E+00	1.694600E+05
$SO + OH \rightarrow SO_2 + H$	1.621810E+08	0.0E+00	2.565926E+03
$SO_2 + H \rightarrow SO + OH$	7.691299E+09	0.0E+00	1.187023E+05
$SO + O_2 \rightarrow SO_2 + O$	4.466832E+05	0.0E+00	2.703222E+04
$SO_2 + O \rightarrow SO + O_2$	1.663412E+06	0.0E+00	7.613643E+04
$SO + O + M \rightarrow SO_2 + M$	8.709647E+09	-1.8E+00	0.000000E+00
$SO_2 + M \rightarrow SO + O + M$	1.905464E+14	0.0E+00	5.207365E+05

Appendix B Kinetic mechanism for flue gas reactions

The chemical kinetic data is given in Chemkin-PRO formation. The rate coefficient is expressed using Equation (A-1). The pre-exponent factor A is given in units of cm-mol-s-k. The temperature exponent b is dimensionless. The activation energy E is given in units of cal/mol.

	REACTIONS CONSIDERED			A	b	E
1.	OH+H2=H2O+H			2.14E+08	1.5	3449.0
2.	O+OH=O2+H			2.02E+14	-0.4	0.0
3.	O+H2=OH+H			5.06E+04	2.7	6290.0
4.	H+O2+M=HO2+M			8.00E+17	-0.8	0.0
	H2O	Enhanced by	2.000E+01			
	N2	Enhanced by	0.000E+00			
	CO2	Enhanced by	4.000E+00			
5.	H+O2+N2=HO2+N2			6.70E+19	-1.4	0.0
6.	OH+HO2=H2O+O2			1.90E+16	-1.0	0.0
7.	H+HO2=2OH			1.69E+14	0.0	874.0
8.	H+HO2=H2+O2			4.28E+13	0.0	1411.0
9.	H+HO2=O+H2O			3.01E+13	0.0	1721.0
10.	O+HO2=O2+OH			3.25E+13	0.0	0.0
11.	2OH=O+H2O			4.33E+03	2.7	-2485.7
12.	H+H+M=H2+M			1.00E+18	-1.0	0.0
	H2O	Enhanced by	0.000E+00			
	H2	Enhanced by	0.000E+00			
	CO2	Enhanced by	0.000E+00			
13.	H+H+H2=H2+H2			9.20E+16	-0.6	0.0
14.	H+H+H2O=H2+H2O			6.00E+19	-1.2	0.0
15.	H+H+CO2=H2+CO2			5.49E+20	-2.0	0.0
16.	H+OH+M=H2O+M			1.60E+22	-2.0	0.0
	H2O	Enhanced by	5.000E+00			

17.	H+O+M=OH+M		6.20E+16	-0.6	0.0
	H2O	Enhanced by 5.000E+00			
18.	O+O+M=O2+M		1.89E+13	0.0	-1788.0
	H2O	Enhanced by 5.000E+00			
	CO	Enhanced by 2.000E+00			
	CO2	Enhanced by 3.000E+00			
	H2	Enhanced by 2.000E+00			
19.	HO2+HO2=H2O2+O2		4.20E+14	0.0	11982.0
	Declared duplicate reaction...				
20.	HO2+HO2=H2O2+O2		1.30E+11	0.0	-1629.0
	Declared duplicate reaction...				
21.	H2O2+M=OH+OH+M		1.30E+17	0.0	45500.0
	H2O	Enhanced by 5.000E+00			
	CO	Enhanced by 2.000E+00			
	CO2	Enhanced by 3.000E+00			
	H2	Enhanced by 2.000E+00			
22.	H2O2+H=HO2+H2		1.69E+12	0.0	3755.0
23.	H2O2+H=OH+H2O		1.02E+13	0.0	3576.0
24.	H2O2+O=OH+HO2		6.63E+11	0.0	3974.0
25.	H2O2+OH=H2O+HO2		7.83E+12	0.0	1331.0
26.	CH3+CH3(+M)=C2H6(+M)		2.10E+16	-1.0	620.0
	Low pressure limit:	0.12600E+51 -0.96700E+01 0.62200E+04			
	TROE centering:	0.53250E+00 0.15100E+03 0.10380E+04 0.49700E+04			
	N2	Enhanced by 1.430E+00			
	H2O	Enhanced by 8.590E+00			
	H2	Enhanced by 2.000E+00			
	CO	Enhanced by 2.000E+00			
	CO2	Enhanced by 3.000E+00			
27.	CH3+H(+M)=CH4(+M)		1.30E+16	-0.6	383.0
	Low pressure limit:	0.17500E+34 -0.47600E+01 0.24400E+04			
	TROE centering:	0.78300E+00 0.74000E+02 0.29410E+04 0.69640E+04			

	H2	Enhanced by	2.860E+00			
	H2O	Enhanced by	8.570E+00			
	CH4	Enhanced by	2.860E+00			
	CO	Enhanced by	2.140E+00			
	CO2	Enhanced by	2.860E+00			
	C2H6	Enhanced by	4.290E+00			
	N2	Enhanced by	1.430E+00			
28.	CH4+O2=CH3+HO2			7.90E+13	0.0	56000.0
29.	CH4+H=CH3+H2			1.30E+04	3.0	8040.0
30.	CH4+OH=CH3+H2O			1.60E+06	2.1	2460.0
31.	CH4+O=CH3+OH			1.02E+09	1.5	8604.0
32.	CH4+HO2=CH3+H2O2			1.80E+11	0.0	18700.0
33.	CH3+HO2=CH3O+OH			8.00E+12	0.0	0.0
34.	CH3+O=CH2O+H			8.00E+13	0.0	0.0
35.	CH3+O2=CH3O+O			2.87E+13	0.0	30481.0
36.	CH3+O2=CH2O+OH			1.85E+12	0.0	20315.0
37.	CH3+O2(+M)=CH3O2(+M)			7.80E+08	1.2	0.0
	Low pressure limit:	0.54000E+26	-0.33000E+01	0.00000E+00		
	N2	Enhanced by	1.100E+00			
	H2O	Enhanced by	1.000E+01			
38.	CH3O2+H=CH3O+OH			1.00E+14	0.0	0.0
39.	CH3O2+O=CH3O+O2			3.60E+13	0.0	0.0
40.	CH3O2+OH=CH3OH+O2			6.00E+13	0.0	0.0
41.	CH3O2+HO2=CH3OOH+O2			2.50E+11	0.0	-1570.0
42.	CH3O2+H2O2=CH3OOH+HO2			2.40E+12	0.0	9940.0
43.	CH3O2+CH2O=CH3OOH+HCO			2.00E+12	0.0	11665.0
44.	CH3O2+CH4=CH3OOH+CH3			1.80E+11	0.0	18500.0
45.	CH3O2+CH3=CH3O+CH3O			2.40E+13	0.0	0.0
46.	CH3O2+CH3O=CH2O+CH3OOH			3.00E+11	0.0	0.0
47.	CH3O2+CH2OH=CH2O+CH3OOH			1.20E+13	0.0	0.0
48.	CH3O2+CH3OH=CH3OOH+CH2OH			1.80E+12	0.0	13700.0

49.	CH3O2+CH3O2=CH3O+CH3O+O2	1.00E+11	0.0	300.0
50.	CH3O2+CH3O2=CH3OH+CH2O+O2	4.00E+09	0.0	-2210.0
51.	CH3OOH=CH3O+OH	6.30E+14	0.0	42300.0
52.	CH3OOH+H=CH3O2+H2	8.80E+10	0.0	1860.0
53.	CH3OOH+H=CH3O+H2O	8.20E+10	0.0	1860.0
54.	CH3OOH+O=CH3O2+OH	1.00E+12	0.0	3000.0
55.	CH3OOH+OH=CH3O2+H2O	1.80E+12	0.0	-378.0
56.	CH2OH+H=CH3+OH	1.00E+14	0.0	0.0
57.	CH3O+H=CH3+OH	1.00E+14	0.0	0.0
58.	CH3+OH=CH2+H2O	7.50E+06	2.0	5000.0
59.	CH3+HCO=CH4+CO	1.20E+14	0.0	0.0
60.	CH3+H=CH2+H2	9.00E+13	0.0	15100.0
61.	CH3+OH(+M)=CH3OH(+M)	6.30E+13	0.0	0.0
	Low pressure limit: 0.18900E+39 -0.63000E+01 0.31000E+04			
	TROE centering: 0.21050E+00 0.83500E+02 0.53980E+04 0.83700E+04			
	N2 Enhanced by 1.430E+00			
	H2O Enhanced by 8.580E+00			
	CO2 Enhanced by 3.000E+00			
	CO Enhanced by 2.000E+00			
	H2 Enhanced by 2.000E+00			
62.	CH3OH+OH=CH2OH+H2O	5.30E+04	2.5	960.0
63.	CH3OH+OH=CH3O+H2O	1.32E+04	2.5	960.0
64.	CH3OH+O=CH2OH+OH	3.88E+05	2.5	3080.0
65.	CH3OH+H=CH2OH+H2	1.70E+07	2.1	4868.0
66.	CH3OH+H=CH3O+H2	4.24E+06	2.1	4868.0
67.	CH3OH+HO2=CH2OH+H2O2	9.64E+10	0.0	12578.0
68.	CH2O+H(+M)=CH3O(+M)	5.40E+11	0.5	2600.0
	Low pressure limit: 0.15400E+31 -0.48000E+01 0.55600E+04			
	TROE centering: 0.75800E+00 0.94000E+02 0.15550E+04 0.42000E+04			
	N2 Enhanced by 1.430E+00			
	H2O Enhanced by 8.580E+00			

	CO	Enhanced by	2.000E+00		
	H2	Enhanced by	2.000E+00		
	CO2	Enhanced by	3.000E+00		
69.	H+CH2O(+M)=CH2OH(+M)		5.40E+11	0.5	3600.0
	Low pressure limit:	0.91000E+32 -0.48200E+01	0.65300E+04		
	TROE centering:	0.71870E+00 0.10300E+03	0.12910E+04	0.41600E+04	
	N2	Enhanced by	1.430E+00		
	H2O	Enhanced by	8.580E+00		
	CO	Enhanced by	2.000E+00		
	CO2	Enhanced by	3.000E+00		
	H2	Enhanced by	2.000E+00		
70.	CH3O+H=CH2O+H2		2.00E+13	0.0	0.0
71.	CH2OH+H=CH2O+H2		2.00E+13	0.0	0.0
72.	CH3O+OH=CH2O+H2O		1.00E+13	0.0	0.0
73.	CH2OH+OH=CH2O+H2O		1.00E+13	0.0	0.0
74.	CH3O+O=CH2O+OH		1.00E+13	0.0	0.0
75.	CH2OH+O=CH2O+OH		1.00E+13	0.0	0.0
76.	CH3O+O2=CH2O+HO2		6.30E+10	0.0	2600.0
77.	CH2OH+O2=CH2O+HO2		1.57E+15	-1.0	0.0
	Declared duplicate reaction...				
78.	CH2OH+O2=CH2O+HO2		7.23E+13	0.0	3577.0
	Declared duplicate reaction...				
79.	CH2+H=CH+H2		1.00E+18	-1.6	0.0
80.	CH2+OH=CH+H2O		1.13E+07	2.0	3000.0
81.	CH2+OH=CH2O+H		2.50E+13	0.0	0.0
82.	CH+O2=HCO+O		3.30E+13	0.0	0.0
83.	CH+O=CO+H		5.70E+13	0.0	0.0
84.	CH+OH=HCO+H		3.00E+13	0.0	0.0
85.	CH+OH=C+H2O		4.00E+07	2.0	3000.0
86.	CH+CO2=HCO+CO		3.40E+12	0.0	690.0
87.	CH+H=C+H2		1.50E+14	0.0	0.0

88.	CH+H2O=CH2O+H			5.72E+12	0.0	-751.0
89.	CH+CH2O=CH2CO+H			9.46E+13	0.0	-515.0
90.	CH+C2H2=C3H2+H			1.00E+14	0.0	0.0
91.	CH+CH2=C2H2+H			4.00E+13	0.0	0.0
92.	CH+CH3=C2H3+H			3.00E+13	0.0	0.0
93.	CH+CH4=C2H4+H			6.00E+13	0.0	0.0
94.	C+O2=CO+O			2.00E+13	0.0	0.0
95.	C+OH=CO+H			5.00E+13	0.0	0.0
96.	C+CH3=C2H2+H			5.00E+13	0.0	0.0
97.	C+CH2=C2H+H			5.00E+13	0.0	0.0
98.	CH2+CO2=CH2O+CO			1.10E+11	0.0	1000.0
99.	CH2+O=CO+H+H			5.00E+13	0.0	0.0
100.	CH2+O=CO+H2			3.00E+13	0.0	0.0
101.	CH2+O2=CO+H2O			2.20E+22	-3.3	2867.0
102.	CH2+O2=CO2+H+H			3.29E+21	-3.3	2867.0
103.	CH2+O2=CH2O+O			3.29E+21	-3.3	2867.0
104.	CH2+O2=CO2+H2			2.63E+21	-3.3	2867.0
105.	CH2+O2=CO+OH+H			1.64E+21	-3.3	2867.0
106.	CH2+CH2=C2H2+H+H			4.00E+13	0.0	0.0
107.	CH2+HCCO=C2H3+CO			3.00E+13	0.0	0.0
108.	CH2+C2H2=H2CCCH+H			1.20E+13	0.0	6600.0
109.	CH2+CH4=CH3+CH3			4.30E+12	0.0	10030.0
110.	CH2O+OH=HCO+H2O			3.43E+09	1.2	-447.0
111.	CH2O+H=HCO+H2			5.70E+07	1.9	2740.0
112.	CH2O+M=HCO+H+M			6.10E+15	0.0	76900.0
	H2	Enhanced by	2.000E+00			
	CO	Enhanced by	2.000E+00			
	CO2	Enhanced by	3.000E+00			
	H2O	Enhanced by	5.000E+00			
113.	CH2O+M=CO+H2+M			2.80E+15	0.0	63800.0
	H2	Enhanced by	2.000E+00			

	CO	Enhanced by	2.000E+00			
	CO2	Enhanced by	3.000E+00			
	H2O	Enhanced by	5.000E+00			
114.	CH2O+O=HCO+OH			1.80E+13	0.0	3080.0
115.	CH2O+CH3=HCO+CH4			7.80E-08	6.1	1967.0
116.	CH2O+HO2=HCO+H2O2			4.10E+04	2.5	10200.0
117.	CH2O+O2=HCO+HO2			5.00E+04	3.0	39000.0
118.	HCO+OH=H2O+CO			1.00E+14	0.0	0.0
119.	HCO+M=H+CO+M			4.80E+17	-1.2	17700.0
	CO	Enhanced by	1.870E+00			
	H2	Enhanced by	1.870E+00			
	CH4	Enhanced by	2.810E+00			
	CO2	Enhanced by	3.000E+00			
	H2O	Enhanced by	5.000E+00			
120.	HCO+H=CO+H2			1.19E+13	0.2	0.0
121.	HCO+O=CO+OH			3.00E+13	0.0	0.0
122.	HCO+O=CO2+H			3.00E+13	0.0	0.0
123.	HCO+O2=HO2+CO			3.40E+12	0.0	0.0
124.	HCO+HO2=CO2+OH+H			3.00E+13	0.0	0.0
125.	HCO+HCO=CO+CH2O			3.00E+13	0.0	0.0
126.	CO+O+M=CO2+M			6.17E+14	0.0	3000.0
	H2	Enhanced by	2.000E+00			
	CO	Enhanced by	2.000E+00			
	CO2	Enhanced by	3.000E+00			
	H2O	Enhanced by	5.000E+00			
127.	CO+OH=CO2+H			1.51E+07	1.3	-758.0
128.	CO+O2=CO2+O			2.53E+12	0.0	47688.0
129.	HO2+CO=CO2+OH			5.80E+13	0.0	22934.0
130.	C2H6+CH3=C2H5+CH4			5.50E-01	4.0	8300.0
131.	C2H6+H=C2H5+H2			5.40E+02	3.5	5210.0
132.	C2H6+O=C2H5+OH			3.00E+07	2.0	5115.0

133.	C2H6+OH=C2H5+H2O	7.23E+06	2.0	864.0
134.	C2H6+O2=C2H5+HO2	5.00E+13	0.0	55000.0
135.	C2H6+HO2=C2H5+H2O2	1.30E+13	0.0	20460.0
136.	C2H4+H=C2H3+H2	5.42E+14	0.0	14902.0
137.	C2H4+O=CH3+HCO	8.10E+06	1.9	180.0
138.	C2H4+O=CH2HCO+H	4.70E+06	1.9	180.0
139.	C2H4+O=CH2CO+H2	6.80E+05	1.9	180.0
140.	C2H4+OH=C2H3+H2O	2.02E+13	0.0	5955.0
141.	C2H4+O2=CH2HCO+OH	2.00E+08	1.5	39000.0
142.	C2H4+HO2=CH3HCO+OH	2.20E+12	0.0	17200.0
143.	C2H4+CH3=C2H3+CH4	5.00E+11	0.0	15000.0
144.	CH2+CH3=C2H4+H	4.00E+13	0.0	0.0
145.	C2H4+H(+M)=C2H5(+M)	1.08E+12	0.5	1822.0
	Low pressure limit: 0.11120E+35 -0.50000E+01 0.44480E+04			
	TROE centering: 0.50000E+00 0.95000E+02 0.95000E+02 0.20000E+03			
	H2 Enhanced by 2.000E+00			
	CO Enhanced by 2.000E+00			
	CO2 Enhanced by 3.000E+00			
	H2O Enhanced by 5.000E+00			
146.	C2H5+H=CH3+CH3	4.89E+12	0.3	0.0
147.	H+C2H5(+M)=C2H6(+M)	5.20E+17	-1.0	1580.0
	Low pressure limit: 0.20000E+42 -0.70800E+01 0.66850E+04			
	TROE centering: 0.84220E+00 0.12500E+03 0.22190E+04 0.68820E+04			
	H2 Enhanced by 2.000E+00			
	CO Enhanced by 2.000E+00			
	CO2 Enhanced by 3.000E+00			
	H2O Enhanced by 5.000E+00			
148.	C2H5+O2=C2H4+HO2	1.00E+10	0.0	-2190.0
149.	C2H5+O=CH3+CH2O	4.20E+13	0.0	0.0
150.	C2H5+O=CH3HCO+H	5.30E+13	0.0	0.0
151.	C2H5+O=C2H4+OH	3.00E+13	0.0	0.0

152.	C2H5+OH=C2H4+H2O	2.40E+13	0.0	0.0
153.	C2H5+HCO=C2H6+CO	1.20E+14	0.0	0.0
154.	C2H5+CH2O=C2H6+HCO	5.50E+03	2.8	5860.0
155.	C2H5+CH3=C2H4+CH4	1.10E+12	0.0	0.0
156.	C2H5+C2H5=C2H6+C2H4	1.50E+12	0.0	0.0
157.	C2H2+O=CH2+CO	6.10E+06	2.0	1900.0
158.	C2H2+O=HCCO+H	1.43E+07	2.0	1900.0
159.	C2H2+O=C2H+OH	3.20E+15	-0.6	15000.0
160.	H2+C2H=C2H2+H	4.09E+05	2.4	864.3
161.	H+C2H2(+M)=C2H3(+M)	3.64E+10	1.1	2640.0
	Low pressure limit: 0.22540E+41 -0.72690E+01 0.65770E+04			
	TROE centering: 0.50000E+00 0.67500E+03 0.67500E+03			
	H2 Enhanced by 2.000E+00			
	CO Enhanced by 2.000E+00			
	CO2 Enhanced by 3.000E+00			
	H2O Enhanced by 5.000E+00			
162.	C2H3+H=C2H2+H2	4.00E+13	0.0	0.0
163.	C2H3+O=CH2CO+H	3.00E+13	0.0	0.0
164.	C2H3+O2=CH2O+HCO	4.58E+16	-1.4	1015.0
165.	C2H3+O2=CH2HCO+O	3.03E+11	-0.3	10.7
166.	C2H3+O2=C2H2+HO2	1.34E+06	1.6	-383.5
167.	C2H3+OH=C2H2+H2O	2.00E+13	0.0	0.0
168.	C2H3+CH2=C3H4+H	3.00E+13	0.0	0.0
169.	C2H3+C2H=C2H2+C2H2	3.00E+13	0.0	0.0
170.	C2H3+CH3=C2H2+CH4	2.10E+13	0.0	0.0
171.	C2H3+CH2O=C2H4+HCO	5.40E+03	2.8	5860.0
172.	C2H3+HCO=C2H4+CO	9.00E+13	0.0	0.0
173.	C2H3+C2H3=H2CCCH+CH3	1.80E+13	0.0	0.0
174.	C2H3+C2H3=C2H4+C2H2	6.30E+13	0.0	0.0
175.	C2H3+CH=CH2+C2H2	5.00E+13	0.0	0.0
176.	OH+C2H2=C2H+H2O	3.37E+07	2.0	14000.0

177.	OH+C2H2=HCCOH+H		5.04E+05	2.3	13500.0
178.	OH+C2H2=CH2CO+H		2.18E-04	4.5	-1000.0
179.	OH+C2H2=CH3+CO		4.83E-04	4.0	-2000.0
180.	OH+C2H2(+M)=C2H2OH(+M)		1.52E+08	1.7	1000.0
	Low pressure limit: 0.18100E+24 -0.20000E+01 0.00000E+00				
	H2	Enhanced by 2.000E+00			
	CO	Enhanced by 2.000E+00			
	CO2	Enhanced by 3.000E+00			
	H2O	Enhanced by 5.000E+00			
181.	HCCOH+H=HCCO+H2		3.00E+07	2.0	1000.0
182.	HCCOH+OH=HCCO+H2O		1.00E+07	2.0	1000.0
183.	HCCOH+O=HCCO+OH		2.00E+07	3.0	1900.0
184.	C2H2OH+H=CH2HCO+H		5.00E+13	0.0	0.0
185.	C2H2OH+O=OCHCHO+H		5.00E+13	0.0	0.0
186.	C2H2OH+O2=OCHCHO+OH		1.00E+12	0.0	5000.0
187.	CH2HCO+H=CH3+HCO		1.00E+14	0.0	0.0
188.	CH2HCO+H=CH3CO+H		3.00E+13	0.0	0.0
189.	CH2HCO+O=CH2O+HCO		5.00E+13	0.0	0.0
190.	CH2HCO+OH=CH2CO+H2O		2.00E+13	0.0	0.0
191.	CH2HCO+OH=CH2OH+HCO		1.00E+13	0.0	0.0
192.	CH2HCO+CH3=C2H5+HCO		5.00E+13	0.0	0.0
193.	CH2HCO+CH2=C2H4+HCO		5.00E+13	0.0	0.0
194.	CH2HCO+CH=C2H3+HCO		1.00E+14	0.0	0.0
195.	CH2HCO+O2=OH+OCHCHO		2.22E+11	0.0	1500.0
196.	OCHCHO+M=HCO+HCO+M		1.00E+17	0.0	25000.0
197.	OCHCHO+H=CH2O+HCO		3.00E+13	0.0	0.0
198.	CH2HCO+M=CH3+CO+M		2.00E+16	0.0	42000.0
	H2	Enhanced by 2.000E+00			
	CO	Enhanced by 2.000E+00			
	CO2	Enhanced by 3.000E+00			
	H2O	Enhanced by 5.000E+00			

199.	CH3HCO+OH=CH3CO+H2O		2.30E+10	0.7	-1110.0
200.	CH3HCO+H=CH3CO+H2		4.10E+09	1.2	2400.0
201.	CH3HCO+CH3=CH3CO+CH4		2.00E-06	5.6	2464.0
202.	CH3CO(+M)=CH3+CO(+M)		2.80E+13	0.0	17100.0
	Low pressure limit:	0.21000E+16 0.00000E+00	0.14000E+05		
	TROE centering:	0.50000E+00 0.10000E-29	0.10000E+31		
	H2	Enhanced by 2.000E+00			
	CO	Enhanced by 2.000E+00			
	CO2	Enhanced by 3.000E+00			
	H2O	Enhanced by 5.000E+00			
203.	CH3CO+H=CH3+HCO		2.10E+13	0.0	0.0
204.	CH3CO+H=CH2CO+H2		1.20E+13	0.0	0.0
205.	CH3CO+O=CH3+CO2		1.50E+14	0.0	0.0
206.	CH3CO+O=CH2CO+OH		4.00E+13	0.0	0.0
207.	CH3CO+OH=CH2CO+H2O		1.20E+13	0.0	0.0
208.	CH3HCO=CH3+HCO		7.10E+15	0.0	81280.0
209.	CH3HCO+O=CH3CO+OH		5.80E+12	0.0	1800.0
210.	CH3HCO+O2=CH3CO+HO2		3.00E+13	0.0	39000.0
211.	CH3HCO+HO2=CH3CO+H2O2		3.00E+12	0.0	12000.0
212.	CH2CO+O=CO2+CH2		1.75E+12	0.0	1350.0
213.	CH2CO+H=CH3+CO		5.93E+06	2.0	1300.0
214.	CH2CO+H=HCCO+H2		3.00E+07	2.0	10000.0
215.	CH2CO+O=HCCO+OH		2.00E+07	2.0	10000.0
216.	CH2CO+OH=HCCO+H2O		1.00E+07	2.0	3000.0
217.	CH2CO+OH=CH2OH+CO		7.20E+12	0.0	0.0
218.	CH2CO+OH=CH3+CO2		3.00E+12	0.0	0.0
219.	CH2+CO(+M)=CH2CO(+M)		8.10E+11	0.5	4510.0
	Low pressure limit:	0.18800E+34 -0.51100E+01	0.70950E+04		
	TROE centering:	0.59070E+00 0.27500E+03	0.12260E+04	0.51850E+04	
	H2	Enhanced by 2.000E+00			
	CO	Enhanced by 2.000E+00			

	CO2	Enhanced by	3.000E+00			
	H2O	Enhanced by	8.580E+00			
	N2	Enhanced by	1.430E+00			
220.	C2H+O2=CO+CO+H			2.52E+13	0.0	0.0
221.	C2H+CH4=CH3+C2H2			7.23E+12	0.0	976.0
222.	CH+CO(+M)=HCCO(+M)			5.00E+13	0.0	0.0
	Low pressure limit:	0.18800E+29	-0.37400E+01	0.19360E+04		
	TROE centering:	0.57570E+00	0.23700E+03	0.16520E+04	0.50690E+04	
	N2	Enhanced by	1.430E+00			
	H2O	Enhanced by	8.580E+00			
	CO	Enhanced by	2.000E+00			
	CO2	Enhanced by	3.000E+00			
	H2	Enhanced by	2.000E+00			
223.	HCCO+C2H2=H2CCCH+CO			1.00E+11	0.0	3000.0
224.	H+HCCO=CH2(S)+CO			1.00E+14	0.0	0.0
225.	O+HCCO=H+CO+CO			1.00E+14	0.0	0.0
226.	HCCO+O2=CO2+CO+H			1.40E+07	1.7	1000.0
227.	HCCO+O2=CO+CO+OH			2.88E+07	1.7	1000.0
228.	CH+HCCO=C2H2+CO			5.00E+13	0.0	0.0
229.	HCCO+HCCO=C2H2+CO+CO			1.00E+13	0.0	0.0
230.	HCCO+OH=C2O+H2O			6.00E+13	0.0	0.0
231.	C2O+H=CH+CO			1.00E+13	0.0	0.0
232.	C2O+O=CO+CO			5.00E+13	0.0	0.0
233.	C2O+OH=CO+CO+H			2.00E+13	0.0	0.0
234.	C2O+O2=CO+CO+O			2.00E+13	0.0	0.0
235.	CH2(S)+M=CH2+M			1.00E+13	0.0	0.0
	H	Enhanced by	0.000E+00			
	H2O	Enhanced by	0.000E+00			
	C2H2	Enhanced by	0.000E+00			
	N2	Enhanced by	0.000E+00			
	AR	Enhanced by	0.000E+00			

236.	CH2(S)+CH4=CH3+CH3	4.00E+13	0.0	0.0
237.	CH2(S)+C2H6=CH3+C2H5	1.20E+14	0.0	0.0
238.	CH2(S)+O2=CO+OH+H	7.00E+13	0.0	0.0
239.	CH2(S)+H2=CH3+H	7.00E+13	0.0	0.0
240.	CH2(S)+H2O=CH3+OH	3.01E+15	-0.6	0.0
241.	CH2(S)+H2O=CH2+H2O	3.00E+13	0.0	0.0
242.	CH2(S)+C2H2=CH2+C2H2	4.00E+13	0.0	0.0
243.	CH2(S)+H=CH2+H	2.00E+14	0.0	0.0
244.	CH2(S)+O=CO+H+H	3.00E+13	0.0	0.0
245.	CH2(S)+OH=CH2O+H	3.00E+13	0.0	0.0
246.	CH2(S)+H=CH+H2	3.00E+13	0.0	0.0
247.	CH2(S)+CO2=CH2O+CO	3.00E+12	0.0	0.0
248.	CH2(S)+CH3=C2H4+H	2.00E+13	0.0	0.0
249.	CH2(S)+CH2CO=C2H4+CO	1.60E+14	0.0	0.0
250.	CH2(S)+N2=CH2+N2	1.26E+13	0.0	430.0
251.	CH2(S)+AR=CH2+AR	1.45E+13	0.0	884.0
252.	C2H+O=CH+CO	5.00E+13	0.0	0.0
253.	C2H+OH=HCCO+H	2.00E+13	0.0	0.0
254.	C2H+OH=C2+H2O	4.00E+07	2.0	8000.0
255.	C2+H2=C2H+H	4.00E+05	2.4	1000.0
256.	C2+O2=CO+CO	5.00E+13	0.0	0.0
257.	C2+OH=C2O+H	5.00E+13	0.0	0.0
258.	C3H+O2=HCCO+CO	1.00E+13	0.0	0.0
259.	C3H+O=C2H+CO	1.00E+13	0.0	0.0
260.	C3H2+H=C3H+H2	1.00E+13	0.0	0.0
261.	C3H2+O2=HCCO+CO+H	2.00E+12	0.0	1000.0
262.	C3H2+O=C2H2+CO	1.00E+14	0.0	0.0
263.	C3H2+OH=C2H2+HCO	5.00E+13	0.0	0.0
264.	H2CCCH+O2=CH2CO+HCO	3.00E+10	0.0	2868.0
265.	H2CCCH+O=CH2O+C2H	1.40E+14	0.0	0.0
266.	H2CCCH+H=C3H2+H2	5.00E+13	0.0	1000.0

267. H2CCCH+H(+M)=H3CCCH(+M) 1.00E+17 -0.8 315.0

Low pressure limit: 0.35000E+56 -0.48800E+01 0.22250E+04

TROE centering: 0.70860E+00 0.13400E+03 0.17840E+04 0.57400E+04

H2 Enhanced by 2.000E+00

CO Enhanced by 2.000E+00

CO2 Enhanced by 3.000E+00

H2O Enhanced by 8.600E+00

268. H2CCCH+H(+M)=H2CCCH2(+M) 1.00E+17 -0.8 315.0

Low pressure limit: 0.35000E+56 -0.48800E+01 0.22250E+04

TROE centering: 0.70860E+00 0.13400E+03 0.17840E+04 0.57400E+04

H2 Enhanced by 2.000E+00

CO Enhanced by 2.000E+00

CO2 Enhanced by 3.000E+00

H2O Enhanced by 8.600E+00

269. H2CCCH+OH=C3H2+H2O 2.00E+13 0.0 0.0

270. CH2CHC.O=C2H3+CO 1.00E+14 0.0 34000.0

271. CH2CHC.O+O=C2H3+CO2 1.00E+14 0.0 0.0

272. CH2CHC.O+O2=CH2HCO+CO2 5.40E+20 -2.7 7000.0

273. H2CCCH2=H3CCCH 2.20E+14 0.0 68100.0

274. H2CCCH2+H=H3CCCH+H 1.00E+13 0.0 5000.0

275. H2CCCH2+H=H2CCCH+H2 3.00E+07 2.0 5000.0

276. H2CCCH2+O=C2H4+CO 1.30E+07 1.9 180.0

277. H2CCCH2+OH=H2CCCH+H2O 2.00E+07 2.0 1000.0

278. H2CCCH2+H(+M)=CH2CHC.H2(+M) 1.20E+11 0.7 3000.0

Low pressure limit: 0.56000E+34 -0.50000E+01 0.44500E+04

TROE centering: 0.70860E+00 0.13400E+03 0.17840E+04 0.57400E+04

279. H2CCCH2+H(+M)=CH2C.CH3(+M) 8.50E+12 0.0 2000.0

Low pressure limit: 0.11000E+35 -0.50000E+01 0.44500E+04

TROE centering: 0.70860E+00 0.13400E+03 0.17840E+04 0.57400E+04

280. H3CCCH+H=H2CCCH+H2 3.00E+07 2.0 5000.0

281. H3CCCH+H=CH3+C2H2 1.00E+14 0.0 4000.0

282.	H3CCCH+H(+M)=CH2C.CH3(+M)			6.50E+12	0.0	2000.0
	Low pressure limit:	0.85000E+40	-0.72700E+01	0.65800E+04		
	TROE centering:	0.70860E+00	0.13400E+03	0.17840E+04	0.57400E+04	
283.	H3CCCH+OH=H2CCCH+H2O			2.00E+07	2.0	1000.0
284.	H3CCCH+O=C2H4+CO			1.50E+13	0.0	2100.0
285.	CH2CHCHO+H=C2H4+HCO			2.00E+13	0.0	3500.0
286.	CH2CHCHO+H=CH2CHC.O+H2			4.00E+13	0.0	4200.0
287.	CH2CHCHO+O=CH2CHC.O+OH			7.20E+12	0.0	1970.0
288.	CH2CHCHO+O=CH2CO+HCO+H			5.00E+07	1.8	76.0
289.	CH2CHCHO+OH=CH2CHC.O+H2O			1.00E+13	0.0	0.0
290.	CH2CHCHO+O2=CH2CHC.O+HO2			3.00E+13	0.0	36000.0
291.	CH2CHC.H2+H=H2CCCH2+H2			5.00E+13	0.0	0.0
292.	CH2CHC.H2+H=CH2CHCH3			1.90E+26	-3.6	5470.0
293.	CH2CHC.H2+O=CH2CHCHO+H			1.80E+14	0.0	0.0
294.	CH2CHC.H2+OH=H2CCCH2+H2O			1.00E+13	0.0	0.0
295.	CH2CHC.H2+HO2=CH2CHCHO+H+OH			1.00E+13	0.0	0.0
296.	CH2CHC.H2+O2=CH2CHCHO+OH			1.80E+13	-0.4	22860.0
297.	CH2CHC.H2+O2=H2CCCH2+HO2			5.00E+15	-1.4	22430.0
298.	CH2CHC.H2+O2=CH2HCO+CH2O			1.10E+10	0.3	12840.0
299.	CH2CHC.H2+O2=C2H2+CH2O+OH			2.80E+25	-4.8	15470.0
300.	CH2CHC.H2+CH3=H2CCCH2+CH4			3.02E+12	-0.3	-131.0
301.	C.HCHCH3+H=CH2CHC.H2+H			1.00E+14	0.0	0.0
302.	C.HCHCH3+H=H3CCCH+H2			2.00E+13	0.0	0.0
303.	C.HCHCH3+H=CH2CHCH3			1.00E+14	0.0	0.0
304.	C.HCHCH3+OH=H3CCCH+H2O			1.00E+13	0.0	0.0
305.	C.HCHCH3+O2=CH3HCO+HCO			1.10E+23	-3.3	3900.0
306.	CH2C.CH3+H=CH2CHC.H2+H			1.00E+14	0.0	0.0
307.	CH2C.CH3+H=H3CCCH+H2			4.00E+13	0.0	0.0
308.	CH2C.CH3+H=CH2CHCH3			5.00E+13	0.0	0.0
309.	CH2C.CH3+O=CH2CO+CH3			1.00E+14	0.0	0.0
310.	CH2C.CH3+OH=H3CCCH+H2O			2.00E+13	0.0	0.0

311.	CH2C.CH3+O2=CH3CO+CH2O	1.10E+22	-3.3	3900.0
312.	CH2CHCH3+H=C2H4+CH3	7.20E+12	0.0	1300.0
313.	CH2CHCH3+H=CH2CHC.H2+H2	1.70E+05	2.5	2490.0
314.	CH2CHCH3+H=CH2C.CH3+H2	4.10E+05	2.5	9800.0
315.	CH2CHCH3+H=C.HCHCH3+H2	8.00E+05	2.5	12300.0
316.	CH2CHCH3+O=C2H5+HCO	1.60E+07	1.8	-1216.0
317.	CH2CHCH3+O=CH2CHC.H2+OH	5.20E+11	0.7	5884.0
318.	CH2CHCH3+O=C.HCHCH3+OH	1.20E+11	0.7	8960.0
319.	CH2CHCH3+O=CH2C.CH3+OH	6.00E+10	0.7	7630.0
320.	CH2CHCH3+O2=CH2CHC.H2+HO2	2.00E+13	0.0	47600.0
321.	CH2CHCH3+O2=C.HCHCH3+HO2	2.00E+13	0.0	47600.0
322.	CH2CHCH3+O2=CH2C.CH3+HO2	2.00E+13	0.0	47600.0
323.	CH2CHCH3+OH=CH2CHC.H2+H2O	3.10E+06	2.0	-298.0
324.	CH2CHCH3+OH=CH2C.CH3+H2O	1.10E+06	2.0	1451.0
325.	CH2CHCH3+OH=C.HCHCH3+H2O	2.10E+06	2.0	2778.0
326.	CH2CHCH3+HO2=CH2CHC.H2+H2O2	9.60E+03	2.6	13909.0
327.	CH2CHCH3=C2H2+CH4	2.50E+12	0.0	70000.0
328.	CH2CHCH3=H2CCCH2+H2	3.00E+13	0.0	80000.0
329.	CH2CHCH3+OH+O2=CH3HCO+CH2O+OH	3.00E+10	0.0	-8280.0
330.	CH2CHCH3+CH3=CH2CHC.H2+CH4	2.22E+00	3.5	5675.0
331.	CH2CHCH3+CH3=CH2C.CH3+CH4	8.43E-01	3.5	11656.0
332.	CH2CHCH3+CH3=C.HCHCH3+CH4	1.35E+00	3.5	12848.0
333.	CH2CHCH3+HCO=CH2CHC.H2+CH2O	1.08E+07	1.9	17010.0
334.	C2H5CHO+H=C2H5CO+H2	8.00E+13	0.0	0.0
335.	C2H5CHO+O=C2H5CO+OH	7.80E+12	0.0	1730.0
336.	C2H5CHO+OH=C2H5CO+H2O	1.20E+13	0.0	0.0
337.	nC3H7=CH2CHCH3+H	1.30E+13	0.0	38500.0
338.	nC3H7+H=CH2CHCH3+H2	1.80E+12	0.0	0.0
339.	nC3H7+O=C2H5CHO+H	1.00E+14	0.0	0.0
340.	nC3H7+OH=CH2CHCH3+H2O	2.40E+13	0.0	0.0
341.	nC3H7+OH=nC3H7OH	2.40E+13	0.0	0.0

342.	nC3H7+O2=CH2CHCH3+HO2			9.00E+14	0.0	0.0
343.	nC3H7+HO2=nC3H7O+OH			2.40E+13	0.0	0.0
344.	nC3H7+CH3=CH2CHCH3+CH4			1.10E+13	-0.3	0.0
345.	nC3H7+nC3H7=C3H8+CH2CHCH3			1.70E+12	0.0	0.0
346.	nC3H7+iC3H7=C3H8+CH2CHCH3			5.10E+13	-0.3	0.0
347.	nC3H7+C3H8=C3H8+iC3H7			8.40E-04	4.0	4726.0
348.	iC3H7=CH2CHCH3+H			6.50E+07	1.8	35360.0
349.	iC3H7=C2H4+CH3			1.00E+12	0.0	0.0
350.	iC3H7+H=CH2CHCH3+H2			3.60E+12	0.0	0.0
351.	iC3H7+O=C2H5CHO+H			4.80E+13	0.0	0.0
352.	iC3H7+O=CH3HCO+CH3			4.80E+13	0.0	0.0
353.	iC3H7+OH=CH2CHCH3+H2O			2.40E+13	0.0	0.0
354.	iC3H7+O2=CH2CHCH3+HO2			1.30E+11	0.0	0.0
355.	iC3H7+HO2=CH3HCO+CH3+OH			2.40E+13	0.0	0.0
356.	iC3H7+CH3=CH2CHCH3+CH4			1.10E+14	-0.6	0.0
357.	iC3H7+iC3H7=C3H8+CH2CHCH3			2.10E+14	-0.7	0.0
358.	nC3H7OH=C2H5O+CH3			1.60E+16	0.0	81674.0
359.	C3H8=nC3H7+H			1.60E+16	0.0	97500.0
360.	C3H8=iC3H7+H			6.30E+15	0.0	94700.0
361.	C3H8=CH3+C2H5			1.10E+17	0.0	84396.0
362.	C3H8(+M)=CH3+C2H5(+M)			7.80E+18	0.0	64980.0
	Low pressure limit:	0.66000E+41	0.00000E+00	0.84400E+05		
	TROE centering:	0.76000E+00	0.19460E+04	0.38000E+02		
363.	C3H8+H=nC3H7+H2			9.30E+12	0.0	8000.0
364.	C3H8+H=iC3H7+H2			3.10E+13	0.0	8000.0
365.	C3H8+O=nC3H7+OH			1.90E+05	2.7	3716.0
366.	C3H8+O=iC3H7+OH			4.80E+04	2.7	2106.0
367.	C3H8+OH=nC3H7+H2O			2.30E+12	0.0	2600.0
368.	C3H8+OH=iC3H7+H2O			5.30E+12	0.0	1950.0
369.	C3H8+O2=nC3H7+HO2			4.00E+13	0.0	50872.0
370.	C3H8+O2=iC3H7+HO2			4.00E+13	0.0	47693.0

371.	C3H8+HO2=nC3H7+H2O2		4.80E+04	2.5	16494.0
372.	C3H8+HO2=iC3H7+H2O2		9.60E+03	2.6	13910.0
373.	C3H8+CH3=nC3H7+CH4		9.00E-01	3.6	7154.0
374.	C3H8+CH3=iC3H7+CH4		1.50E+00	3.5	5481.0
375.	H+NO+M=HNO+M		4.00E+20	-1.8	0.0
	H2O	Enhanced by 1.000E+01			
	O2	Enhanced by 1.500E+00			
	H2	Enhanced by 2.000E+00			
	CO2	Enhanced by 3.000E+00			
	N2	Enhanced by 1.000E+00			
376.	H+NO+N2=HNO+N2		7.00E+19	-1.5	0.0
377.	NO+O(+M)=NO2(+M)		1.30E+15	-0.8	0.0
	Low pressure limit: 0.75000E+20 -0.14100E+01 0.00000E+00				
	N2	Enhanced by 1.700E+00			
	O2	Enhanced by 1.500E+00			
	H2O	Enhanced by 1.000E+01			
378.	NO+OH(+M)=HONO(+M)		2.00E+12	-0.1	-721.0
	Low pressure limit: 0.50000E+24 -0.25100E+01 -0.68000E+02				
	N2	Enhanced by 1.000E+00			
	O2	Enhanced by 1.000E+00			
	H2O	Enhanced by 6.700E+00			
	AR	Enhanced by 6.700E-01			
379.	NO+HO2=NO2+OH		2.10E+12	0.0	-480.0
380.	NO2+H=NO+OH		1.30E+14	0.0	362.0
381.	NO2+O=NO+O2		3.90E+12	0.0	-238.0
382.	NO2+O(+M)=NO3(+M)		1.30E+13	0.0	0.0
	Low pressure limit: 0.10000E+29 -0.40800E+01 0.24700E+04				
	N2	Enhanced by 1.500E+00			
	O2	Enhanced by 1.500E+00			
	H2O	Enhanced by 1.000E+01			
383.	NO2+HO2=HONO+O2		6.30E+08	1.2	5000.0

384.	NO2+H2=HONO+H			4.50E+12	0.0	27600.0
385.	NO2+NO2=NO3+NO			9.60E+09	0.7	20900.0
386.	NO3+H=NO2+OH			6.00E+13	0.0	0.0
387.	NO3+O=NO2+O2			1.00E+13	0.0	0.0
388.	NO3+OH=NO2+HO2			1.40E+13	0.0	0.0
389.	NO3+HO2=NO2+O2+OH			1.50E+12	0.0	0.0
390.	NO3+NO2=NO+NO2+O2			5.00E+10	0.0	2940.0
391.	HNO+H=NO+H2			4.40E+11	0.7	650.0
392.	HNO+O=NO+OH			2.30E+13	0.0	0.0
393.	HNO+OH=NO+H2O			3.60E+13	0.0	0.0
394.	HNO+O2=HO2+NO			2.00E+13	0.0	16000.0
395.	HNO+NO2=HONO+NO			6.00E+11	0.0	2000.0
396.	HNO+HNO=N2O+H2O			9.00E+08	0.0	3100.0
397.	HON+M=NO+H+M			5.10E+19	-1.7	16045.0
	AR	Enhanced by	7.000E-01			
	H2O	Enhanced by	7.000E+00			
	CO2	Enhanced by	2.000E+00			
398.	HON+H=HNO+H			2.00E+13	0.0	0.0
399.	HON+H=OH+NH			2.00E+13	0.0	0.0
400.	HON+O=OH+NO			7.00E+13	0.0	0.0
401.	HON+OH=HONO+H			4.00E+13	0.0	0.0
402.	HON+O2=NO2+OH			1.00E+12	0.0	4968.0
403.	H2NO+M=HNO+H+M			2.80E+24	-2.8	64915.0
	H2O	Enhanced by	1.000E+01			
404.	H2NO+M=HNOH+M			1.10E+29	-4.0	44000.0
	H2O	Enhanced by	1.000E+01			
405.	H2NO+H=HNO+H2			3.00E+07	2.0	2000.0
406.	H2NO+H=NH2+OH			5.00E+13	0.0	0.0
407.	H2NO+O=HNO+OH			3.00E+07	2.0	2000.0
408.	H2NO+OH=HNO+H2O			2.00E+07	2.0	1000.0
409.	H2NO+HO2=HNO+H2O2			2.90E+04	2.7	1600.0

410.	H2NO+O2=HNO+HO2	3.00E+12	0.0	25000.0
411.	H2NO+NO=HNO+HNO	2.00E+04	2.0	13000.0
412.	H2NO+NH2=HNO+NH3	3.00E+12	0.0	1000.0
413.	H2NO+NO2=HONO+HNO	6.00E+11	0.0	2000.0
414.	HONO+H=HNO+OH	5.60E+10	0.9	5000.0
415.	HONO+H=NO+H2O	8.10E+06	1.9	3850.0
416.	HONO+O=NO2+OH	1.20E+13	0.0	6000.0
417.	HONO+OH=NO2+H2O	4.00E+12	0.0	0.0
418.	HONO+HONO=NO+NO2+H2O	3.50E-01	3.6	12100.0
419.	HNOH+M=HNO+H+M	2.00E+24	-2.8	58934.0
	H2O Enhanced by 1.000E+01			
420.	HNOH+H=NH2+OH	4.00E+13	0.0	0.0
421.	HNOH+H=HNO+H2	4.80E+08	1.5	378.0
422.	HNOH+O=HNO+OH	7.00E+13	0.0	0.0
	Declared duplicate reaction...			
423.	HNOH+O=HNO+OH	3.30E+08	1.5	-358.0
	Declared duplicate reaction...			
424.	HNOH+OH=HNO+H2O	2.40E+06	2.0	-1192.0
425.	HNOH+HO2=HNO+H2O2	2.90E+04	2.7	-1600.0
426.	HNOH+O2=HNO+HO2	3.00E+12	0.0	25000.0
427.	HNOH+NH2=NH3+HNO	1.80E+06	1.9	-1152.0
428.	HNOH+NO2=HONO+HNO	6.00E+11	0.0	2000.0
429.	NH3+M=NH2+H+M	2.20E+16	0.0	93470.0
430.	NH3+H=NH2+H2	6.40E+05	2.4	10171.0
431.	NH3+O=NH2+OH	9.40E+06	1.9	6460.0
432.	NH3+OH=NH2+H2O	2.00E+06	2.0	566.0
433.	NH3+HO2=NH2+H2O2	3.00E+11	0.0	22000.0
434.	NH2+H=NH+H2	4.00E+13	0.0	3650.0
435.	NH2+O=HNO+H	6.60E+14	-0.5	0.0
436.	NH2+O=NH+OH	6.80E+12	0.0	0.0
437.	NH2+OH=NH+H2O	4.00E+06	2.0	1000.0

438.	NH2+HO2=H2NO+OH	5.00E+13	0.0	0.0
439.	NH2+HO2=NH3+O2	9.20E+05	1.9	-1152.0
440.	NH2+O2=H2NO+O	2.50E+11	0.5	29586.0
441.	NH2+O2=HNO+OH	6.20E+07	1.2	35100.0
442.	NH2+NH2=NH3+NH	5.00E+13	0.0	10000.0
443.	NH2+NH=NH3+N	9.20E+05	1.9	2444.0
444.	NH2+N=N2+H+H	7.00E+13	0.0	0.0
445.	NH2+NO=N2+H2O	2.80E+20	-2.7	1258.0
446.	NH2+NO=NNH+OH	2.30E+10	0.4	-814.0
447.	NH2+NO2=N2O+H2O	1.60E+16	-1.4	268.0
448.	NH2+NO2=H2NO+NO	6.50E+16	-1.4	268.0
449.	NH2+HNO=NH3+NO	3.60E+06	1.6	-1250.0
450.	NH2+HONO=NH3+NO2	7.10E+01	3.0	-4940.0
451.	NH+H=N+H2	3.00E+13	0.0	0.0
452.	NH+O=NO+H	9.20E+13	0.0	0.0
453.	NH+OH=HNO+H	2.00E+13	0.0	0.0
454.	NH+OH=N+H2O	5.00E+11	0.5	2000.0
455.	NH+O2=HNO+O	4.60E+05	2.0	6500.0
456.	NH+O2=NO+OH	1.30E+06	1.5	100.0
457.	NH+NH=N2+H+H	2.50E+13	0.0	0.0
458.	NH+N=N2+H	3.00E+13	0.0	0.0
459.	NH+NO=N2O+H	2.90E+14	-0.4	0.0
	Declared duplicate reaction...			
460.	NH+NO=N2O+H	-2.20E+13	-0.2	0.0
	Declared duplicate reaction...			
	Warning...negative pre-exponential factor for forward rate constant...			
461.	NH+NO=N2+OH	2.20E+13	-0.2	0.0
462.	NH+NO2=N2O+OH	1.00E+13	0.0	0.0
463.	NH+HONO=NH2+NO2	1.00E+13	0.0	0.0
464.	N+OH=NO+H	3.80E+13	0.0	0.0
465.	N+O2=NO+O	6.40E+09	1.0	6280.0

466.	N+NO=N2+O	3.30E+12	0.3	0.0
467.	N2H2+H=NNH+H2	5.00E+13	0.0	1000.0
468.	N2H2+O=NH2+NO	1.00E+13	0.0	0.0
469.	N2H2+O=NNH+OH	2.00E+13	0.0	1000.0
470.	N2H2+OH=NNH+H2O	1.00E+13	0.0	1000.0
471.	N2H2+NO=N2O+NH2	3.00E+12	0.0	0.0
472.	N2H2+NH2=NH3+NNH	1.00E+13	0.0	1000.0
473.	N2H2+NH=NNH+NH2	1.00E+13	0.0	1000.0
474.	NNH=N2+H	6.50E+07	0.0	0.0
475.	NNH+H=N2+H2	1.00E+14	0.0	0.0
476.	NNH+O=N2O+H	1.00E+14	0.0	0.0
477.	NNH+O=N2+OH	8.00E+13	0.0	0.0
478.	NNH+O=NH+NO	5.00E+13	0.0	0.0
479.	NNH+OH=N2+H2O	5.00E+13	0.0	0.0
480.	NNH+O2=N2+HO2	2.00E+14	0.0	0.0
481.	NNH+O2=N2+H+O2	5.00E+13	0.0	0.0
482.	NNH+NH=N2+NH2	5.00E+13	0.0	0.0
483.	NNH+NH2=N2+NH3	5.00E+13	0.0	0.0
484.	NNH+NO=N2+HNO	5.00E+13	0.0	0.0
485.	N2O(+M)=N2+O(+M)	1.30E+12	0.0	62570.0
	Low pressure limit: 0.40000E+15 0.00000E+00 0.56600E+05			
	N2 Enhanced by 1.700E+00			
	O2 Enhanced by 1.400E+00			
	CO2 Enhanced by 3.000E+00			
	H2O Enhanced by 1.200E+01			
486.	N2O+H=N2+OH	3.30E+10	0.0	4729.0
	Declared duplicate reaction...			
487.	N2O+H=N2+OH	4.40E+14	0.0	19254.0
	Declared duplicate reaction...			
488.	N2O+O=NO+NO	9.20E+13	0.0	27679.0
489.	N2O+O=N2+O2	3.70E+12	0.0	15936.0

490.	N2O+OH=N2+HO2			1.30E-02	4.7	36560.0
491.	N2O+OH=HNO+NO			1.20E-04	4.3	25080.0
492.	N2O+NO=NO2+N2			5.30E+05	2.2	46280.0
493.	HCN+M=H+CN+M			3.40E+35	-5.1	133000.0
	N2	Enhanced by	0.000E+00			
	O2	Enhanced by	1.500E+00			
	H2O	Enhanced by	1.000E+01			
	CO2	Enhanced by	1.500E+00			
494.	HCN+N2=H+CN+N2			3.60E+26	-2.6	124890.0
495.	HCN+M=HNC+M			1.60E+26	-3.2	54600.0
	AR	Enhanced by	7.000E-01			
	H2O	Enhanced by	7.000E+00			
	CO2	Enhanced by	2.000E+00			
496.	CN+H2=HCN+H			1.10E+05	2.6	1908.0
497.	HCN+O=NCO+H			7.60E+10	0.5	7810.0
498.	HCN+O=CN+OH			4.20E+10	0.4	20665.0
499.	HCN+O=NH+CO			3.50E+03	2.6	4980.0
500.	HCN+OH=CN+H2O			3.90E+06	1.8	10300.0
501.	HCN+OH=HOCN+H			5.90E+04	2.4	12500.0
502.	HCN+OH=HNCO+H			2.00E-03	4.0	1000.0
503.	HCN+OH=NH2+CO			7.80E-04	4.0	4000.0
504.	HCN+O2=CN+HO2			3.00E+13	0.0	75100.0
505.	HCN+CN=NCCN+H			1.50E+07	1.7	1530.0
506.	HNC+H=HCN+H			7.80E+13	0.0	3600.0
507.	HNC+O=NH+CO			4.60E+12	0.0	2200.0
508.	HNC+OH=HNCO+H			2.80E+13	0.0	3700.0
509.	HNC+CN=NCCN+H			1.00E+13	0.0	0.0
510.	CN+O=CO+N			1.90E+12	0.5	723.0
511.	CN+OH=NCO+H			1.00E+15	-0.4	0.0
512.	CN+O2=NCO+O			7.20E+12	0.0	-417.0
	Declared duplicate reaction...					

513.	CN+O2=NCO+O			2.80E+17	-2.0	0.0
	Declared duplicate reaction...					
514.	CN+O2=NO+CO			2.80E+17	-2.0	0.0
515.	CN+CO2=NCO+CO			3.70E+06	2.2	26900.0
516.	CN+CH2O=HCN+HCO			4.20E+13	0.0	0.0
517.	CN+NO=NCO+N			9.60E+13	0.0	42100.0
518.	CN+NO2=NCO+NO			5.30E+15	-0.8	344.0
519.	CN+NO2=CO+N2O			4.90E+14	-0.8	344.0
520.	CN+NO2=N2+CO2			3.70E+14	-0.8	344.0
521.	CN+HNO=HCN+NO			1.80E+13	0.0	0.0
522.	CN+HONO=HCN+NO2			1.20E+13	0.0	0.0
523.	CN+N2O=NCN+NO			3.80E+03	2.6	3700.0
524.	CN+HNCO=HCN+NCO			5.00E+12	0.0	0.0
525.	CN+NCO=NCN+CO			1.80E+13	0.0	0.0
526.	HNCO+M=CO+NH+M			1.10E+16	0.0	86000.0
	N2	Enhanced by	1.000E+00			
	CO2	Enhanced by	2.000E+00			
	AR	Enhanced by	7.000E-01			
527.	HNCO+H=NH2+CO			3.60E+04	2.5	2345.0
528.	HNCO+H=NCO+H2			9.00E+07	1.7	13900.0
529.	HNCO+O=NCO+OH			2.20E+06	2.1	11430.0
530.	HNCO+O=NH+CO2			9.60E+07	1.4	8520.0
531.	HNCO+O=HNO+CO			1.50E+08	1.6	44012.0
532.	HNCO+OH=NCO+H2O			6.45E+05	2.0	2563.0
533.	HNCO+OH=NH2+CO2			1.80E+06	1.5	3597.0
534.	HNCO+HO2=NCO+H2O2			3.00E+11	0.0	22000.0
535.	HNCO+O2=HNO+CO2			1.00E+12	0.0	35000.0
536.	HNCO+NH=NH2+NCO			3.00E+13	0.0	23700.0
537.	HOCN+H=HNCO+H			3.10E+08	0.8	1917.0
538.	HOCN+H=NH2+CO			1.20E+08	0.6	2076.0
539.	HOCN+H=H2+NCO			2.40E+08	1.5	6617.0

540.	HOCN+O=OH+NCO			1.70E+08	1.5	4133.0
541.	HOCN+OH=H2O+NCO			1.20E+06	2.0	-248.0
542.	HOCN+NH2=NCO+NH3			9.20E+05	1.9	3646.0
543.	HCNO=HCN+O			4.20E+31	-6.1	61210.0
544.	HCNO+H=HCN+OH			7.20E+10	0.8	8612.0
545.	HCNO+O=HCO+NO			6.30E+13	0.0	0.0
546.	HCNO+OH=CH2O+NO			1.00E+12	0.0	0.0
547.	HCNO+O=NCO+OH			7.00E+12	0.0	0.0
548.	HCNO+OH=NO+CO+H2			6.50E+12	0.0	0.0
549.	HCNO+OH=NCO+H+OH			4.50E+12	0.0	0.0
550.	HCNO+OH=NCO+H2O			3.50E+12	0.0	0.0
551.	HCNO+OH=HCO+HNO			4.50E+12	0.0	0.0
552.	NCO+M=N+CO+M			2.20E+14	0.0	54050.0
	N2	Enhanced by	1.500E+00			
	CO2	Enhanced by	2.000E+00			
553.	NCO+H=CO+NH			7.20E+13	0.0	1000.0
554.	NCO+O=NO+CO			2.00E+15	-0.5	0.0
555.	NCO+OH=HON+CO			5.30E+12	-0.1	5126.0
556.	NCO+OH=H+CO+NO			8.30E+12	-0.1	18042.0
557.	NCO+HO2=HNCO+O2			2.00E+13	0.0	0.0
558.	NCO+O2=NO+CO2			2.00E+12	0.0	20000.0
559.	NCO+HCO=HNCO+CO			3.60E+13	0.0	0.0
560.	NCO+NO=N2O+CO			6.16E+17	-1.7	763.0
561.	NCO+NO=N2+CO2			7.84E+17	-1.7	763.0
562.	NCO+NO2=CO+NO+NO			2.50E+11	0.0	-707.0
563.	NCO+NO2=CO2+N2O			3.00E+12	0.0	-707.0
564.	NCO+HNO=HNCO+NO			1.80E+13	0.0	0.0
565.	NCO+HONO=HNCO+NO2			3.60E+12	0.0	0.0
566.	NCO+N=N2+CO			2.00E+13	0.0	0.0
567.	NCO+NH3=HNCO+NH2			2.80E+04	2.5	980.0
568.	NCO+NCO=CO+CO+N2			1.80E+13	0.0	0.0

569.	C2N2+O=NCO+CN	4.60E+12	0.0	8880.0
570.	C2N2+OH=HOCN+CN	1.90E+11	0.0	2900.0
571.	NCN+O=CN+NO	1.00E+14	0.0	0.0
572.	NCN+OH=HCN+NO	5.00E+13	0.0	0.0
573.	NCN+H=HCN+N	1.00E+14	0.0	0.0
574.	NCN+O2=NO+NCO	1.00E+13	0.0	0.0
575.	H+CH3CN=HCN+CH3	4.00E+07	2.0	2000.0
576.	H+CH3CN=CH2CN+H2	3.00E+07	2.0	1000.0
577.	O+CH3CN=NCO+CH3	1.50E+04	2.6	4980.0
578.	OH+CH3CN=CH2CN+H2O	2.00E+07	2.0	2000.0
579.	CH2CN+O=CH2O+CN	1.00E+14	0.0	0.0
580.	CN+CH2OH=CH2CN+OH	5.00E+13	0.0	0.0
581.	H2CN=HCN+H	4.00E+28	-6.0	29897.0
582.	H2CN+H=HCN+H2	2.40E+08	1.5	-894.0
583.	H2CN+O=HCN+OH	1.70E+08	1.5	-894.0
584.	H2CN+OH=HCN+H2O	1.50E+19	-2.2	2166.0
	Declared duplicate reaction...			
585.	H2CN+OH=HCN+H2O	1.20E+06	2.0	-1192.0
	Declared duplicate reaction...			
586.	H2CN+O2=CH2O+NO	3.00E+12	0.0	5961.0
587.	H2CN+N=N2+CH2	2.00E+13	0.0	0.0
588.	H2CN+NH2=HCN+NH3	9.20E+05	1.9	-1152.0
589.	HCNH=HCN+H	6.10E+28	-5.7	24271.0
590.	HCNH+H=H2CN+H	2.00E+13	0.0	0.0
591.	HCNH+H=HCN+H2	2.40E+08	1.5	-894.0
592.	HCNH+O=HNCO+H	7.00E+13	0.0	0.0
593.	HCNH+O=HCN+OH	1.70E+08	1.5	-894.0
594.	HCNH+OH=HCN+H2O	1.20E+06	2.0	-1192.0
595.	NCCN+M=CN+CN+M	1.10E+34	-4.3	130079.0
	N2 Enhanced by 1.500E+00			
	O2 Enhanced by 1.500E+00			

	H2	Enhanced by	1.500E+00			
	H2O	Enhanced by	1.000E+01			
	CO2	Enhanced by	3.000E+00			
596.	NCCN+O=CN+NCO			4.60E+12	0.0	8880.0
597.	NCCN+OH=CN+HOCN			1.90E+11	0.0	2900.0
598.	CO+NO2=CO2+NO			9.00E+13	0.0	33779.0
599.	CO+N2O=N2+CO2			3.20E+11	0.0	20237.0
600.	CO2+N=NO+CO			3.01E+08	0.0	0.0
601.	NH+CO2=CO+HNO			8.20E+13	0.0	34500.0
602.	CH2O+NCO=HNCO+HCO			6.00E+12	0.0	0.0
603.	CH2O+NO2=HCO+HONO			8.00E+02	2.8	13730.0
604.	HCO+NO=HNO+CO			7.00E+13	-0.4	0.0
605.	HCO+NO2=CO+HONO			1.20E+23	-3.3	2355.0
606.	HCO+NO2=H+CO2+NO			8.40E+15	-0.8	1930.0
607.	HCO+HNO=CH2O+NO			6.00E+11	0.0	2000.0
608.	CH4+CN=CH3+HCN			6.20E+04	2.6	-437.0
609.	NCO+CH4=CH3+HNCO			9.80E+12	0.0	8120.0
610.	CH3+NO=HCN+H2O			1.50E-01	3.5	3950.0
611.	CH3+NO=H2CN+OH			1.50E-01	3.5	3950.0
612.	CH3+N=H2CN+H			7.10E+13	0.0	0.0
613.	CH3+CN=CH2CN+H			1.00E+14	0.0	0.0
614.	CH3+HOCN=CH3CN+OH			5.00E+12	0.0	2000.0
615.	CH2+NO=HCN+OH			2.20E+12	0.0	-378.0
616.	CH2+NO=HCNO+H			1.30E+12	0.0	-378.0
617.	CH2+NO2=CH2O+NO			5.90E+13	0.0	0.0
618.	CH2+N=HCN+H			5.00E+13	0.0	0.0
619.	CH2+N2=HCN+NH			1.00E+13	0.0	74000.0
620.	CH2(S)+NO=HCN+OH			2.00E+13	0.0	0.0
621.	CH2(S)+NO=CH2+NO			1.00E+14	0.0	0.0
622.	CH2(S)+HCN=CH3+CN			5.00E+13	0.0	0.0
623.	CH+NO2=HCO+NO			1.00E+14	0.0	0.0

624.	CH+NO=HCN+O			4.80E+13	0.0	0.0
625.	CH+NO=HCO+N			3.40E+13	0.0	0.0
626.	CH+NO=NCO+H			1.90E+13	0.0	0.0
627.	CH+N=CN+H			1.30E+13	0.0	0.0
628.	CH+N2=HCN+N			3.70E+07	1.4	20723.0
629.	CH+N2O=HCN+NO			1.90E+13	0.0	-511.0
630.	C+NO=CN+O			2.00E+13	0.0	0.0
631.	C+NO=CO+N			2.80E+13	0.0	0.0
632.	C+N2=CN+N			6.30E+13	0.0	46019.0
633.	C+N2O=CN+NO			5.10E+12	0.0	0.0
634.	C2H6+CN=C2H5+HCN			1.20E+05	2.8	-1788.0
635.	C2H6+NCO=C2H5+HNCO			1.50E-09	6.9	-2910.0
636.	C2H4+CN=C2H3+HCN			5.90E+14	-0.2	0.0
637.	C2H3+NO=C2H2+HNO			1.00E+12	0.0	1000.0
638.	C2H3+N=HCN+CH2			2.00E+13	0.0	0.0
639.	C2H2+NCO=HCCO+HCN			1.40E+12	0.0	1815.0
640.	C2H+NO=CN+HCO			2.10E+13	0.0	0.0
641.	CH2CO+CN=HCCO+HCN			2.00E+13	0.0	0.0
642.	HCCO+NO=HCNO+CO			5.00E+13	0.0	800.0
643.	HCCO+NO=HCN+CO2			1.00E+10	1.0	616.0
644.	HCCO+NO2=HCNO+CO2			1.60E+13	0.0	0.0
645.	HCCO+N=HCN+CO			5.00E+13	0.0	0.0
646.	C3H8+CN=nC3H7+HCN			2.10E+09	1.1	-564.0
647.	C3H8+CN=iC3H7+HCN			2.00E+11	0.6	-648.0
648.	C3H8+NO=nC3H7+HNO			5.00E+13	0.0	51000.0
649.	C3H8+NO=iC3H7+HNO			5.00E+13	0.0	51000.0
650.	H2S+M=S+H2+M			1.60E+24	-2.6	89100.0
	N2	Enhanced by	1.500E+00			
	SO2	Enhanced by	1.000E+01			
	H2O	Enhanced by	1.000E+01			
651.	H2S+H=SH+H2			1.20E+07	2.1	700.0

652.	H2S+O=SH+OH	7.50E+07	1.8	2900.0
653.	H2S+OH=SH+H2O	2.70E+12	0.0	0.0
654.	H2S+S=SH+SH	8.30E+13	0.0	7400.0
655.	H2S+S=HS2+H	2.00E+13	0.0	7400.0
656.	S+H2=SH+H	1.40E+14	0.0	19300.0
657.	SH+O=H+SO	1.00E+14	0.0	0.0
658.	SH+OH=S+H2O	1.00E+13	0.0	0.0
659.	SH+HO2=HSO+OH	1.00E+12	0.0	0.0
660.	SH+O2=HSO+O	1.90E+13	0.0	17925.0
661.	S+OH=H+SO	4.00E+13	0.0	0.0
662.	S+O2=SO+O	5.20E+06	1.8	-1200.0
663.	SH+SH=S2+H2	1.00E+12	0.0	0.0
664.	SH+S=S2+H	3.00E+13	0.0	0.0
665.	S2+M=S+S+M	4.80E+13	0.0	77000.0
666.	S2+H+M=HS2+M	1.00E+16	0.0	0.0
667.	S2+O=SO+S	1.00E+13	0.0	0.0
668.	HS2+H=S2+H2	1.20E+07	2.1	700.0
669.	HS2+O=S2+OH	7.50E+07	1.8	2900.0
670.	HS2+OH=S2+H2O	2.70E+12	0.0	0.0
671.	HS2+S=S2+SH	2.00E+13	0.0	7400.0
672.	HS2+H+M=H2S2+M	1.00E+16	0.0	0.0
673.	H2S2+H=HS2+H2	1.20E+07	2.1	700.0
674.	H2S2+O=HS2+OH	7.50E+07	1.8	2900.0
675.	H2S2+OH=HS2+H2O	2.70E+12	0.0	0.0
676.	H2S2+S=HS2+SH	2.00E+13	0.0	7400.0
677.	SO3+H=HOSO+O	2.50E+05	2.9	50300.0
678.	SO3+H=SO2+OH	8.40E+09	1.2	3319.0
679.	SO3+O=SO2+O2	2.80E+04	2.6	29212.0
680.	SO3+SO=SO2+SO2	7.60E+03	2.4	2980.0
681.	SO3+OH=SO2+HO2	4.80E+04	2.5	27225.0
682.	SO2+OH=HOSO+O	3.90E+08	1.9	76000.0

683. SO2+O(+M)=SO3(+M) 3.70E+11 0.0 1689.0

Low pressure limit: 0.24000E+28 -0.36000E+01 0.51860E+04

TROE centering: 0.44200E+00 0.31600E+03 0.74420E+04

SO2 Enhanced by 1.000E+01

H2O Enhanced by 1.000E+01

N2 Enhanced by 0.000E+00

CO2 Enhanced by 2.500E+00

684. SO2+O(+N2)=SO3(+N2) 3.70E+11 0.0 1689.0

Low pressure limit: 0.29000E+28 -0.35800E+01 0.52060E+04

TROE centering: 0.43000E+00 0.37100E+03 0.74420E+04

685. SO2+OH(+M)=HOSO2(+M) 5.70E+12 -0.3 0.0

Low pressure limit: 0.17000E+28 -0.40900E+01 0.00000E+00

TROE centering: 0.10000E+01 0.10000E-29 0.41200E+03

N2 Enhanced by 1.000E+00

SO2 Enhanced by 5.000E+00

H2O Enhanced by 5.000E+00

CO2 Enhanced by 2.500E+00

686. SO+O(+M)=SO2(+M) 3.20E+13 0.0 0.0

Low pressure limit: 0.12000E+22 -0.15400E+01 0.00000E+00

TROE centering: 0.55000E+00 0.10000E-29 0.10000E+31

N2 Enhanced by 1.500E+00

SO2 Enhanced by 1.000E+01

H2O Enhanced by 1.000E+01

687. SO+M=S+O+M 4.00E+14 0.0 107000.0

688. SO+OH(+M)=HOSO(+M) 1.60E+12 0.5 -400.0

Low pressure limit: 0.95000E+28 -0.34800E+01 0.97000E+03

N2 Enhanced by 1.500E+00

SO2 Enhanced by 1.000E+01

H2O Enhanced by 1.000E+01

CO2 Enhanced by 2.500E+00

689. SO+O2=SO2+O 7.60E+03 2.4 2970.0

690.	HSO+H=HSOH	2.50E+20	-3.1	920.0
691.	HSO+H=SH+OH	4.90E+19	-1.9	1560.0
692.	HSO+H=S+H2O	1.60E+09	1.4	-340.0
693.	HSO+H=H2SO	1.80E+17	-2.5	50.0
694.	HSO+H=H2S+O	1.10E+06	1.0	10400.0
695.	HSO+H=SO+H2	1.00E+13	0.0	0.0
696.	HSO+O+M=HSO2+M	1.10E+19	-1.7	-50.0
697.	HSO+O=SO2+H	4.50E+14	-0.4	0.0
698.	HSO+O+M=HOSO+M	6.90E+19	-1.6	1590.0
699.	HSO+O=O+HOS	4.80E+08	1.0	5340.0
700.	HSO+O=OH+SO	1.40E+13	0.1	300.0
701.	HSO+OH=HOSHO	5.20E+28	-5.4	3170.0
702.	HSO+OH=HOSO+H	5.30E+07	1.6	3750.0
703.	HSO+OH=SO+H2O	1.70E+09	1.0	470.0
704.	HSO+O2=SO2+OH	1.00E+12	0.0	10000.0
705.	HSOH=SH+OH	2.80E+39	-8.8	75200.0
706.	HSOH=S+H2O	5.80E+29	-5.6	54500.0
707.	HSOH=H2S+O	9.80E+16	-3.4	86500.0
708.	H2SO=H2S+O	4.90E+28	-6.7	71700.0
709.	HOSO(+M)=HSO2(+M)	1.00E+09	1.0	50000.0
	Low pressure limit: 0.17000E+36 -0.56400E+01 0.55400E+05			
	TROE centering: 0.40000E+00 0.10000E-29 0.10000E+31			
	N2 Enhanced by 1.000E+00			
	SO2 Enhanced by 1.000E+01			
	H2O Enhanced by 1.000E+01			
	CO2 Enhanced by 2.500E+00			
710.	HOSO+M=O+HOS+M	2.50E+30	-4.8	119000.0
711.	HOSO+OH=SO2+H2O	1.00E+12	0.0	0.0
712.	HSO2+OH=SO2+H2O	1.00E+13	0.0	0.0
713.	HOSO2=HOSO+O	5.40E+18	-2.3	106300.0
714.	HOSO2=SO3+H	1.40E+18	-2.9	54900.0

715.	HOSO2+H=SO2+H2O	1.00E+12	0.0	0.0
716.	HOSO2+O=SO3+OH	5.00E+12	0.0	0.0
717.	HOSO2+OH=SO3+H2O	1.00E+12	0.0	0.0
718.	HOSO2+O2=HO2+SO3	7.80E+11	0.0	656.0
719.	HOSHO=HOSO+H	6.40E+30	-5.9	73800.0
720.	HOSHO=SO+H2O	1.20E+24	-3.6	59500.0
721.	HOSHO+H=HOSO+H2	1.00E+12	0.0	0.0
722.	HOSHO+O=HOSO+OH	5.00E+12	0.0	0.0
723.	HOSHO+OH=HOSO+H2O	1.00E+12	0.0	0.0
724.	H+SO2(+M)=HSO2(+M)	5.31E+08	1.6	2472.0
	Low pressure limit: 0.14100E+32 -0.51900E+01 0.45130E+04			
	TROE centering: 0.39000E+00 0.16700E+03 0.21910E+04			
	N2 Enhanced by 1.000E+00			
	SO2 Enhanced by 1.000E+01			
	H2O Enhanced by 1.000E+01			
	CO2 Enhanced by 2.500E+00			
725.	H+SO2(+M)=HOSO(+M)	2.37E+08	1.6	7339.0
	Low pressure limit: 0.18500E+38 -0.61400E+01 0.11075E+05			
	TROE centering: 0.28300E+00 0.27200E+03 0.39950E+04			
	N2 Enhanced by 1.000E+00			
	SO2 Enhanced by 1.000E+01			
	H2O Enhanced by 1.000E+01			
	CO2 Enhanced by 2.500E+00			
726.	H+SO2(+M)=OH+SO(+M)	9.19E+25	2.8	20850.0
	Low pressure limit: 0.13500E+23 -0.23000E+01 0.30965E+05			
	TROE centering: 0.28300E+00 0.27200E+03 0.39950E+04			
	N2 Enhanced by 1.000E+00			
	SO2 Enhanced by 1.000E+01			
	H2O Enhanced by 1.000E+01			
	CO2 Enhanced by 2.500E+00			
727.	HOSO+O2=SO2+HO2	9.60E+01	2.4	-10130.0

728.	HOSO+H=SO(S)+H2O			2.40E+14	0.0	0.0
729.	HOSO+H=SO2+H2			1.80E+07	1.7	-1286.0
730.	HSO+M=SO+H+M			8.43E+15	0.0	58600.0
	N2	Enhanced by	1.500E+00			
	SO2	Enhanced by	1.000E+01			
	H2O	Enhanced by	1.000E+01			
731.	SO2+S=SO+SO			6.00E-16	8.2	9600.0
732.	HSO2+H=SO2+H2			5.00E+12	0.5	-262.0
733.	HSO2+O2=HO2+SO2			1.10E+03	3.2	-235.0
734.	SO+HO2=SO2+OH			3.70E+03	2.4	7660.0
735.	SO(S)+M=SO+M			1.00E+13	0.0	0.0
736.	SO(S)+O2=SO2+O			1.00E+13	0.0	0.0
737.	SO2+CO=SO+CO2			1.90E+13	0.0	65900.0
738.	CO+SO=CO2+S			5.10E+13	0.0	53400.0
739.	SO+NO2=SO2+NO			8.40E+12	0.0	0.0
740.	SO2+NO2=SO3+NO			6.30E+12	0.0	27000.0
741.	HSO+NO2=HOSO+NO			5.80E+12	0.0	0.0
742.	SO3+H2O=H2SO4			7.23E+08	0.0	0.0

Appendix C Henry's law constants used in ASPEN Plus

Henry's law constants for the species involved in the absorber column were incorporated in ASPEN Plus, based on the compilation by Sander [97]. Henry's constant at a given temperature can be defined as:

$$H(T) = H^o \times \exp\left(-\frac{\Delta_{sol}h}{R}\left(\frac{1}{T}-\frac{1}{T^o}\right)\right) \quad \text{(C-1)}$$

Where H^o is the Henry solubility at standard temperature T^o. The expression $\Delta_{sol}h$ is the molar enthalpy of dissolution, R is the gas constant and T is the temperature in K.

Table C-1 Temperature dependent Henry's Law constants used in ASPEN Plus

	H^o (at $T^o = 298.15\ K$)	$-\frac{\Delta_{sol}h}{R}$
	$(mol.m^{-3}.Pa^{-1})$	(K)
Ar	1.4E-5	1700
O_2	1.2E-5	1700
CO_2	3.3E-4	2400
NO	1.9E-5	1600
NO_2	1.2E-4	2400
N_2O_3	5.9E-3	
N_2O_4	1.33E-2	1100
HNO_2	4.8E-1	4800
HNO_3	2.1E+3	8700
SO_2	1.3E-3	2900
SO_3	1.0E+4	
H_2SO_4	2.9E+7	10000